Alternative Topological Approaches to the Electronic Lamp Ballast

by

Eric Bertrand Shen

S.B., Massachusetts Institute of Technology (1993)
S.M., Massachusetts Institute of Technology (1993)

Submitted to the Department of Electrical Engineering and Computer Science
in partial fulfillment of the requirements for the degree of

Doctor of Philosophy

at the

MASSACHUSETTS INSTITUTE OF TECHNOLOGY

May 1997
[June 1997]

Author .....
Department of Electrical Engineering and Computer Science
May 19, 1997

Certified by .....
Martin F. Schlecht
Professor of Electrical Engineering
Thesis Supervisor

Accepted by .....
Arthur C. Smith
Chairman, Departmental Committee on Graduate Students

Alternative Topological Approaches to the Electronic Lamp Ballast

by

Eric Bertrand Shen

Submitted to the Department of Electrical Engineering and Computer Science
on May 19, 1997, in partial fulfillment of the
requirements for the degree of
Doctor of Philosophy

Abstract

The electronic ballast industry has matured to the point of diminishing returns with conventional ballast topologies. We have undertaken this project and collaborated closely with the industry with the goal of making significant improvements upon the state of the art. By wiping the slate clean and asking ourselves the fundamental question "What does the ballast need to accomplish?" we have invented a new class of circuits suitable for driving discharge lamps. These topologies show promise in terms of size, cost, and performance relative to exisiting ballast technology. This thesis describes these new topologies and compares their merits to existing ballast topologies.

The general philosophy of our topologies is to drive the lamp with a square wave of current synchronized to the 60 Hz utlitity. This has enabled us to use dc–dc conversion techniques, and has resulted in unique circuit topologies. These topologies have enabled us to address the issue of minimizing the size of the 120 Hz load balancing energy storage capacitor present in all ballast topologies. Two basic types of topologies are presented. The series capacitor topology is an elegant solution in that it functions simply as a series element in between the lamp and utility. Because of this, the series capacitor is limited to driving lamps with arc voltages around the average of the utility ($\approx 100\ V$). It is capable of delivering power to a 100 watt load at 96% efficiency. The autotransformer topology takes the series capacitor topology one step further with the addition of a shunt path. This enables the autotransformer topology to drive lamps of any arc voltage with power factor correction on the utility current. A prototype has been shown to deliver 60 watts at 93% efficiency.

This document presents background information on fluorescent and HID type discharge lamps. The current conventional ballast circuits are explained. The new topologies are described in detail and evaluated in terms of size, cost, and performance.

Thesis Supervisor: Martin F. Schlecht
Title: Professor of Electrical Engineering

Acknowledgments

First and foremost, I would like to thank my thesis supervisor, Professor Marty Schlecht, for his help and guidance over the past several years. This work would not have been possible without him. I would also like to thank my thesis readers, Professor Jeff Lang and Professor Jim Roberge, for their helpful comments and suggestions.

I have to acknowledge Professor Steve Leeb and Paul Warren for all the help with laboratory equipment. The following MIT students gave me help and advice along the way: Roxann Blanchard, Rod Hinman, Deron Jackson, Joe Kung, David Martin, and David Perreault. I would also like to thank Beth Chung, Vivian Mizuno, and Marilyn Pierce, for taking care of all the details so that I could graduate.

The following people at Philips Research supported this project: Gert Bruning, Paulo Caldeira, Chin Chang, Joan Fuller, P. D. Goodell, Wen-Jian Gu, Betsy McIlvaine, and Satyen Mukherjee. I have to give special thanks to Mark Fellows of Philips Lighting for the many telephone conversations. I would like to thank David Longden at Philips Components for supplying me with parts. I also owe a debt of gratitude to Richard Osborn and the generous people at Tektronix for their donations.

Finally, I would like to thank God, my family, Nina and the Irani family, the Keyamanesh family, Cristin O'Neal, and all my friends for their support.

This research was funded in part by Philips Research.

Contents

List of Figures

Chapter 1

Introduction

This thesis documents work in the area of electronic lamp ballasts for driving discharge lamps. An entirely new class of lamp ballast circuit topologies, is presented. In addition, the necessary background information on discharge lamps is presented along with the past and present state of the art of lamp ballasts.

This chapter presents a general background of artificial lighting devices and describes the relative merits of each. An outline of the thesis contents is also given.

1.1 Light Sources

The invention of the carbon filament incandescent lamp by Thomas A. Edison in 1879 is arguably one of man's greatest achievements. We have evolved from a society once chained to the daily cycle of daytime and nighttime, into a society that can function productively at any hour and any time. Today we think nothing of illuminating our homes, driveways, streets, offices, and highways. In fact, most of us could not imagine a world without artificial lighting — it is something that we all take for granted. In the United States and around the world, over 25% of all the electrical energy used is consumed by artificial lighting [1, 2, 3].

There are two general classes of artificial light sources, incandescent lamps and gaseous discharge lamps. Incandescent lamps are perhaps the most familiar to us and are common in most households. These lamps consist of a glass bulb containing a

tungsten filament. The filament has some electrical resistance, and when connected to the utility, current flows thereby heating the filament to incandescence. A GE *watt-miser* incandescent lamp gives 1030 lumens of light output for 67 watts of input power over a lifetime of 1000 hours. An important figure of merit for all lamps is the lumen per watt ratio (also referred to as efficacy), or the light output for a given input power; refer to Figure 1-1 for the definition of a lumen. The GE watt-miser yields about 15 lm/W, and most incandescent lamps have efficacies ranging between 11 and 25 lm/W [1, 4]. Only 10% or less of the total input energy is actually radiated as light [4], and the rest is dissipated as heat.

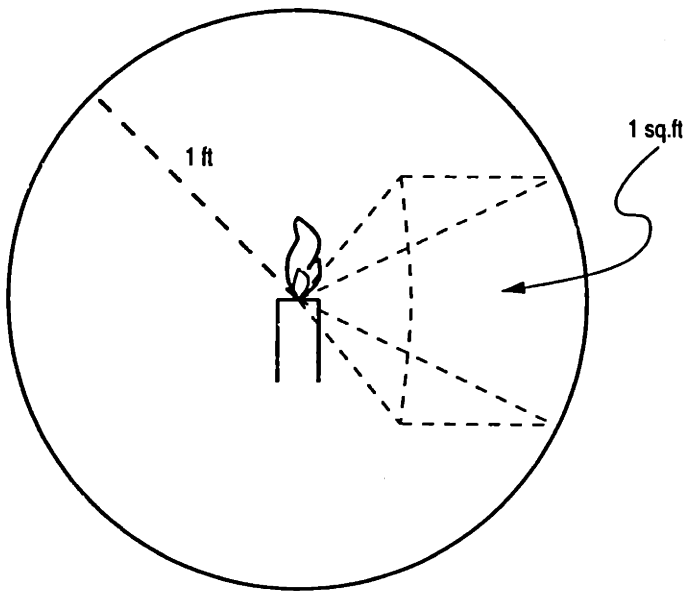

Figure 1-1: Definition of a lumen

Gaseous discharge lamps, or electric discharge lamps, generally consist of a gas sealed within a glass tube with one electrode at each end. An arc, or discharge, is struck between the electrodes causing light to be radiated by collision processes within the tube. There are two classes of discharge lamps, the popular fluorescent type and the high intensity discharge (HID) type. Perhaps half of all artificial lighting is produced by discharge lamps [5], and there is good reason why. Discharge lamps are much more efficient than incandescents, converting 25 to 30% of the total energy into

light [5]. Fluorescent lamps, for instance, generate roughly 80 lm/W for an efficacy six times greater than that of incandescent lamps [6, 7, 8]. Certain types of HID lamps can yield efficacies of up to 140 lm/W [1] while retaining the compact size of incandescents. In addition to increased efficacy, discharge lamps also have long lifetimes of 10,000 hours to 24,000 hours [5].

While discharge lamps are more efficient and last longer than incandescents, there are still other tradeoffs to consider. Incandescents are relatively inexpensive to install and replace, which makes them ideal for consumers [6]. Discharge lamps, on the other hand, have a high initial cost and require external circuitry, called a ballast, to operate from the utility [5]. The discharge lamp benefits of long life and increased efficacy are hard to ignore, however, and with improvements in lamp technology and ballast technology, discharge lamp usage will certainly increase [5].

The ballast circuitry is the focus of the work in this thesis. All discharge lamps have a negative resistance characteristic and thus require intermediate circuitry to interface the lamp to the utility. The primary role of the ballast is to limit the lamp current to the desired operating value. Old electromagnetic ballasts use only simple reactive components like inductors and capacitors to perform this function, while newer electronic ballasts use power conversion circuitry that performs power factor correction and high frequency inversion to drive the lamps at high frequency.

The electronic ballast is a very elegant solution that results in very high ballast–lamp system efficiency. However, electronic ballasts are very expensive compared to electromagnetic ballasts. Also, attempts to reduce the physical size of the electronic ballast have been limited by features fundamental to the ballast topology. This thesis presents several alternative topological approaches to the electronic lamp ballast. The new topologies focus on the reduction of the size of the ballast components, and further improvement in ballast efficiency. In certain applications, these new ballasts may represent cheaper, more easily manufactured solutions.

1.2 Outline

The remaining chapters of this thesis present more detailed background information as well as information pertaining to the new circuit inventions. This thesis is intended to teach a basic understanding of discharge lamp phenomena so that the reader will understand the key issues regarding using lamps as circuit loads. The new circuit topologies are conceptual innovations unlike current and past ballast technologies. A background of ballast technology is presented so that the motivation and scope of the new inventions can be put into perspective.

Chapters 2 and 3 describe the construction and mechanisms by which discharge lamps produce light. Both fluorescent and HID lamp types are covered, each having different properties. This sets the background for the requirements of the ballast — the circuit used to drive these discharge lamps.

Chapter 4 covers ballasts specifically. Both the older, electromagnetic ballasts and the newer, electronic ballasts are described. The advantages and disadvantages of each ballast type are discussed.

Chapter 5 describes our approach to the electronic lamp ballast problem. Issues and concerns are presented from the circuit perspective and the lamp perspective. Basic comparisons are drawn between our approach and existing approaches.

The remaining chapters present the actual circuit topologies that were invented during the course of this research. Two basic "types" of circuit topologies (named series capacitor and autotransformer) are explained in Chapters 6 and 7, first from a conceptual viewpoint, and second from a circuit implementation viewpoint. The circuit topologies evolved into different forms during the course of this project, and these topological evolutions are presented. A final variation of the autotransformer topology, called the auto UDII topology, is presented in Chapter 8. This topology has the most potential for commercial viability.

Simulations and evaluations of the topologies are given along with comparisons to existing ballast topologies. Two different prototypes, one series capacitor type and one auto UDII type, were constructed and tested. Those results are presented in the

relevant chapters.

Chapter 9 summarizes the thesis, draws conclusions, and discusses possible future work.

Chapter 2

Fluorescent Lamps

Discharge lamps produce light by means of sustaining an electric arc through a gas, creating radiation of some sort. The specific details are different for each lamp type. Because of the arc-nature of the discharge lamps, they present unique problems to the circuit designer. This chapter describes the basic construction of the fluorescent lamp. The details of the discharge are presented which explain the physical processes involved in producing light. Also discussed is the efficacy of the fluorescent lamp, and the parameters which affect the efficacy. This background is necessary so that the requirements of the ballast circuit are fully understood.

2.1 Construction

The construction of a typical fluorescent lamp is shown in Figure 2-1. It consists of a long glass tube (typically one to one and a half inches in diameter) with electrodes at both ends. The electrodes are usually made of coiled coil tungsten wire coated with an electron emissive material. The negative end of the lamp is called the cathode, and the positive end is called the anode. A fluorescent powder, or phosphor, coats the inside of the tube. The tube is filled with an inert gas, such as argon, along with a small amount of mercury (a few milligrams) [9].

In operation, an electric field between the anode and the cathode causes electrons to be emitted from the hot cathode electrode, forming an arc through the gas. Some

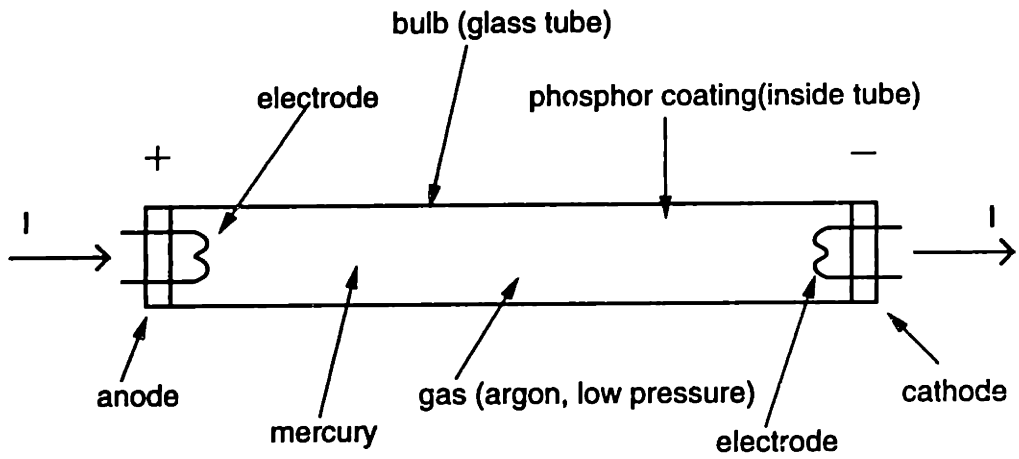

Figure 2-1: Fluorescent lamp

mercury atoms are ionized, while others emit ultra-violet (UV) radiation. This UV radiation excites the phosphors yielding visible light.

2.1.1 The Bulb

The fluorescent lamp bulb is usually a straight soda-lime silicate glass tube, but it may also be circular or U-shaped. There are many different types of fluorescent lamps ranging from half a foot to eight feet in length, and from half an inch to one and a half inches in diameter. The diameter of the bulb is specified in eights of an inch. For example, a T8 lamp is 1 inch in diameter, and a T12 lamp is 1.5 inches in diameter; the "T" stands for tubular. Perhaps the most common fluorescent lamp is the F40T12, or 40 watt T12 lamp, which is 4 feet in length. Also common is the F32T8 lamp, which is a 32 watt, 4 foot long lamp. The dimensions greatly affect the efficacy of the lamp. This is explained in Section 2.3.2. Phosphors, which convert the ultra-violet radiation into visible light, coat the inside of the tube.

2.1.2 The Electrodes

The purpose of the electrodes is to function as both anode and cathode, since virtually all lamps are operated on alternating current. The job of the cathode is perhaps the

most demanding because it is difficult, in general, to get electrons to leave a metal and enter a gas [10]. The function of the anode is simply to collect the electrons at the positive end of the tube. Coiled-coil or triple coiled tungsten wire, coated with an electron emissive material, is used for the electrodes. The electron emissive material is some form of alkaline earth oxide, such as carbonates of barium, strontium, or calcium [10]. Its job is to increase the electrode temperature to the point where electrons are emitted thermionically, without increasing the temperature to the point where the emitter material evaporates. The life of the lamp is directly related to the life of the electrodes, since whenever the electrode can no longer emit electrons, the lamp will cease to function. Sputtering damage during lamp starting and evaporation of the emitter material are the main causes of electrode failure [5].

2.1.3 The Gas

As was previously mentioned, light is produced by exciting mercury atoms to emit UV radiation. A certain amount of mercury is introduced into the tube which yields the proper vapor pressure at a desired operating temperature (eg. 10 mg Hg, vapor pressure $3\text{–}10\times10^{-3}$ torr). The pressure is important because if it is too low, there is an insufficient number of electron and mercury atom collisions. If it is too high, the mercury radiation begins to be re-absorbed instead of reaching the phosphors at the tube wall.

In addition to the mercury, an inert gas at a pressure of 1 to 3 torr [11] is also required in the tube for a variety of reasons. The main need for the inert gas is to control the electron mobility. With the electron path unimpeded, the electrons may strike the tube wall or the electrodes at high speeds while the chance of collisions with the mercury atoms is very small. The inert gas increases the number of electron collisions with mercury atoms while reducing losses at the tube wall. Of course, the electrons also collide with the inert gas atoms. These elastic collisions do not excite radiation, since the gas is inert, but they do represent a source of loss. For this reason, using heavier inert gases results in lower elastic collision losses and more efficient radiation. Out of the possible helium, neon, argon, krypton, and xenon, argon

is primarily used for performance and cost reasons because it gives the maximum reduction of wall losses with the minimum elastic collision losses [6]. Helium and neon are light and result in significant elastic collision losses, while krypton and xenon are relatively expensive. Again, gas pressure is important with the main tradeoff being increased wall losses at low pressure and increased elastic collision losses at high pressure. The inert gas also facilitates the starting of the discharge.

2.2 The Discharge

This section describes the physical process in the discharge and the mechanisms by which light is produced. First, the basics of the discharge are presented as a prelude to more detailed discussion. Second, a characterization of the low pressure discharge is given. Next, the negative resistance characteristic of discharges is explained. Finally, the details of the radiation and the phosphors are described.

2.2.1 Discharge Basics

As described briefly in the previous section, an electric discharge lamp, such as a fluorescent lamp, produces light by means of passing an electric current through a gas. The atoms of the gas are excited to produce radiation in a spectrum that is dependent upon the elements of the gas and the construction of the lamp. A simple illustration of a gas discharge is shown in Figure 2-2.

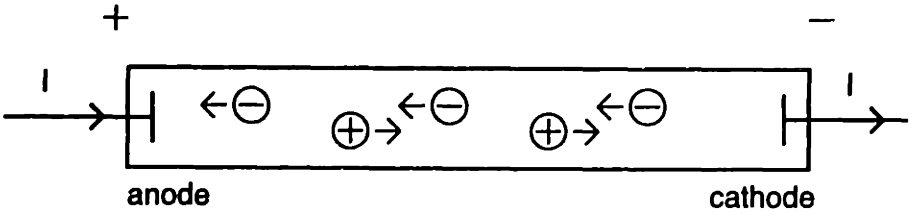

Figure 2-2: Gas discharge

Normally, a gas is an insulator and no electrical current can pass through it.

However, if the gas is ionized, producing free electrons and positive ions, a current can be supported. This flow of electricity through a gas is defined as a discharge. As shown in Figure 2-2, positive ions drift towards the cathode and electrons drift towards the anode under an applied electric field. The total current through the lamp is the sum of the ion and electron currents. Because the electrons are several thousand times lighter than the ions, most of the discharge current is from the flow of electrons. In fact, only 0.1 to 1% of the total current is carried by the ions [6].

Before the discharge is formed, the gas is essentially an insulator. Ignition is accomplished by doing two things. First, free electrons must be emitted into the gas from the cathode. By action of heating the cathode, which is coated with an electron emissive material, electrons may be emitted thermionically. Second, a high voltage must be applied across the lamp. This high voltage assists the cathode by generating electrons through field emission. More importantly, the electric field across the anode and cathode accelerates the electrons through the gas, generating more electrons through impact ionization. This process continues in a cumulative fashion, or avalanche, forming the discharge.

2.2.2 Low Pressure Discharges

Under certain conditions, the discharge can be classified as a low pressure discharge. Consider a discharge tube that is a few centimeters in diameter and roughly a meter in length. If it contains one or more gases at a total pressure of about 1/100 atm, and is operated on low currents (1 or 2 amps), then there is negligible heating of the gas. These are the conditions which define a low pressure discharge [6]. Fluorescent lamps are low pressure discharges, as opposed to HID lamps, which are high pressure discharges. The reason for having this distinction is that the radiation processes are different between high and low pressure discharges. This is briefly explained below.

Ignoring the area immediately surrounding each electrode, the large uniform region of the discharge between the electrodes is called the positive column. In this region, neutral gas atoms, mercury ions, and electrons are moving largely at random, although there is a general drift of charged particles due the the applied electric

field. Electrons gain kinetic energy from the accelerating electric field and lose energy through collisions with gas atoms. The electrons have energies corresponding to electron temperatures of 10,000 K to 20,000 K. The gas atoms, however, are much heavier than the electrons and reach temperatures of only 10°C to 30°C higher than the tube surroundings.

Because of this disparity in energies, the electrons behave like a separate gas at a higher temperature, with a Maxwellian distribution of energies; refer to Appendix A. At an electron temperature of 7737 K, the mean energy of the electrons is 1 eV [6]. Some electrons have energies great enough to produce excitation of radiation in the mercury atoms or even ionization of the mercury atoms.

With low pressure discharges, the radiation produced is in a discrete line spectrum. That is, there are resonant peaks where most of the radiation energy is concentrated. This type of radiation is called resonance radiation. In high pressure discharges, the resonant radiation is absorbed and the radiated energy occurs in a broad spectrum. This is explained in more detail later in Section 3.2.

2.2.3 Negative Resistance

Throughout the positive column, electrons and positive mercury ions exist in equal numbers. With no net space charge, the gas can be called a charge neutral plasma. Because of the applied electric field, the electrons and ions drift on average towards the anode and cathode, respectively. However, the electrons and ions also drift radially towards the tube wall, where they recombine into neutral atoms. Since the electrons are lighter and have higher diffusion rates than the ions, they diffuse faster than the ions. This leaves more ions in the plasma, causing a radial electric field which slows down the electrons and speeds up the ions. In the end, both ions and electrons diffuse at the same rate, preserving charge neutrality. This process is called ambipolar diffusion [5].

For the discharge to be in the steady state, the rate of generation and rate of loss of carriers must balance. That is, the ionization rate must equal the loss of electrons and ions by ambipolar diffusion. The electrical conductivity of the discharge

is proportional to the electron density (or plasma density) in the plasma. The plasma density increases with increasing discharge current. The result of this is that with greater and greater currents, the conductivity of the discharge increases, and less voltage is required to maintain the discharge. Thus, the discharge has a negative voltage to current relationship. Under voltage source operation, the discharge is not current limiting, and a series impedance is required to limit the current. This is the primary role of the ballast. A typical negative resistance characteristic is shown in Figure 2-3.

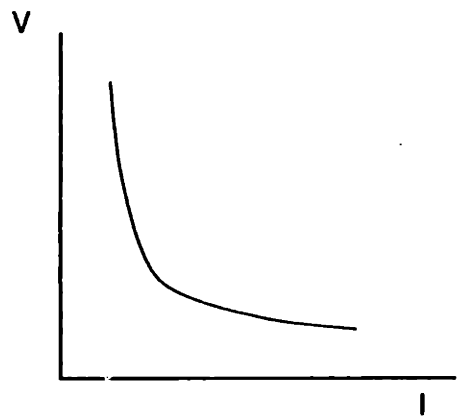

Figure 2-3: Negative resistance characteristic of the discharge

2.2.4 Radiation

When an electron collides with a neutral gas atom, several things can happen.

1. The electron can rebound with a small loss in kinetic energy. This is called an elastic collision.
2. An electron in the atom can be excited to a higher energy level.
3. An electron in the atom can be freed completely. This is called ionization.

The probabilities of each event depend on the energies of the colliding electrons. The ionization potential of mercury is 10.4 eV while argon is 15.7 eV. So in a common gas

mixture of argon and mercury, the mercury is preferentially ionized, not the argon. The electron collisions with the argon atoms are essentially elastic, causing a slight heating of the gas.

For purposes of radiation, the important event is the excitation of a mercury atom by a colliding electron. This process is illustrated in Figure 2-4. When an orbiting

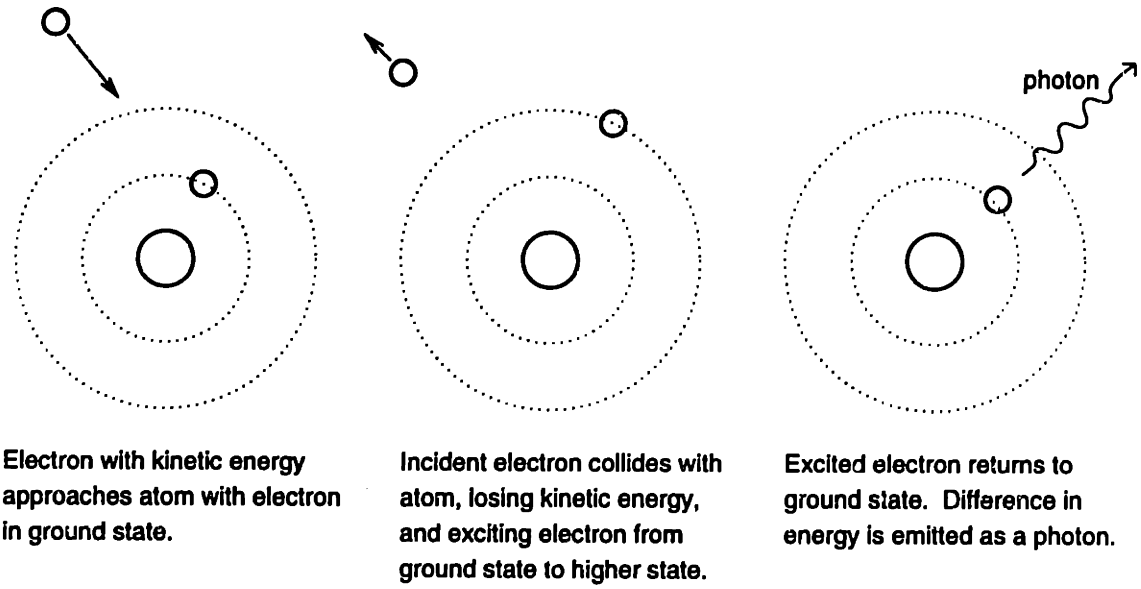

Figure 2-4: Excitation and radiation

electron in a gas atom absorbs the energy from a colliding electron, it is excited to a higher energy state. Eventually, the excited electron returns to its ground state with the difference in energy emitted as a photon.

In a low pressure discharge, the positive column radiates energy at characteristic frequencies, yielding a discrete line spectrum. With mercury vapor, many states are excited, but the lowest excited state is excited the most and produces what is called resonance radiation. At low pressure, this resonance radiation is usually very efficiently generated [10].

Figure 2-5 shows a simplified energy level diagram of the mercury atom. The radiation from the 4.89 eV state to the ground state is the main resonance radiation for a low pressure mercury discharge. Since the energy between the two levels is

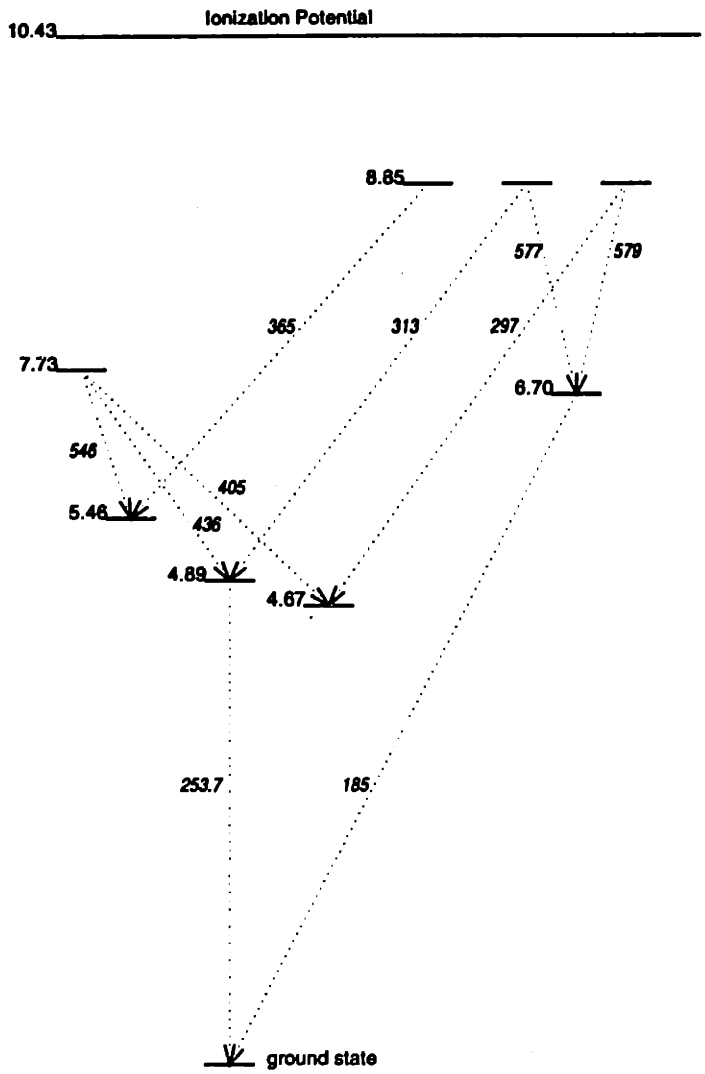

Figure 2-5: Simplified energy level diagram for mercury (energy in eV and radiated wavelength in nm)

known to be 4.89 eV, the wavelength of the radiation can be calculated as follows. The frequency of the radiation ν can be calculated from the Bohr frequency condition

$$\Delta E = h\nu \tag{2.1}$$

where ΔE is the energy difference in joules and h is Planck's constant ($6.63 \times 10^{-34}\ Js$). Also note that 1 eV is $1.602 \times 10^{-19}\ J$. The wavelength λ of the ra-

diation is given by

$$\lambda = \frac{c}{\nu} \tag{2.2}$$

where c is the speed of light ($3 \times 10^8\ m/s$). With an energy difference of 4.89 eV, the wavelength of the emitted radiation λ is 253.7 nm. This radiation is ultra-violet and is not in the visible spectrum (380 nm – 780 nm). Fluorescent lamps use phosphors to convert the 253.7 nm resonance radiation into radiation in the visible spectrum.

From Figure 2-5 one can see that there is also radiation from the 6.70 eV state at 185 nm. This is, of course, at a higher energy state than the 253.7 nm radiation, so the probability of exciting the 253.7 nm radiation is greater. But note also the two states immediately surrounding the 4.89 eV state at 5.46 eV and 4.67 eV. These two states are metastable states and cannot radiate to the ground state. Any electron that ends up in these states will sit there until another state change. The electrons in these states need only a small amount of energy to shift into the 4.89 eV state. This is another reason why the 253.7 nm resonance radiation dominates in mercury.

The efficiency of the radiation is limited by resonance radiation imprisonment, where the radiation is repeatedly re-absorbed and re-emitted until it reaches the tube wall. At higher pressures and gas temperatures, this effect is more pronounced, and the resonance radiation can be suppressed. The resonance radiation phenomenon is thus an important characteristic of low pressure discharges such as the fluorescent lamp.

2.2.5 Phosphors

The chemical phosphors that coat the inside of the tube convert the 253.7 nm ultra-violet radiation into visible light. The atoms in the phosphors absorb the UV radiation and emit radiation in the visible spectrum. The re-emitted radiation is always of a longer wavelength than the exciting radiation. Because the 253.7 nm radiation is very close to the visible spectrum, the conversion to the visible spectrum can be efficient.

Different phosphors are mixed to obtain the desired color of light. The main phosphor used in fluorescent lamps is calcium halo phosphate. Calcium halo phosphate is

excited by radiation wavelengths between 180 nm and 320 nm with a peak sensitivity around 250 nm. The emitted radiation has wavelengths between 350 nm and 750 nm with a peak around 580 nm. Calcium halo phosphate is ideal because it has peak sensitivity right near the 253.7 nm UV radiation, and it re-emits radiation throughout the visible spectrum [9]. The visible spectrum is shown in Figure 2-6. Note that the human eye has maximum sensitivity to wavelengths of 555 nm.

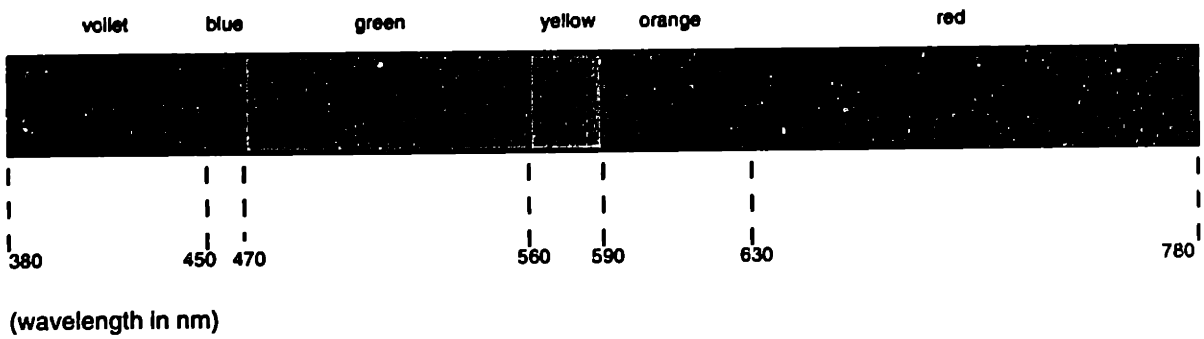

Figure 2-6: Visible spectrum

2.2.6 Summary

The fluorescent lamp generates light through two processes. The first process is the creation of 253.7 nm resonance radiation through excitation of the mercury vapor atoms in the tube. This resonance radiation is possible because of the low pressure discharge. The second process is the conversion of the 253.7 nm radiation to visible light by the coating of chemical phosphors on the inside of the tube wall. Because of the nature of the discharge, the lamp has a negative resistance characteristic and requires a current limiting impedance, or ballast, in operation.

2.3 Efficacy of the Fluorescent Lamp

This section describes the sources of loss in the fluorescent lamp. The efficacy as a function of lamp parameters is presented. High frequency operation of fluorescent

lamps is also discussed.

2.3.1 Loss in Fluorescent Lamps

The fluorescent lamp is an excellent source of artificial light due to its relative superiority in efficacy over incandescent filament lamps. Figure 2-7 shows the sources of loss in the common F40T12 fluorescent lamp. Of the total power delivered to the lamp, 15% is lost at the electrodes while the remaining 85% is dissipated in the positive column. The energy lost in the electrodes is due to the non-zero voltage drops at the anode and cathode. A certain amount of power must also be dissipated in the

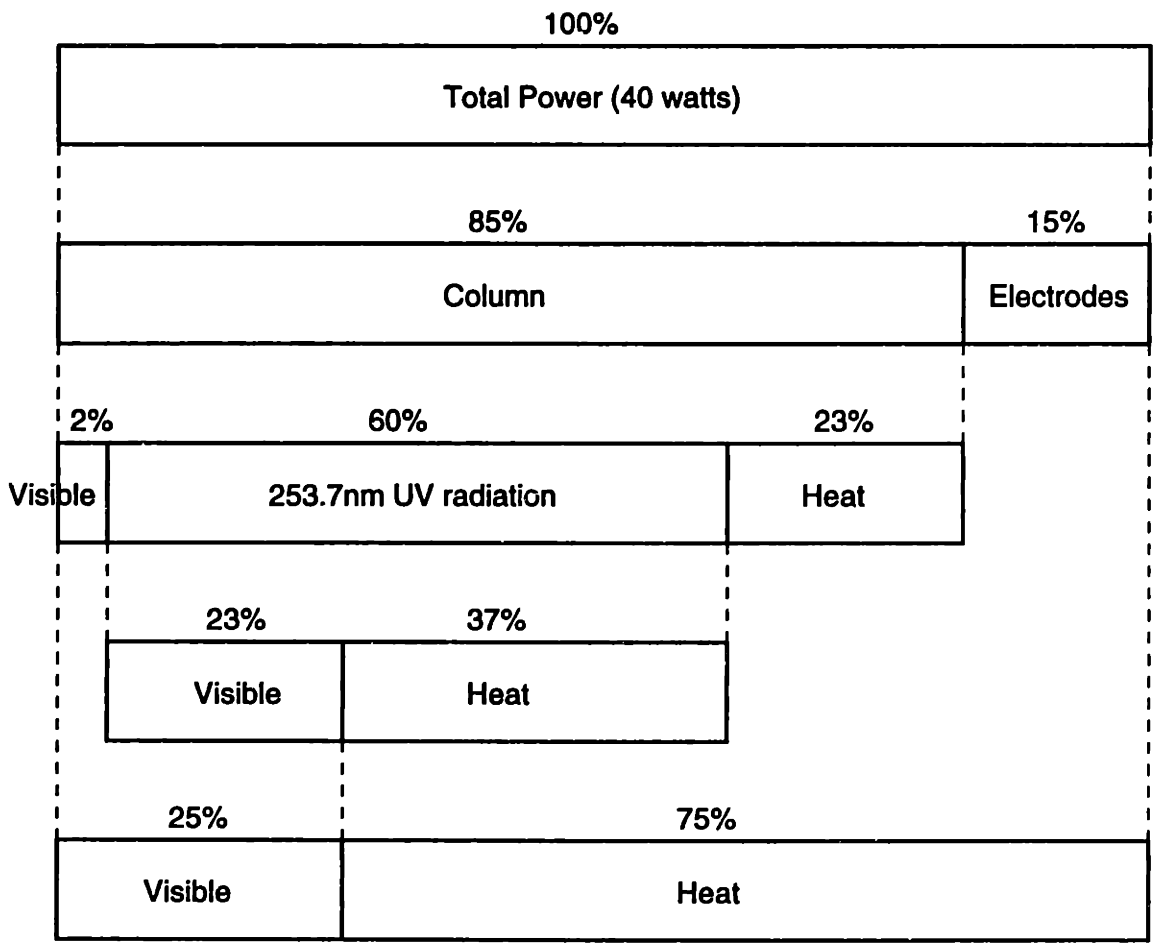

Figure 2-7: Power balance of F40T12 fluorescent lamp

electrodes as heat to assist in the thermionic emission process.

Within the positive column there are still significant sources of loss. Of the 85% power in the positive column, 2% is converted directly into visible light. This is from certain state transitions in mercury that generate radiation in the visible spectrum from 400 nm to 580 nm (see Figure 2-5). About 23% is lost as heat in the positive column. This loss comes mostly from heating of the inert gas through elastic collisions with electrons. The remaining 60% produces the desired resonance radiation at 253.7 nm.

To this point, 60% of the total power delivered to the lamp has resulted in the generation of 253.7 nm radiation. Now it is the job of the phosphors to convert the 253.7 nm radiation into visible light. The conversion of this UV radiation to visible wavelengths can only be done at a maximum theoretical efficiency of around 45% [10, 11]. This number is known as the average energy factor or quantum ratio, and is given by the ratio of the exciting wavelength to emitted wavelength. In this case, the ratio can be approximated as $\lambda_{253.7}/\lambda_{555}$ (which equals 0.46) where the 555 nm radiation represents the maximum light sensitivity to the human eye. The phosphors radiate energy in a broad spectrum, so the actual conversion efficiency is something less than the simple ratio (about 0.45). The phosphors themselves will have a conversion efficiency of around 85% due to phosphor imperfections, coating absorption, and bulb absorption. The net result of all these factors is that of the 60% power that produced 253.7 nm radiation, 23% produces visible light and the remaining 37% is lost as heat [10, 5, 9, 11, 12].

The final result is that a total of 25% of the power delivered to the lamp is converted into visible light. The other 75% is dissipated as heat through the various loss processes discussed previously. About 40% of the heat is radiated and 60% is dissipated by convection to ambient and conduction through fixture parts. The F40T12 40 watt fluorescent lamp has an efficacy of around 85 lm/watt when operated at 60 Hz.

Figure 2-8 shows a similar power balance for the F32T8 32 watt lamp. This lamp was designed specifically for high frequency operation (above 25 kHz). The efficacy

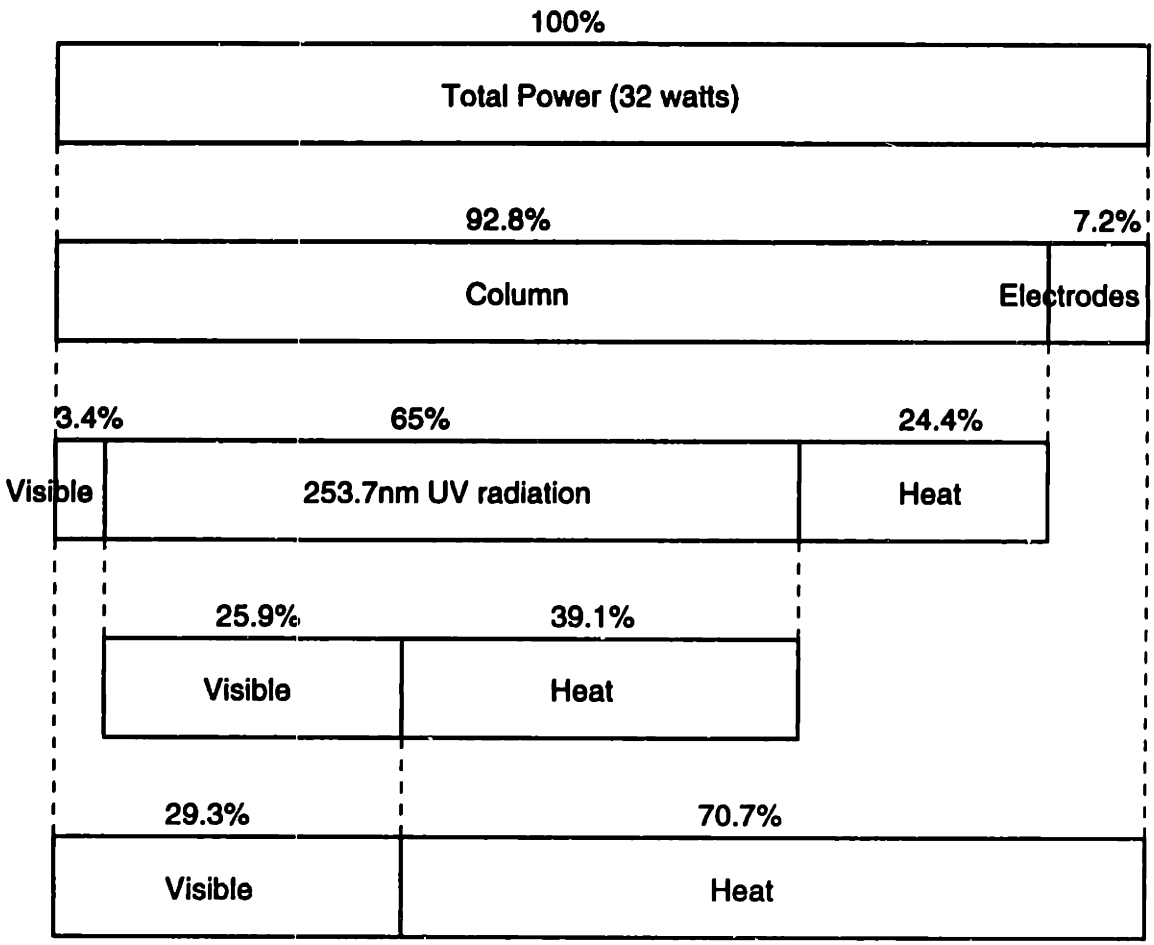

Figure 2-8: Power balance of F32T8 fluorescent lamp

of the lamp is around 100 lm/watt.

2.3.2 Efficacy as a Function of Parameters

Mercury Vapor Pressure

The efficacy of the lamp varies with vapor pressure. In fact, there is an optimum pressure above or below which the efficacy falls. If the pressure is too low, the probability of electron–mercury collisions is too small. If the pressure is too high, the discharge will begin to re-absorb the resonance radiation. That is, the frequency of collisions

is so high that a radiated photon will have difficulty reaching the phosphors without being re-absorbed and re-emitted. The optimum mercury vapor pressure for common fluorescent lamps is generally around $3\text{–}10\times10^{-3}$ torr at 40°C wall temperature [10, 6].

Tube Dimensions

There is an optimum tube diameter for a given current. As the diameter is decreased, the current density increases. The efficiency of resonance radiation decreases with increasing current density due to cumulative excitation (more energy goes into ionizing mercury rather than exciting UV radiation). As the diameter is increased, the distance the 253.7 nm radiation must travel to reach the phosphors increases. Therefore, the likelihood of the photon being re-absorbed is greater and the efficacy of the lamp once again decreases.

As the length of the tube increases, the lamp becomes more efficacious. The voltage drops at the anode and cathode are independent of the tube length. As the tube length is increased, the losses at the electrodes become a smaller fraction of the total power. The combined anode and cathode potentials are on the order of seven to fifteen volts for common lamps. An arc length of four feet is common so that the efficacy of the lamp does not suffer excessively from the electrode losses.

Current

It was already mentioned that the efficiency of the resonance radiation decreases with increasing current due to ionization losses. There are also secondary effects such as the increased temperature and vapor pressure associated with the increased current density. Because the lamp efficacy decreases with increasing current, this suggests that the form of the current will affect the efficacy of the lamp. The highest efficiency of resonance radiation is obtained with a dc current drive. Sinusoidal or peaky waveforms are less efficient because for a given operating power, the current will have periods of high ionization losses during the portions of the ac cycle where the current density is high. A dc current drive has the advantage that the lamp

is operating at the optimum current all the time. The efficiency of the resonance radiation is 5 to 10% higher with a dc drive than with a 60 Hz sinusoidal drive [5].

In practice, dc operation is not used since a resistor must be used for the ballast impedance. This resistor tends to dissipate as much power as the lamp itself. Also, under dc operation, the mercury ions tend to migrate on average towards the cathode. The anode end then produces less light than the rest of the tube due to the local shortage of mercury atoms. For this reason, periodic polarity reversal of the lamp is desired. A square wave of current would achieve the polarity reversal while retaining the efficacy of a dc drive.

2.3.3 High Frequency Operation

Lamp operation at high frequencies yields significant improvements in efficacy for a number of reasons. The electron density decay time constant is around 0.5 ms [5] which is an appreciable fraction of a 60 Hz cycle. When lamps are operated on 60 Hz sinusoidal waveforms, the lamp can actually extinguish at the zero crossings, requiring reignition each half cycle. With higher frequencies, the decay time becomes less of a factor, and the lamp can make a transition through zero voltage or current without any significant decay of charge in the tube [13, 7].

Lamps operated at 60 Hz also suffer from a visible 120 Hz luminous ripple or flicker. Besides the inefficiency in light output, the flicker can create stroboscopic effects with machinery and other problems such as nausea and visual fatigue [14, 7, 15, 16]. With higher frequencies, the lamp flicker becomes negligible. Another factor involved is the afterglow of the phosphors. All these factors contribute to the increased efficacy of fluorescent lamps at high frequency operation [10].

The main improvement at high frequencies, however, is the reduction in anode fall voltage. The cathode has a certain zero-field thermionic emission. For current densities above this, accelerating fields must be present, which require the presence of positive ions and a positive cathode fall. Because of these fields, there is a region of high density plasma surrounding the cathode due to the increased ion concentration. At frequencies above a few kilohertz or so, the plasma density does not decay during

the half period that the polarity of the lamp is reversed. The anode then is immersed in a high density of carriers and can collect current at lower potentials. Thus, the efficacy of the lamp is improved by this reduction in the anode potential [5, 10, 17, 18, 19].

In practice, lamps are operated at frequencies above 20 kHz so that any noise generated is above the range of human hearing. The potential for improvement in efficacy with a high frequency drive depends on the type of lamp. For longer lamps, the improvement is small because the electrode losses are already a small fraction of the total losses. In typical lamps, the anode fall is around one to ten volts, while the cathode fall is five to fifteen volts. Efficacy improvements at high frequencies of 5% to 10% are typical in common lamps [14, 20, 21, 22, 1]. For example, the F40T12 lamp exhibits a 9% gain in efficacy over 60 Hz sinusoidal operation when operated at frequencies above 20 kHz. Similarly, the F32T8 lamp shows an efficacy increase of about 5.5% [23, 24].

Chapter 3

High Intensity Discharge Lamps

The previous chapter described the fluorescent lamp, which is one type of discharge lamp. Its defining characteristic is a discharge that is operated at low pressure. This chapter describes the other major type of discharge lamp called the high intensity discharge lamp or HID lamp. HID lamps, like fluorescents, produce light by sustaining an electric arc through a gas. But unlike fluorescents, which are low pressure discharges, the HID lamps operate on a high pressure discharge. This chapter discusses the various HID lamp types and their construction, as well as the features of the high pressure discharge.

3.1 HID Lamp Types and Construction

HID lamps generally have much smaller arc tubes than fluorescent lamps. While a typical fluorescent lamp will have an arc tube four feet long, HID arc tubes are usually less than several inches long. These short arc tubes operate a discharge at high temperature and pressure with high power densities. The high pressure discharge has different radiation properties than a low pressure discharge. In addition, the high operating pressures and temperatures allow different elements and gases to be used with the arc, also creating different radiating spectra. HID lamps generally have long life and good efficacy, and are compact like incandescents. Most high intensity discharge lamps operate at high power and light intensity, which makes them suitable

for outdoor use more so than indoor use in general. A disadvantage of HID lamps is that once the arc is extinguished, the lamp must cool for 5 to 15 minutes before it can be reignited. There are several different types of HID lamps, including the mercury vapor, metal halide, and high pressure sodium lamps. The features and construction of these lamp types are explained in the following sections.

3.1.1 High Pressure Mercury Vapor Lamps

The construction of a mercury vapor lamp is shown in Figure 3-1. It consists of an inner and outer envelope. The inner envelope is the arc tube, which is made of quartz or fused silica, and contains the actual discharge. Fused silica can withstand temperatures of up to 800°C. The operating temperatures of mercury vapor lamps are usually within the range of 600°C to 750°C. The arc tube is filled with mercury and argon, where the argon is used primarily for starting the discharge. Operating pressures of the gas are 2–10 atm. The outer envelope is an elliptical bulb made of hard borosilicate glass (lamps with wattages less than 125 watts may use soda lime glass) and exists mainly to provide a protective environment for the arc tube. In addition to protecting the arc tube from drafts and ambient conditions, the outer bulb contains an inert gas such as nitrogen to protect internal parts from oxidation. Phosphors may also be used, in which case the outer bulb provides the surface for the phosphor coating.

The mercury vapor lamp produces light by passing an electric discharge through mercury vapor in the arc tube. Under high pressure operation, the mercury radiates in a broader spectrum of wavelengths than for low pressure operation, some of which are of visible wavelengths. This is in contrast to a low pressure mercury discharge (fluorescent) where resonance radiation occurs in an ultra-violet wavelength of 253.7 nm. There are five principle visible radiation wavelengths in mercury, 405 nm, 436 nm, 547 nm, 577 nm, and 579 nm; refer to Figure 2-5. These produce yellow, green, violet, and blue colors with a strong absence of red. Phosphors, such as vanadate phosphor, can be used to convert the ultra-violet radiation into the orange-red spectrum to improve the color of the light output. Without the color correction, red

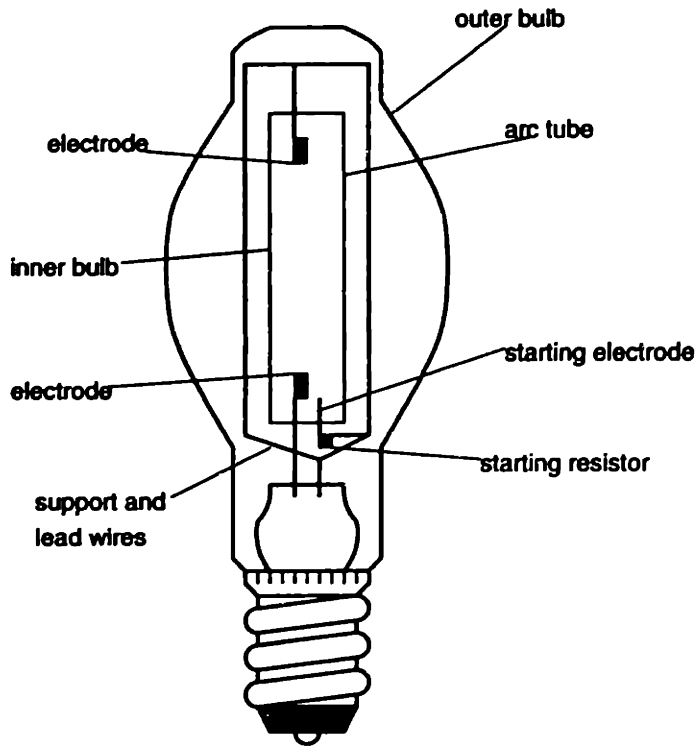

Figure 3-1: High pressure mercury vapor lamp

objects appear black or dark brown.

The electrodes are made from tungsten with an electron emissive material and are heated during operation by bombardment from the arc current. A starting electrode with a starting resistor is used to initiate the arc during ignition. The starting electrode is made of molybdenum or tungsten and is placed in close proximity to the main electrode but at the opposite polarity of voltage. The starting resistor is usually between 10 kΩ and 20 kΩ and is used to limit current during starting. The life of the lamp ends with the loss of emission material from the electrodes. Lamp lifetimes are on the order of 24,000 hours [4].

Commercial mercury vapor lamps vary in wattage from 40 to 2000 watts. Higher power lamps yield higher efficacies. For example, a 50 W mercury lamp yields efficacies around 40 lm/W, while a 1000 W mercury lamp yields efficacies around 60 lm/W [6]. These lamps generally achieve efficacies of only 30 to 65 lm/W [11, 4, 1]. Because

lamp operation is not affected by ambient conditions, the mercury vapor lamp is used in outdoor and industrial plant type applications. Mercury lamps have a negative resistance characteristic and require a ballast for starting and current limiting during operation.

3.1.2 Metal Halide Lamps

Metal halide lamps are very similar to high pressure mercury lamps. The construction of a metal halide lamp is shown in Figure 3-2. The main difference is the addition of metal halides to the arc tube which alter the radiating properties of the discharge. Like the mercury vapor lamp, the inner arc tube is made of quartz or fused silica and is filled with some mercury and a rare gas such as argon for starting, along with one or more metal halides. The outer bulb is made of hard glass.

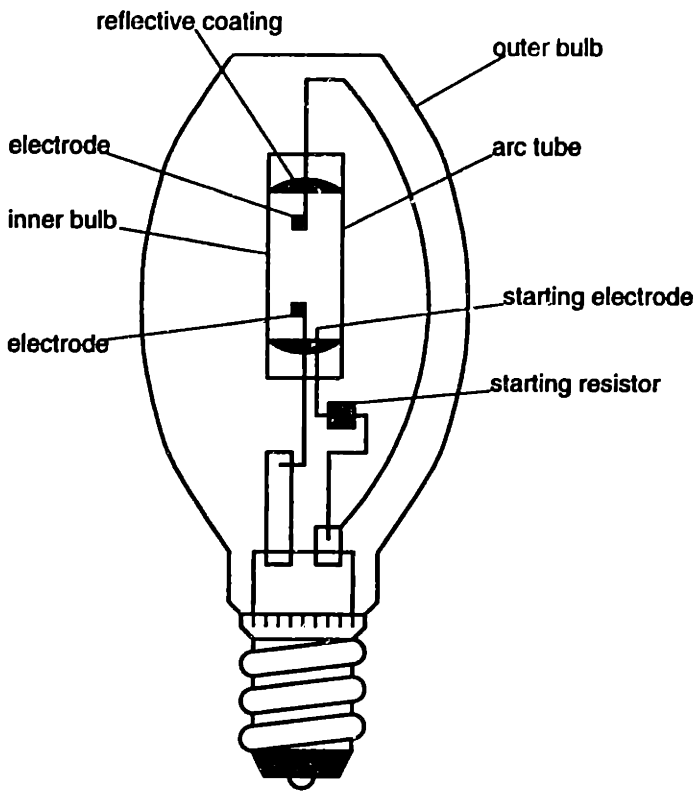

Figure 3-2: Metal halide lamp

There are two main electrodes made from thorium-tungsten. These electrodes must be designed to withstand chemical reaction with the metal halides. A heat-reflecting surface, such as zirconium dioxide, applied to the surrounding area of the electrodes prevents the condensation of the metal halides away from the arc. A starting electrode and resistor, similar to those used in the mercury lamp, are used for initiating the discharge.

Metal halides are combinations or molecules of metals and halogens. Typical metals used include sodium, thalium, indium, scandium, and dysprosium. The halogens include fluorine, chlorine, bromine, and iodine, but iodine is usually used since the others tend to react with the tube parts. Some metals in metallic form cannot be vaporized at temperatures that the arc tube can withstand. However, these problems can be overcome by using the metals in the form of a metal halide. The halides are vaporized at operating temperatures, and they do not react with the arc tube [11, 6, 5].

The halide cycle is the primary phenomenon that characterizes metal halide lamps. When the arc is ignited, the mercury in the arc tube is vaporized, while the metal halides are in solid form on the tube wall. As the arc tube wall temperature increases, the metal halides are vaporized and travel to the center of the tube by diffusion and convection. In the center of the arc, the temperature is high enough to cause the dissociation of the metal halide into metal and halogen atom . The metals are then excited by bombarding electrons to produce their characteristic radiation spectrum. The metals and halogens recombine at the cooler arc tube wall, completing the halide cycle [6].

The metals are introduced to improve the color and efficacy of the lamp. The halide form of the metals must be used to achieve vaporization and dissociation at operating temperatures that the arc tube can support. There are three typical halides used.

1. Sodium, thallium, indium iodides.

2. Sodium, scandium iodides.

3. Dysprosium, thallium iodides.

The metals sodium, thallium, and indium radiate line spectra of 589 nm, 535 nm, and 435 nm respectively. Multi-line spectra are radiated by scandium and dysprosium [11]. Good color is achieved by using combinations of metal halides which emit line spectra and halides which emit multi-line spectra.

The metal halide HID lamps have good color and excellent efficacies [25]. Typical efficacies range from 75 to 125 lm/W [11, 4, 1]. Lifetimes range from 6,000 to 10,000 hours [4]. Because of the warmer color, the metal halide lamps are suitable for indoor use in addition to outdoor applications such as flood lighting, sports lighting, and street lighting. Recently, low wattage lamps have been developed which are well-suited for consumer use. A 70 watt metal halide lamp has an efficacy around 100 lm/W, using an arc tube 1.3 cm in length and 0.7 cm in diameter. A 30 watt metal halide lamp has an efficacy of 85 lm/W, using an arc tube 0.6 cm long and 0.6 cm in diameter [26]. All metal halide lamps have a negative impedance characteristic and require a ballast for starting and current limiting during steady state operation.

3.1.3 High Pressure Sodium Lamps

High pressure sodium lamps generate light by passing an electric arc through sodium vapor. This necessitates different lamp design than the previous mercury vapor and metal halide HID lamps. A sodium lamp is shown in Figure 3-3. Again there are two envelopes, an inner arc tube and an outer bulb. The inner arc tube is made from a ceramic called translucent polycrystalline alumina, or PCA, which is resistant to chemical reaction from sodium. Furthermore, it has a high melting point and has good transmission of light. The PCA allows operation at the higher temperatures and pressures necessary for the sodium vapor discharge. The outer envelope is made of borosilicate glass. The volume of the outer envelope is generally a vacuum or inert argon gas, and functions to isolate the arc tube from the ambient conditions.

The arc tube contains mercury, xenon, and sodium. The mercury and xenon gases

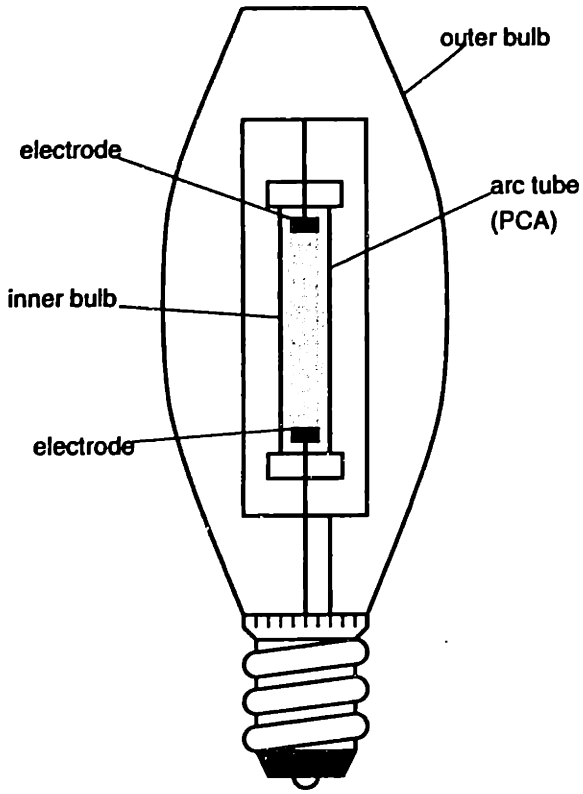

Figure 3-3: High pressure sodium lamp

function as a buffer gas, and raise the operating arc voltage and pressure. At low pressure, sodium exhibits two resonance radiation lines at 589.0 nm and 589.6 nm. By increasing the pressure to about 200 torr, these radiation lines become self-absorbed, and the radiation spectrum broadens. The emitted spectrum is largely golden-white in color.

The electrodes are tungsten with an electron emissive coating of barium and calcium oxides. The metal end cap seal makes the manufacture of a starting probe difficult [5]. The end cap seal is required because the PCA is difficult to work with and cannot be sealed conventionally. Since there is no starting electrode, the lamp is ignited by a high voltage, high frequency pulse from an electronic ignitor.

High pressure sodium lamps have efficacies of around 80 to 140 lm/W [1]. A typical 400 W lamp has an arc tube that is 3.75 inches long and 3/8 of an inch in diameter. They have long lifetimes of around 24,000 hours. High pressure sodium

lamps are used mainly in street lighting and general outdoor lighting.

3.2 High Pressure Discharges

Section 2.2.2 described the principal radiation mechanisms in low pressure discharges. The majority of the radiation produced is from resonance radiation, where atoms are excited by colliding electrons and the emitted radiation occurs when exited valence electrons return to the ground state. When the pressure of the gas in a discharge tube is increased to a few atmospheres, the radiation spectrum changes and the discharge is then known as a high pressure discharge. This section describes the various characteristics of the high pressure discharge.

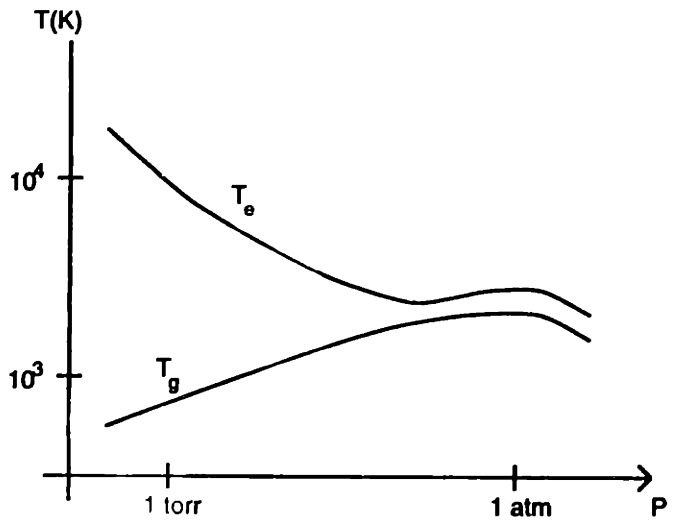

Figure 3-4: Electron temperature and gas temperature with increasing pressure

In a low pressure discharge, the electron temperature is much higher than the gas temperature. As the pressure is increased, there is an increasing number and probability of collisions between particles in the tube. The electrons lose more and more energy to the gas atoms, while the atoms in turn, gain more energy. This process continues with increasing pressure until a point is reached where the electron temperature and the gas temperature are nearly identical. Figure 3-4 illustrates this.

Because the average flow of energy is from the electrons to the gas atoms, the electron temperature is always higher than the gas temperature.

With the gas temperature increasing, there are an increasing number and variety of collision processes within the arc tube that affect the radiation spectrum of the discharge. The general effect of the increasing pressure is that the resonance radiation becomes self-absorbed or imprisoned, and any discrete spectral lines tend to broaden. At higher pressures still, spectral lines can broaden and merge, forming a continuous radiated spectrum. Discharge lamps can take advantage of this radiation broadening by radiating energy directly into the visible spectrum, eliminating the need for an intermediate conversion step of UV radiation to visible radiation.

The self-absorption of strong spectral lines is due primarily to repeated absorption and re-emission of the resonance radiation. The broadening of the emitted spectrum is due to many different collision processes. Collisions between an emitting atom and a neutral buffer gas atom can broaden the radiation and shift the line spectrum. Broadening and shifting of line spectra can occur from electric field interactions in collisions between emitting atoms and charged particles. Collisions between excited and ground state atoms of the same type also cause radiation broadening [6]. Along with broadening lines merging to form a continuous spectrum, recombining positive ions and electrons also cause the emission of a continuous spectrum [27]. All these processes are difficult to quantify, but in general there are random perturbations in energy levels resulting from collisions between radiating or excited atoms with other atoms or electrons. With increased variation in energy levels, the emitted spectrum also varies, resulting in broadening of the spectrum.

3.3 Lamp Efficacy

Less is known about quantifying the exact loss processes in HID lamps than in fluorescent lamps [5]. High pressure mercury lamps emit around 80% of the total power as radiation, where only 16% to 23% is emitted in the visible spectrum. This yields mediocre efficacies around 60 lm/W. High pressure sodium lamps radiate around 40%

of the total power in a band surrounding the 589 nm resonance lines, and therefore achieve high efficacies around 120 lm/W. Metal halide lamps radiate as much as 50% of the energy across the entire visible spectrum yielding efficacies around 100 lm/W [5].

The efficiency of HID lamps increases with increasing current density, due to the increased loading on the arc tube. In fact, the load (watts per unit length of arc tube) is the primary factor in determining the lamp efficacy [27]. Of the loss mechanisms in the lamp, which include convection, diffusion, and conduction, the conduction losses dominate. Conduction losses are roughly independent of lamp parameters, and thus can be considered to be constant [27]. With increasing power, these losses become a smaller fraction of the total and the lamp efficacy increases. At higher loading, more of the critical material is vaporized in the discharge, again yielding increased efficacy. In general, the high wattage HID lamps have higher efficacies [6, 27], because the higher arc loading and pressure results in higher light intensity [1].

As in the case of fluorescent lamps, it is desirable to operate HID lamps at high frequencies due to the reduction in size and weight of the ballast and due to the increased efficacy of the lamp itself [28]. However, the gains in efficacy at high frequency operation are not as dramatic as those in fluorescent lamps [29, 30]. More importantly, high frequency operation can excite acoustic resonances in the arc tube which can cause many problems.

3.4 Acoustic Resonance

Acoustic resonances are caused by the periodic input power giving rise to pressure perturbations within the arc tube [2, 31, 32]. If a resonant frequency is approached, a standing pressure wave mode can propagate. These pressure waves perturb the discharge path and lead to arc instabilities — the arc may move rapidly, the light output may fluctuate, the lamp voltage may increase rapidly which can lead to extinction of the arc. In the worst case, the arc may touch the tube wall causing a temperature rise which can damage or break the arc tube [6, 28, 2].

The resonant frequencies of the arc tube are a function of the gas mixture, tube dimensions, and even the electrode structure, and exist in frequency bands from as low as 500 Hz to as high as 100 kHz [2]. Several techniques are used in practice to achieve high frequency operation without exciting the acoustic resonances. It is possible to operate the lamp in a range of frequencies free of arc resonances, but these bands are usually too narrow to insure reliable operation. Furthermore, the resonant frequencies can change during the lifetime of the lamp [32, 31]. There are typically larger resonance free bands below 10 kHz, but operation there is not desirable due to noise being generated within the range of human hearing. It is possible, but not often practical, to operate the lamps at very high frequencies. Very high frequency operation (above 100 kHz or 200 kHz) can lead to significant losses in the ballast as well as radiated electromagnetic noise. It is possible to modulate the operating frequency to avoid acoustic resonances, because the arc movements due to resonances are slow and cannot be excited when the driving frequency of the lamp is changed rapidly. It is even possible to detect the onset of a resonance and then shift the operating frequency to either side of the resonating frequency [31, 30, 33, 34].

Acoustic resonances are a very troublesome problem. Troubling enough that in practice, high frequency ac operation is often avoided all together. Because the resonances are excited by ac power input fluctuations, a dc or square wave drive is very effective in avoiding resonances [31, 35, 32, 36]. As in fluorescents, dc is not practical because of the need for a resistive ballast and the need to reverse the polarity of the lamp. Square wave operation is often considered to be the ideal drive for HID lamps.

Chapter 4

Ballasts

This chapter introduces lamp ballasts. The introductory sections discuss the general requirements of the ballast and the basic types of ballasts. A brief background of lamp waveforms is presented as background for the more specific discussion of ballast impedances. Finally the two main types of ballasts, electromagnetic and electronic, are discussed in depth. A brief status of the economic market for electronic ballasts is also given.

4.1 Introduction to Ballasts

4.1.1 Requirements of the Ballast

The primary role of the ballast is to limit the lamp current to a desired operating value. If no current limiting were available, the lamp current would increase without bound under voltage source operation due to the negative resistance characteristic of the discharge. As the lamp current increases, the current density in the lamp increases causing more gas atoms to be ionized. This increased ionization rate increases the plasma density in the discharge, resulting in an increased electrical conductivity of the lamp. In order to maintain a steady state value of current, the electric field across the lamp must decrease. Under voltage source operation, the current will not be limited and the lamp will become an electrical short circuit. Therefore, the ballast

must provide a current limiting impedance in series with the lamp.

In addition to current limiting, the ballasts must also provide for ignition of the lamp. Before the arc is established, the lamp is essentially an open circuit. The ballast must be able to generate a sufficient voltage across the lamp to ionize the gas and ignite the arc. Depending upon the procedures used in starting the lamp, the ballast may also have to provide voltage to heat the electrodes to thermionic emission temperatures. These starting procedures are explained in more detail in the following sections.

It was stated earlier that the electron density decay time constant in the plasma is about half a millisecond, which is a significant fraction of a 60 Hz cycle. Under 60 Hz operation, the lamp can actually extinguish each time the utility approaches zero because the plasma density can decay significantly. The ballast must provide suitable operating conditions such that the lamp is re-ignited every half cycle.

The ballast must of course operate the lamp at the desired operating conditions. Frequently, typical lamps have operating voltages around 100 Vrms. Depending upon the voltage of the utility, the ballast may have to provide for voltage step-up or step-down via transformer or autotransformer. When transformers are used, the ballast current limiting impedance is usually incorporated into the transformer itself. The ballast should also provide some degree of regulation of lamp power with changes in the utility.

Besides these general requirements of the ballast, the ballast should interface the lamp to the utility without adverse effects. For instance, the ballast should draw power from the utility with a high power factor and without generating significant line harmonic distortion or electrical interference. Power factor is defined as

$$PF = \frac{Real\ Power}{Apparent\ Power} \tag{4.1}$$

where the real power is given by

$$Real\ Power = \frac{1}{T}\int_0^T v(t)\, i(t)\, dt \tag{4.2}$$

and the apparent power is

$$Apparent\ Power = v_{rms}\, i_{rms} \tag{4.3}$$

With a low power factor, the utility must handle higher circulating currents which requires heavier transmission and distribution cables and generation equipment [37]. Electrical noise in the form of radio frequency interference (RFI) and electromagnetic interference (EMI) can disturb the operation of other surrounding equipment. The ballast may also be required to limit in-rush currents, since many ballast units drawing large instantaneous currents can trip circuit breakers.

4.1.2 Lamp Voltage and Current

Figure 4-1 shows a typical discharge lamp voltage constructed from the static v-i curve with a sinusoidal input current. During ac operation at 60 Hz, however, the waveforms do not follow the static curve precisely because the ionization conditions in the lamp cannot follow the changes in current. Figure 4-2 shows the actual lamp waveform at 60 Hz with sinusoidal input current versus the voltage waveform derived from the static characteristic. Notice that the lamp voltage lies above the static value during the first part of the cycle where the current is increasing. Conversely, the lamp voltage lies below the static value when the current is decreasing. This can be explained qualitatively as follows. In the steady state, the rate of production of ion-electron pairs by ionization must equal the rate of loss of ion-electron pairs by ambipolar diffusion. This can be expressed as

$$\nu_i = \left(\frac{2.4}{R}\right)^2 D_a \tag{4.4}$$

where ν_i is the ionization frequency, D_a is the ambipolar diffusion constant, and R is the radius of the discharge tube; refer to Appendix B. Under 60 Hz ac operation, the ionization frequency is higher at the beginning of a half cycle when the current

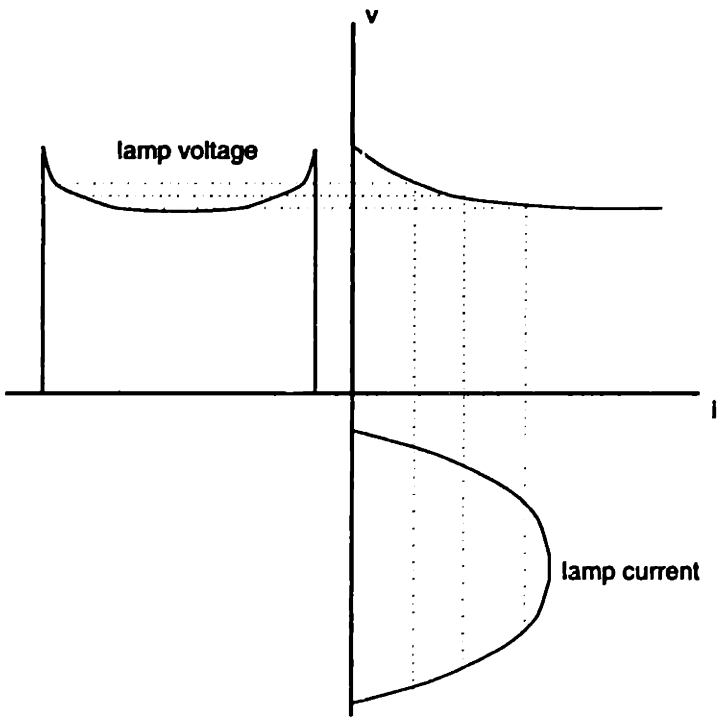

Figure 4-1: Lamp voltage and current constructed from static v-i curve

and electron density are increasing. So equation 4.4 must be modified to

$$\nu_i = \left(\frac{2.4}{R}\right)^2 D_a + \frac{1}{n_e}\frac{dn_e}{dt} \tag{4.5}$$

where the added term represents the rate of change of electron density n_e.

Looking at the static v-i curve in Figure 4-3, notice that the region above the static line represents increasing electron density. The region below the static line represents decreasing electron density. The static curve itself represents the steady state condition where the electron density is constant.

It can be inferred that when the ionization frequency is greater than the loss rate during periods of increasing current, $\frac{dn_e}{dt}$ must be greater than zero and the lamp voltage must then lie above the static value. Similarly, when the lamp current is decreasing, the ionization frequency must be less than the loss rate. Then $\frac{dn_e}{dt}$ is less than zero and the lamp voltage must lie below the static value. This explains the

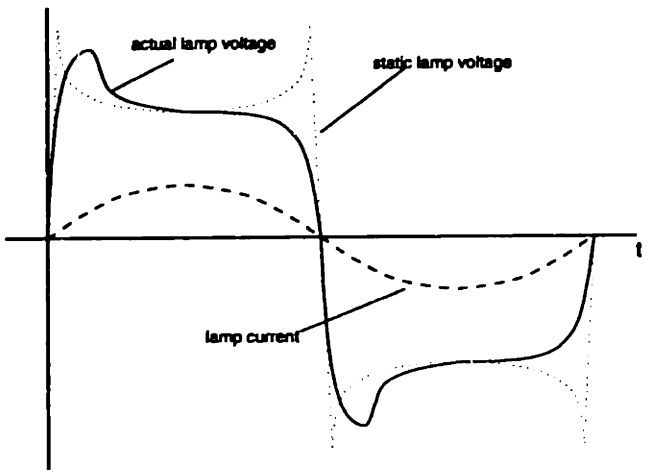

Figure 4-2: Actual lamp voltage versus time

waveforms shown in Figure 4-2.

At higher frequencies, on the order of several kilohertz, the electron density does not vary significantly during each complete ac cycle. Since the electron density is roughly constant, the conductivity of the discharge remains constant and the lamp behaves dynamically like a resistor. Under these conditions, both the lamp voltage and current are approximately sinusoidal.

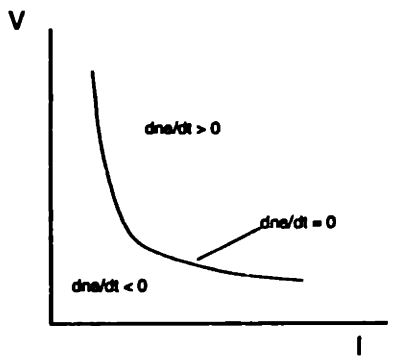

Figure 4-3: Static v-i curve showing regions of changing electron density

4.1.3 Ballast Impedances

Resistor

Perhaps the simplest stabilizing impedance is a resistor in series with the lamp. The resistor ballast regulates the lamp current by creating a voltage drop that is proportional to the current. Some 60 Hz waveforms are shown in Figure 4-4 of a lamp

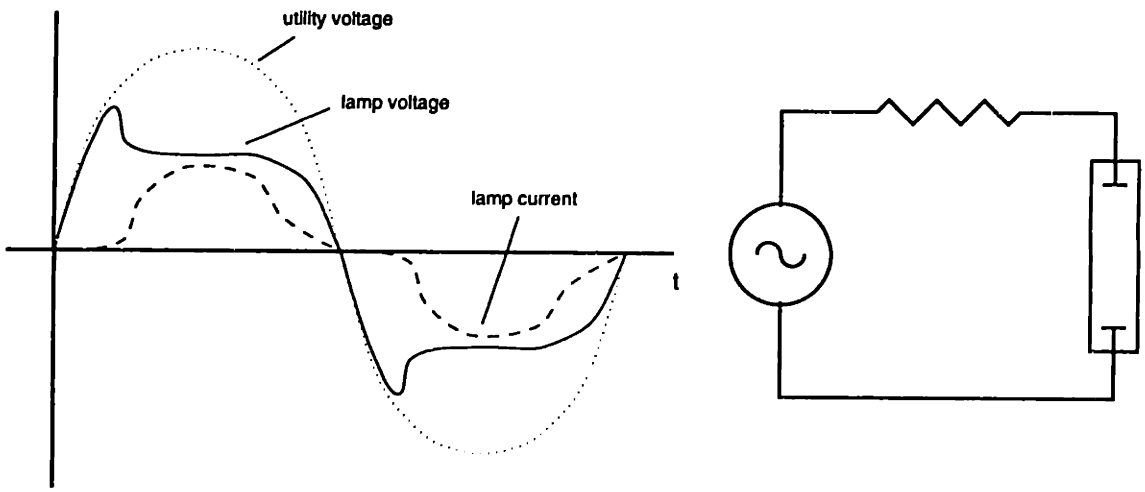

Figure 4-4: 60 Hz lamp waveforms for a resistive ballast

operated with a resistor ballast. Notice that when the utility is crossing zero, the lamp extinguishes and no current flows. The full utility voltage then appears across the lamp until the voltage is high enough to restart the lamp. Once the discharge is re-established, current again flows through the lamp. The peak of the lamp voltage waveform is often referred to as a reignition peak. Resistors are not desirable as ballasts because they dissipate considerable power, in most cases as much power as the lamp itself. Furthermore, the periods of zero current are significant enough to cause noticeable flicker.

Inductor

When lamps are operated on ac waveforms, reactive impedances may be used for the

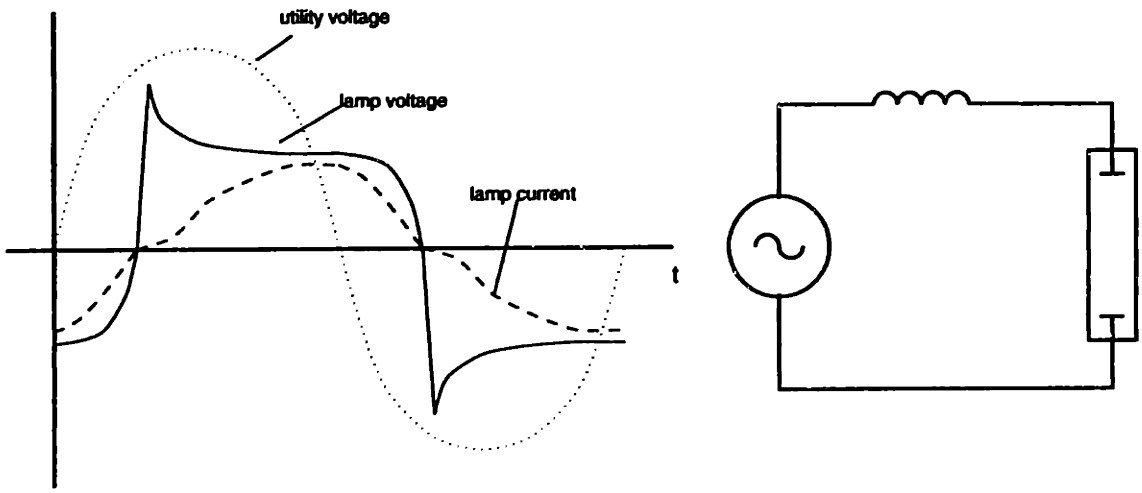

Figure 4-5: 60 Hz lamp waveforms for an inductive ballast

ballast. An inductor may be used to regulate the lamp current by creating a voltage drop proportional to the time rate of change of current. The waveforms of a lamp operated at 60 Hz with an inductor ballast are shown in Figure 4-5. In this case, there is a phase lag between the lamp voltage and the utility voltage. This produces more sustaining, or reignition, voltage available when the lamp switches polarity so that there is no significant period of time with zero current as in the resistor ballast case. The resulting flicker is slight. The power losses in this case are due to the coil resistance and the core losses in the inductor, which are significantly less than the reactive power handled by the inductor. Because of the lagging lamp waveforms, this type of ballast is often referred to as a lag ballast. The current lags the utility voltage, however, which creates an undesirable value of power factor. The power factor can be corrected, which will be explained in Section 4.2.1.

Capacitor

A capacitive impedance seems ideal for a ballast due to the low losses, but capacitors are never used at utility frequencies because of the excessive distortion of the lamp current. The waveforms of a lamp operated at 60 Hz on a capacitor ballast are shown in Figure 4-6. Note that changes in the lamp voltage polarity occur instanta-

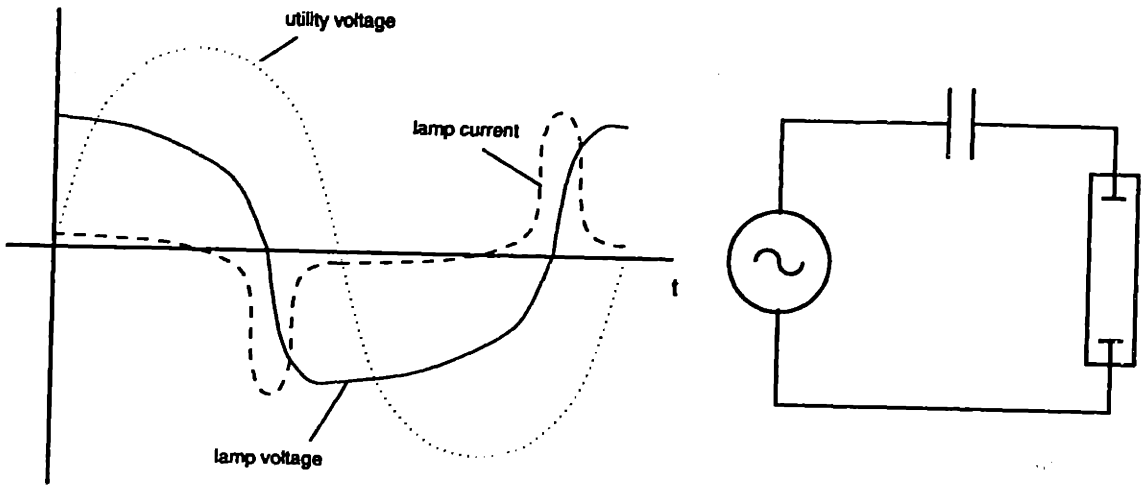

Figure 4-6: 60 Hz lamp waveforms for a capacitive ballast

neously relative to changes in the utility voltage. This rapid change in voltage must occur across the capacitor, which causes highly peaked surges of current through the lamp. The light is radiated in flashes, and the lamp life suffers due to damage of the electrodes. At high frequencies, capacitors can be used as ballast impedances with satisfactory results [38].

4.1.4 Lamp Starting

There are three general types of lamp starting.

1. Preheat or switch-start
2. Instant start
3. Rapid start

Preheat or switch-starting is illustrated in Figure 4-7. In this case, a single inductor is used as the ballast impedance. When the switch is closed, current flows and heats the electrodes. When the switch is opened, the sudden interruption of the current generates an inductive kick in voltage which ignites the lamp. The switch may be a manual switch, as in many desk type lamps, or it may be a bimetallic switch which is

closed at cold temperatures and opens when heated, or it may even be an electronic circuit [39].

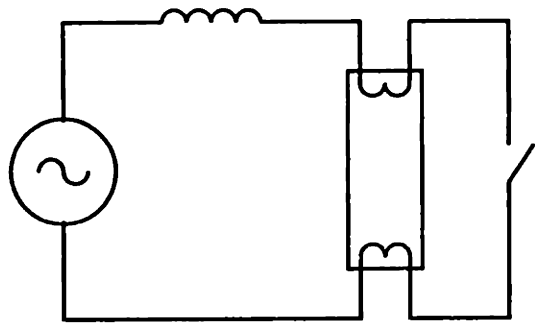

Figure 4-7: Preheat or switch-start ballast

Instant start ballasts ignite the lamp simply by applying a high enough voltage to the lamp to ionize the gas. The electrodes are not preheated. This high voltage is usually in the range of 400 to 1000 volts for common lamps. Once the arc is established, the electrodes are heated by the arc current. A starting aid, in the form of a grounded conducting surface near the lamp assists in ignition by generating lateral electric fields in addition to the applied axial electric field [40]. The starting aid is usually specified to be one inch wide at a distance of half an inch to one inches away from the lamp along the entire length of the lamp [41]. The most typical way of implementing the starting aid is to ground the metal light fixture or luminaire housing the lamps.

Rapid start is the method used most commonly in recent ballasts. In this method, the electrodes are heated for a period of time (approximately half a second) before the high starting voltage is applied to the lamp. The electrodes are usually heated by low voltage windings from a transformer. By heating the electrodes, the starting voltage is lowered compared to the value required for instant starting. Typical ignition voltages may range from 300 to 500 volts. Starting aids are also used in the rapid start scenario. Rapid starting is similar to preheat starting except that the electrode heating is done automatically and no manual switch is required.

4.2 Electromagnetic Ballast Circuits

Ballasts fall into two basic categories, electromagnetic ballasts and electronic baliasts. The electromagnetic ballasts were the first types to be used and are characterized by having only passive components, such as inductors and capacitors. Electronic ballasts use combinations of passive components and active semiconductor devices and usually drive the lamps at frequencies much greater than the line frequency. This section discusses electromagnetic ballasts.

4.2.1 Simple Ballasts

Lag Ballasts

In countries which have 220-240 volt utilities, transformers are not generally required to operate lamps and the most common ballast circuit is the lag circuit consisting of a single inductor in series with the lamp as shown in Figure 4-8a. The inductor, or choke, is made of a coil of copper wire around a high permeability core of silicon-iron laminations. The laminations are insulated from each other to reduce eddy current losses in the core. Because the use of an inductor creates a lagging power factor, a capacitor may be placed across the line to create a leading component of current to correct the power factor. Typical losses in a lag ballast are on the order of 7 to 15 watts for a 40 watt lamp [42, 43].

Lead-Lag Ballasts

Another common ballast circuit is the lead-lag circuit of Figure 4-8b. Again, this circuit is common in situations with high utility voltages of 220 to 240 volts, since no step-up of voltage is required to operate lamps of around 100 volts. In this case, one lamp is operated with a lag circuit and a lagging power factor, and a second lamp is added on a parallel circuit branch operating on a leading power factor. The leading power factor is created with an inductor and capacitor in series with the lamp. A capacitor alone cannot be used for the reasons described in Section 4.1.3. Together, the branch currents add and are drawn from the utility at near unity power factor.

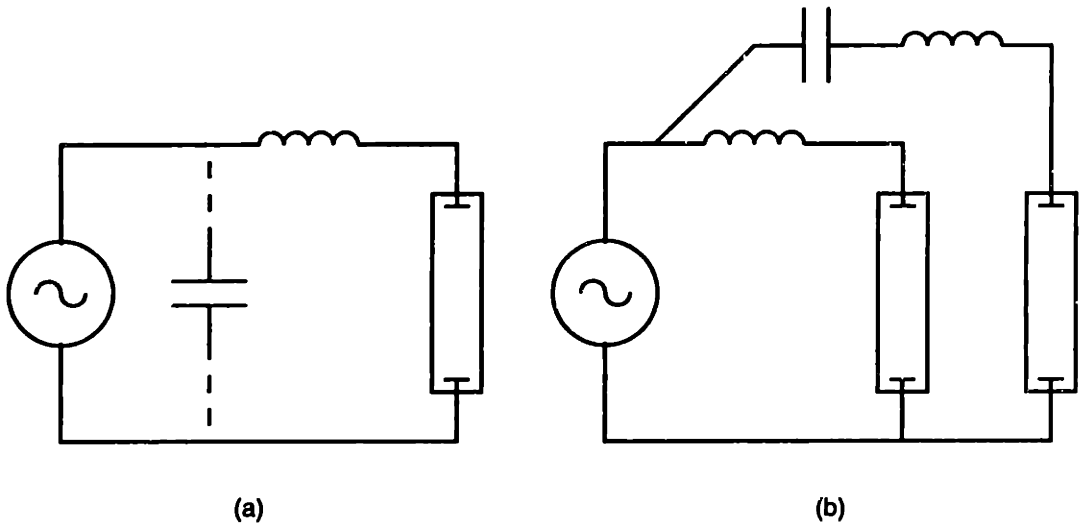

Figure 4-8: Simple ballast circuits (a) lag ballast (b) lead-lag ballast

In the past when the phosphor coatings were not perfected, lamps operating at mains frequencies had noticeable flicker. The lead-lag ballast was a good solution, since the leading and lagging lamps were out of phase. The total flicker from the combination of the two lamps was reduced, and the frequency of the flicker was doubled [44]. The phosphors have since been improved with longer afterglows, so the lead-lag ballast is not so common today.

4.2.2 Autotransformer Ballasts

This section describes the benefits of using the autotransformer and the various ballast circuits derived from it. A section on hybrid ballasts, which are essentially electromagnetic ballasts that include switching devices, is included.

Voltage Step-Up

In countries where the utility voltage is between 110-120 volts, some form of step-up in voltage is required to ignite and operate common lamps which generally have arc voltages around 100 volts. The economics favor the autotransformer over a standard isolated transformer where voltage step-up is required. For an example, Figure 4-9

shows a comparison between the autotransformer and standard transformer. In both cases, a voltage step up of two from input to output is achieved. The current load on the secondary is 200 mA.

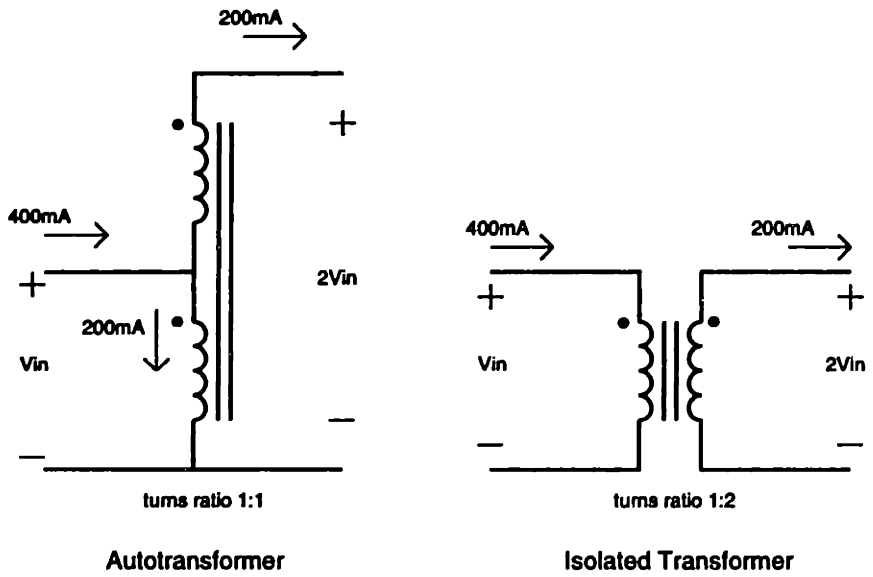

Figure 4-9: Comparison of autotransformer and standard isolated transformer

In the case of the standard transformer, a turns ratio of 1:2 is required. In the autotransformer, the turns ratio is 1:1. Given equivalent turns and wire size on the primaries of the autotransformer and the standard transformer, the standard transformer has primary losses of $(400\ mA)^2 R_p$, where R_p is the primary resistance. The autotransformer has losses of only $(200\ mA)^2 R_p$ since its primary carries only half the current that the standard transformer primary carries. In this case, the autotransformer primary losses are one fourth of the standard transformer primary losses.

Both the standard transformer and autotransformer secondaries carry the same current. The secondary losses in the standard transformer are $(200\ mA)^2 R_s$, where R_s is the secondary resistance. The secondary of the autotransformer has half the number of turns as the standard transformer, resulting in half the resistance for a loss of $(200\ mA)^2 \frac{1}{2} R_s$. The autotransformer secondary losses are one half of the standard transformer secondary losses. So in both cases of primary and secondary losses, the

autotransformer shows considerable advantage over the standard transformer for the same application. Note that the autotransformer connection does not have electrical isolation between the input and output while the standard transformer does.

Autotransformer Ballast Circuits

The same types of ballast impedances presented previously may be employed in autotransformer ballast circuits. An inductor may be used as the ballast impedance, but in the case of the autotransformer, the inductor can be conveniently implemented as a leakage inductance. This is shown in Figure 4-10. The leakage inductance can be

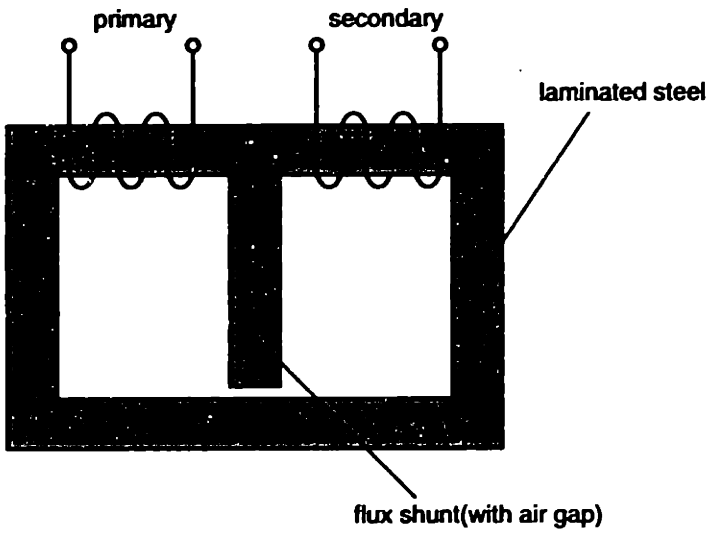

Figure 4-10: Autotransformer with shunt for leakage inductance

increased by deliberately having loose coupling between the primary and secondary. However, the leakage is usually explicitly generated by introducing a shunt in the magnetic path. In this case, some flux is shunted away from the secondary through the alternate leg of the core.

Figure 4-11a shows an autotransformer ballast with the ballast impedance implemented as a leakage inductance. As in the case of the lag ballast, the power factor may be corrected by adding a capacitor across the utility. An even more economical way to increase the power factor is shown in Figure 4-11b. In this circuit, the induc-

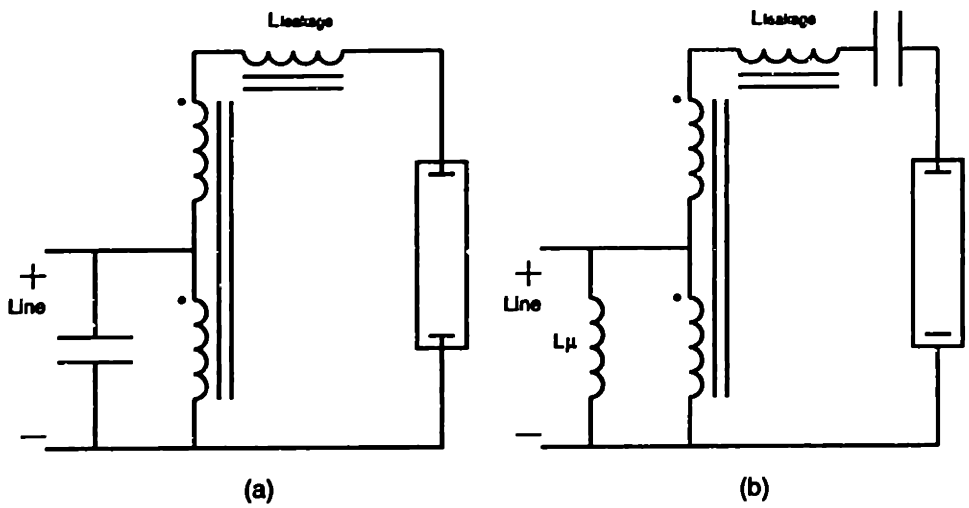

Figure 4-11: Autotransformer ballasts (a) lag with line capacitor (b) lead with magnetizing inductance

tance is still a leakage inductance, but a capacitor is added to the ballast impedance to create a leading power factor. Since the secondary, and therefore the primary, currents are both leading the utility, a lagging component must be introduced. This is accomplished by increasing the primary magnetizing current, which lags the utility. Increasing the primary magnetizing current involves decreasing the primary inductance, which also allows a reduction in secondary turns for a given turns ratio. Both of these actions result in a smaller transformer. This method of power factor correction is therefore favored by economics [5].

Perhaps the most common electromagnetic ballast circuit is the rapid start autotransformer leakage ballast shown in Figure 4-12 [45]. This type of ballast is used most often in a two lamp series configuration. Again an autotransformer is used for voltage step-up and provides an inductance through a leakage reactance. A capacitor is used to provide a leading phase of current so that the power factor may be adjusted by decreasing the primary inductance. Low voltage turns on the secondary are coupled to the electrodes to provide heating of the filaments prior to starting. A starting capacitor provides an electrical path to the lower lamp when both lamps are extinguished. During ignition, the open circuit voltage is applied to the lower lamp. The lower lamp ignites, becomes a near short circuit, and the open circuit voltage

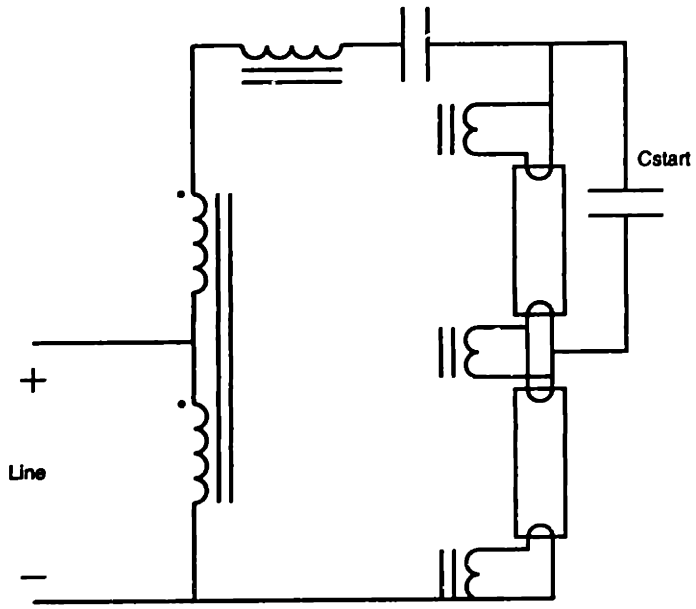

Figure 4-12: Rapid start autotransformer leakage ballast

is then applied to the top lamp. This arrangement is called a sequence start circuit. The two lamp configuration is most common because it requires only a little bit above one lamp ignition voltage (23%) to ignite two lamps [46].

For a ballast circuit like this operating two F40T12 lamps (40 watts each) the ballast losses are around 15 to 16 watts [46, 14, 47] for a ballast efficiency of around 80 to 85%. This type of ballast has been optimized over many years. Further improvements have been made by using lower resistance copper wire with square cross section and higher quality silicon steel in the core laminations. These reduced loss electromagnetic ballasts have losses around 8 watts for two F40T12 lamps [14, 48].

Hybrid Ballasts

The first step towards improving the electromagnetic ballasts involved using lower resistance wire and higher quality core materials. The next step in improving the efficiency of electromagnetic ballasts came in the form of hybrid ballasts [49, 50, 51]. The general approach of the hybrid ballast is to heat the electrodes prior to ignition and deactivate the heating coils to the electrodes after ignition. The normal operating

current heats the electrodes sufficiently during operation to insure thermionic emission of electrons. The hybrid ballast concept is shown in Figure 4-13.

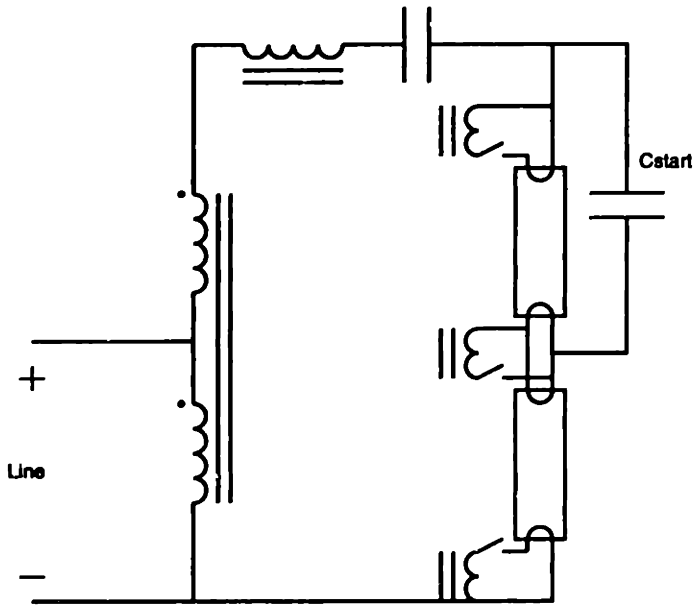

Figure 4-13: Hybrid ballast

Original implementations of the hybrid ballast concept involved relays, thermal cutout switches, and solid state components that resulted in a very expensive ballast. More recent implementations use an auxiliary filament transformer that is activated only during ignition. A sidac senses high open circuit voltage and breaks over when the lamps are not ignited, activating the auxiliary transformer. Still more recent implementations use optocouplers and power triacs to deactivate the filament windings. The hybrid ballast approach can result in an additional savings of around 5 watts over the reduced loss electromagnetic ballast for two F40T12 lamps.

Additional Ignition Circuits

Sometimes the ballast must provide even more increased open circuit voltage to insure starting of the lamps. This is often accomplished with a splined gap peaking

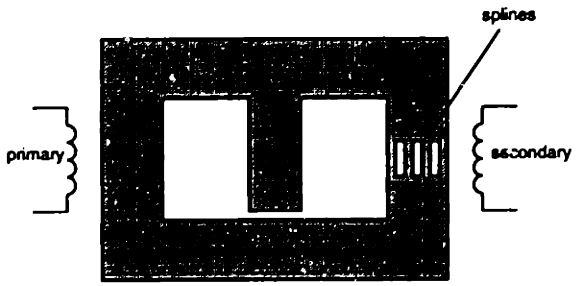

Figure 4-14: Splined gap peaking transformer

transformer as shown in Figure 4-14. The splines form a region with significantly less cross sectional area than the rest of the core. When the primary volts are at a maximum, the primary current and magnetic flux are near zero. The splines are unsaturated and have high permeability, so the flux follows the all iron path through the splines linking the secondary. With the primary voltage near maximum, the secondary voltage is also a high value. At all other times, the splines are saturated

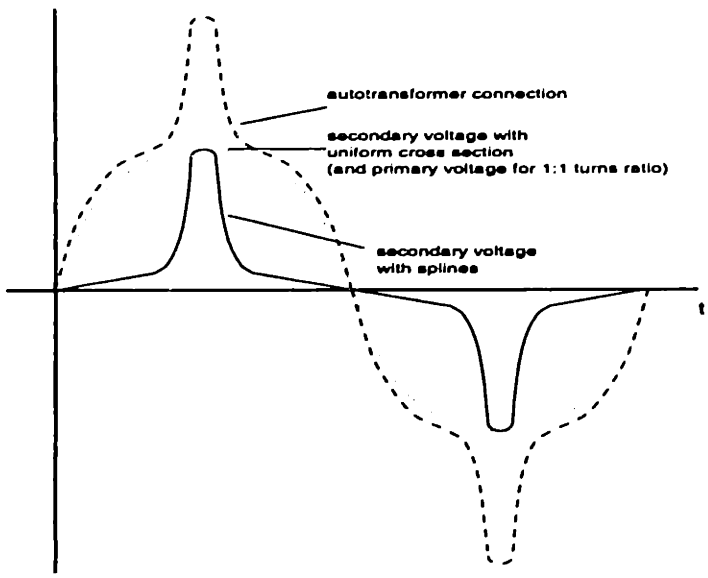

Figure 4-15: Splined gap peaking transformer secondary waveforms

and behave like an air gap with low permeability. If the gap of the shunt path is

suitably sized, most of the flux will travel through the shunt, bypassing the secondary. The secondary voltage is then very low. In this way, a peaked voltage waveform can be generated as shown in Figure 4-15.

Electronic Ignitor

The electromagnetic ballast circuits for HID lamps are very similar to the types already presented in this chapter. The exception is that HID lamps typically require much higher starting voltages than fluorescent lamps (up to several kilovolts) [52]. The ignition function is usually separated from the ballast and is accomplished with a separate electronic ignitor circuit. One such circuit is shown in Figure 4-16. The capacitor C_1 is charged to a voltage by the utility. With a gate control signal to the thyristor, the energy in the capacitor is discharged into part of the ballast inductor winding. The pulse is increased by the turns ratio of the ballast inductor winding, and creates a short pulse of 3 to 4 kV. Most electronic ignitors operate on this principle of discharging the energy stored in a capacitor into an inductor [53].

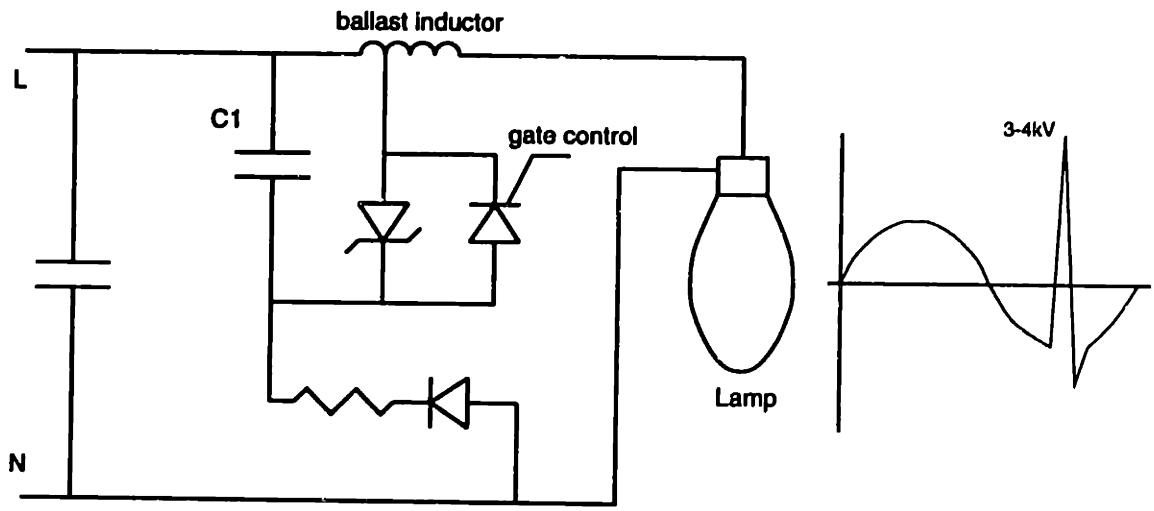

Figure 4-16: Electronic ignitor for HID lamps

4.3 Electronic Ballasts

This section introduces electronic ballast circuits. An overview of the advantages and disadvantages of the electronic ballast is given. Then, a basic electronic ballast circuit is described followed by more detailed discussion of the individual functional stages of the ballast.

4.3.1 Introduction to Electronic Ballasts

Electronic ballasts use active switching devices in addition to passive components to drive discharge lamps. In most cases, the electronic ballast drives the lamp at frequencies greater than 20 kHz. The electronic ballast offers many advantages over the electromagnetic ballast. These advantages include:

1. Improved lamp efficacy with high frequency drive
2. Improved ballast efficiency
3. Extended lamp life
4. No visible flicker
5. Less audible noise
6. Smaller ballast size and weight

These advantages do not come without disadvantages. The disadvantages of electronic ballasts include:

1. High cost
2. Reduced reliability
3. Electrical interference (RFI and EMI)

The development of the electronic ballast was driven by the discovery that discharge lamps were more efficient when driven at high frequencies than at line frequencies. The typical electronic ballast converts 60 Hz line power into high frequency sinusoidal

power to drive the lamp. In the process, numerous advantages arise. The first and foremost is the increased efficacy of the lamp itself, as discussed in Section 2.3.3. Typical lamps show increases in efficacy of 10% at frequencies around 20 kHz. In addition to the increased efficacy, lamps driven at high frequency have no visible flicker. The problems associated with the 120 Hz flicker of lamps using electromagnetic ballasts were mentioned in Section 2.3.3 [54, 55, 14].

Electronic ballast circuits can deliver power with good efficiency compared to electromagnetic ballasts. Typical losses in an electronic ballast are on the order of 6 watts compared to the 10 to 15 watts of loss in electromagnetic ballasts. With improved lamp efficacy and improved ballast efficiency, the electronic ballast–lamp combination can result in energy savings of 20 to 25% for a given light output compared to electromagnetic ballasts [42, 13, 29]. In industrial and office space type applications, there can be substantial savings in air conditioning costs when using electronic ballasts due to the reduced ballast dissipation [14]. It should be noted that the efficiency of an electromagnetic ballast can always be improved by increasing the size and cost of the ballast. So the issue is never strictly efficiency alone, but efficiency at what cost, size and weight.

It is generally accepted that lamps operated on electronic ballasts have longer lifetimes than when operated on magnetic ballasts [14, 2, 43]. The extended lamp life results from the improved lamp waveforms at high frequencies, since the voltage and current waveforms are essentially sinusoidal at frequencies above a few kilohertz compared to the distorted waveforms at 60 Hz. High current crest factors in particular, result in the shortening of electrode life. Additionally, electronic ballasts can regulate the lamp power more effectively than electromagnetic ballasts in the face of changing line and lamp conditions.

Because electronic ballasts use power conversion circuitry switching at high frequencies, the filter elements can be substantially smaller than the components in a 60 Hz ballast. This results in a smaller and lighter ballast. Furthermore, electronic ballasts work at frequencies above 20 kHz which is out of the range of human hearing, so there is virtually no audible noise compared to the 120 Hz buzzing in electromag-

netic ballasts [48, 56].

The main disadvantage of electronic ballasts is their high cost relative to electromagnetic ballasts. Section 4.4 covers this in more detail. Because of the complicated nature of the electronic ballast circuitry the ballasts can be more prone to failure, although since electronic ballasts are relatively new, limited field test data have been gathered [2]. But initial electronic ballasts had significantly higher failure rates than electromagnetic ballasts [57, 58, 59].

Perhaps a more troubling disadvantage of electronic ballasts is radio frequency interference (RFI) and electromagnetic interference (EMI) generated by the ballast circuitry and the lamp. High harmonic currents generated by the ballast and conducted back into the utility can cause many problems such as excessive neutral currents, overheated transformers, and interference with sensitive electronic equipment [60, 61]. The ballast itself does not tend to radiate EMI since it is encased in a grounded metal enclosure. But the lamps can generate EMI and RFI. Infrared radiation from lamps can interfere with television and videocasette recorder remote controls [62, 63]. Radiated electric noise from the lamps can be amplified by hearing aids. Household security systems can be rendered inoperative. The electronic ballast design must take steps to minimize the generation of EMI and RFI. The Federal Communications Commission (FCC) regulates conducted and radiated EMI for electronic ballasts under the Code of Federal Regulations, Section 47, Part 18, entitled *RF Lighting Devices* [64].

4.3.2 The Typical Electronic Ballast Circuit

Virtually all electronic ballasts are based on resonant inverter circuits. A typical electronic ballast circuit topology is shown in Figure 4-17. The utility is rectified with a full-wave rectifier bridge of four diodes. The rectified utility is then boosted to a high dc voltage on the capacitor C_e and power factor correction on the input current is performed in the process. The power factor correction is shown here as a boost converter but other circuits or passive components may be used instead. This is explained in Section 4.3.3. The capacitor C_e performs two functions. First, it must

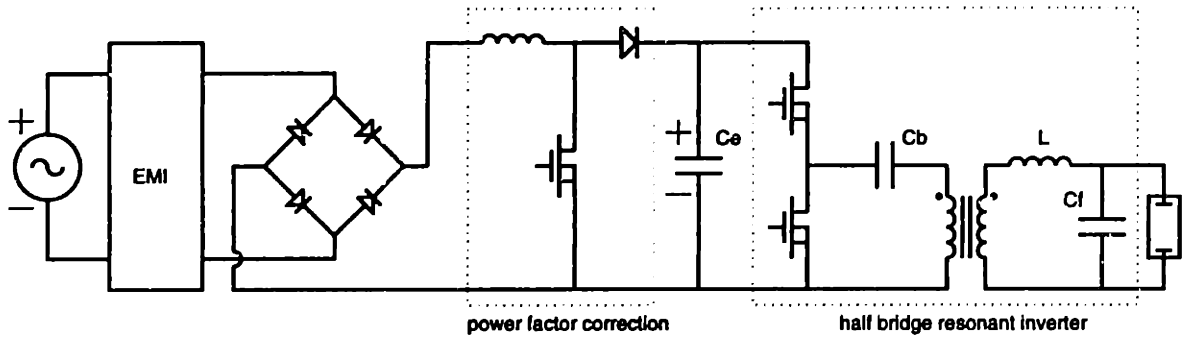

Figure 4-17: Typical electronic ballast

provide a dc voltage for input to the resonant inverter. Second, it must balance the cyclic energy flow between the load and the utility. The resonant inverter output stage is the heart of the ballast. This stage converts the dc voltage on C_e to a high frequency sinusoidal drive for the lamp. The two switches shown in a half bridge configuration operate at 50% duty cycle to chop the dc voltage into a high frequency square wave. A capacitor C_b blocks dc components from an isolation transformer. The second order filter formed by the inductor L and capacitor C_f filters the square wave so that the lamp sees sinusoidal voltage and current at the fundamental of the switching frequency. The transformer is used for both isolation and turns ratio.

Functionally, most electronic ballasts are equivalent to the one shown in Figure 4-17. In practice, the power factor correction stage and the resonant inverter stage can be implemented in many different ways. The following sections describe the functional blocks of the electronic ballast in greater detail.

4.3.3 Power Factor Correction

Not all ballasts use power factor correction. Figure 4-18 shows the input stage of a non-power factor corrected ballast. The energy storage capacitor follows the bridge rectifiers immediately with no intermediate circuitry. The capacitor is charged to the peak of the utility each half cycle and only draws current during those short instants where the utility is greater than the capacitor voltage. This results in poor power

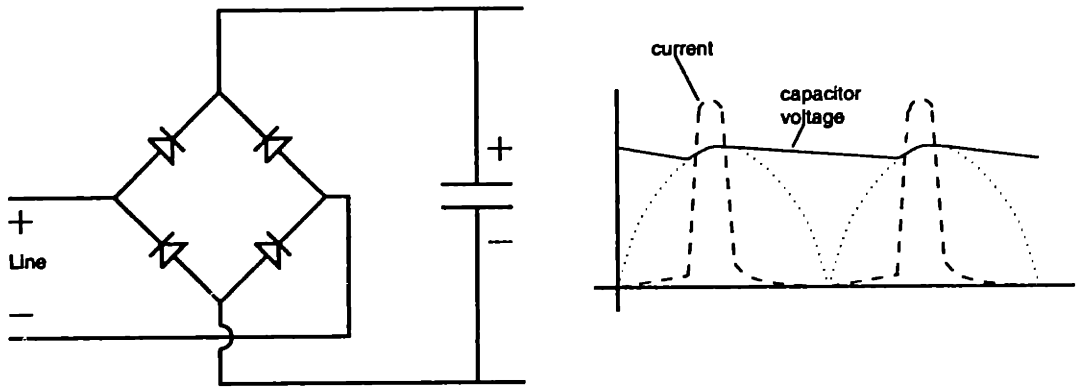

Figure 4-18: Diode rectifier bridge with no power factor correction

factor and very high harmonic distortion of the line current, in addition to very large peak currents. There are two basic approaches to correcting the power factor — passive and active.

Passive Power Factor Correction

There are many different approaches to passive power factor correction. Perhaps the simplest is the addition of an inductor between the rectifier bridge and the energy storage capacitor as shown in Figure 4-19a. The inductor works to stretch out the conduction angle of the input current. Figure 4-19b is another passive approach consisting of an LC filter in front of the diode bridge. Figure 4-19c is a parallel LC filter which can be tuned to attenuate the third harmonic (which is especially troublesome in three-phase systems).

All these passive approaches consist of inductors or capacitors placed before or after the diode bridge. The advantage of passive approaches is that they are relatively simple to implement. However, these filter elements are relatively large and bulky because they operate at line frequencies. Because of the series components in the filter, the efficiency of the converter is degraded. At higher power levels, the passive filter size and expense increases [65, 66, 67, 68].

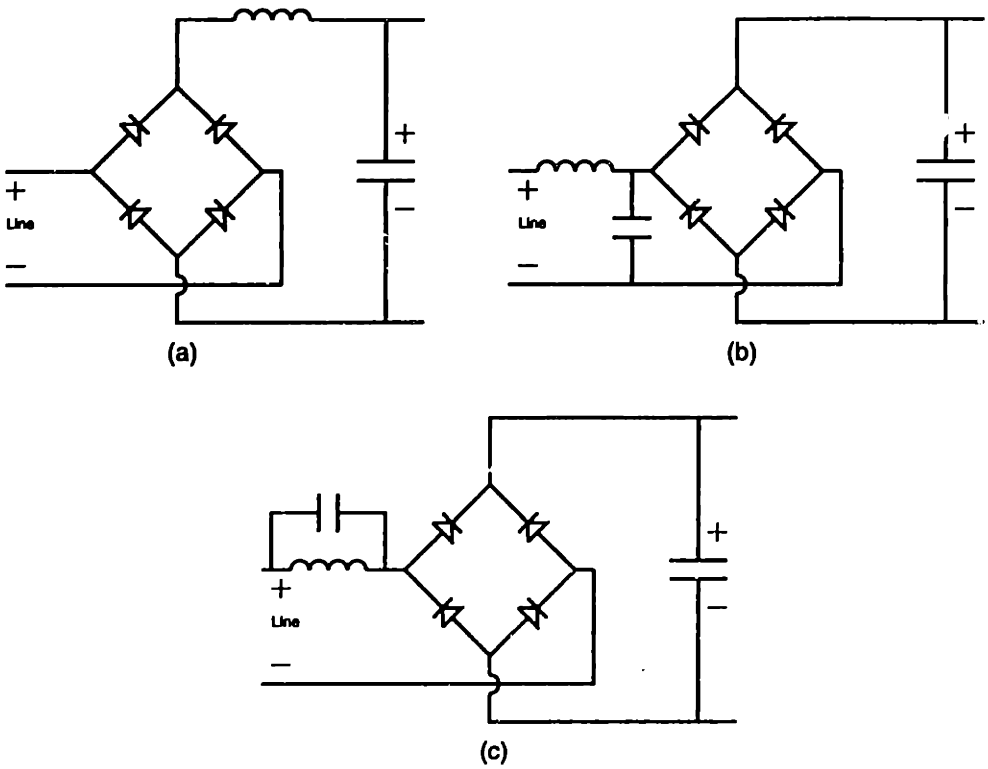

Figure 4-19: Passive power factor correction

Active Power Factor Correction

Active power factor correction is generally more complex and expensive to implement than passive methods. The cost can be comparable in some cases, and the active methods can usually achieve much greater power factor and much lower harmonic distortion. By using a high frequency switching converter, the additional filter components can be smaller than the line frequency components present in a passive approach. As a result, an active power factor correction stage can be added without significantly increasing the size or weight of the ballast. There are several topologies that can be used — the buck, the flyback, and the boost converter topologies.

The buck converter is shown in Figure 4-20. The buck converter is generally not a good choice. It is a down converter, so the output voltage must be less than the input voltage. The buck converter is therefore applicable in situations where the dc bus voltage on the capacitor is substantially less than the peak of the utility, which

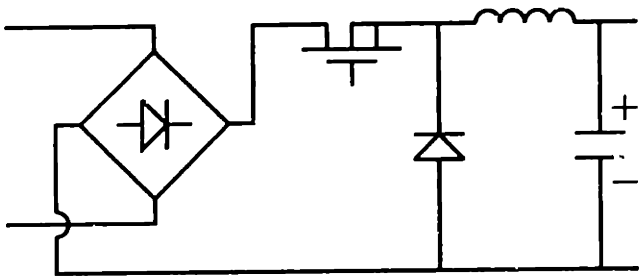

Figure 4-20: Buck converter

is not often the case in electronic ballasts. Because there is a switch immediately following the diode bridge, the current drawn from the utility is chopped and further filtering is required. The active switch is also relatively difficult to drive, since it is a high side switch and requires some form of level shifting circuitry.

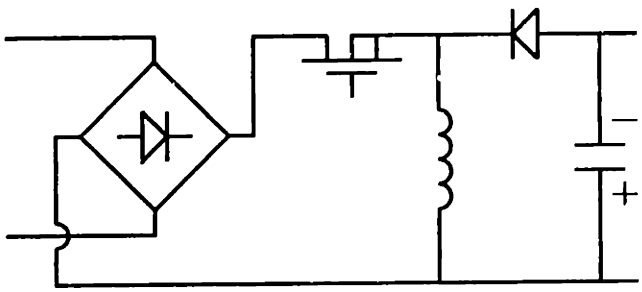

Figure 4-21: Flyback converter

The flyback converter is shown in Figure 4-21. The chief advantage of the flyback converter is that the output voltage may be above or below the input voltage (albeit with a polarity reversal). Implementing a discontinuous mode control is easy because with a fixed switch on time, the input current will follow the input voltage. However, the switches must withstand the sum of the input and output voltages, and again the active switch requires a high side drive. The input current is again chopped, requiring more filtering to the line. The inductor tends to be larger than the inductors in the buck or boost converters.

The boost converter shown in Figure 4-22 is the most popular choice for active

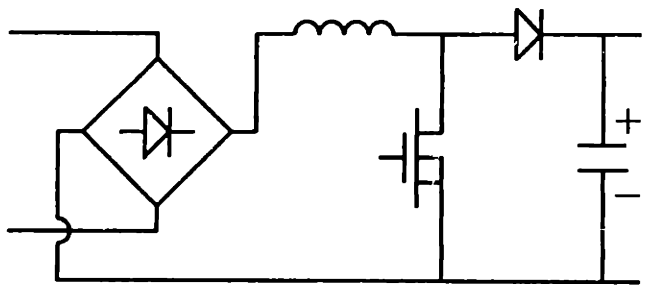

Figure 4-22: Boost converter

power factor correction in electronic ballasts [67, 69]. The only requirement of the boost converter is that the output voltage must be greater than the input voltage. In the case of the electronic ballasts, this is actually desirable. The energy storage capacitor can store energy with less capacitance at higher voltages for a given allowable ripple voltage. Also, the resonant inverter stage may require a high dc input voltage. The boost converter can work over virtually the entire input voltage range, eliminating distortion and achieving very high power factor. When operated in the continuous mode, the inductor current is not chopped and additional filtering of the input current is easy. The active switch is ground referenced and is simple to drive. The boost converter can also be operated in the discontinuous mode at the expense of a larger input EMI filter. Under discontinuous conduction operation, the inductor current reaches zero for a period of time during each switching period. The diode can undergo reverse recovery during this time and an ultrafast recovery diode may not be necessary.

4.3.4 Resonant Inverter

There are many different implementations for the resonant inverter output state of the ballast. This section describes the different bridges and filters that can be used. In terms of control, the two different types of resonant inverters are free-running and controlled. These are explained as well with several examples.

Bridge Implementation

The bridge implementation shown in Figure 4-23 is a half bridge called an asymmetrical bridge. The input to the filter is alternately connected to the full dc bus

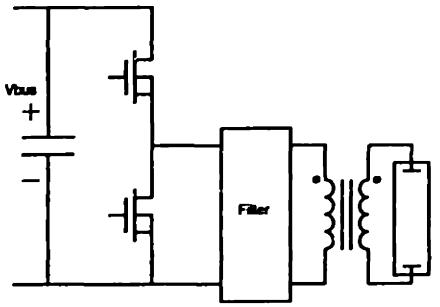

Figure 4-23: Asymmetrical half bridge

voltage and ground. The output from the bridge has a dc component at half the bus voltage that must be removed by a series capacitor in the filter before the transformer. This is essentially the same implementation shown in the basic electronic ballast of Figure 4-17.

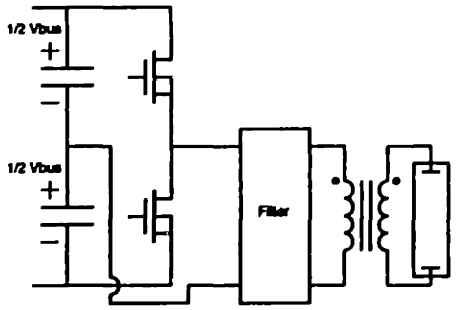

Figure 4-24: Half bridge

The bridge implementation shown in Figure 4-24 is a true half bridge which uses a connection between two energy storage capacitors. The input to the filter is alternately connected to $+\frac{1}{2}$ the bus voltage and $-\frac{1}{2}$ the bus voltage, so no dc blocking

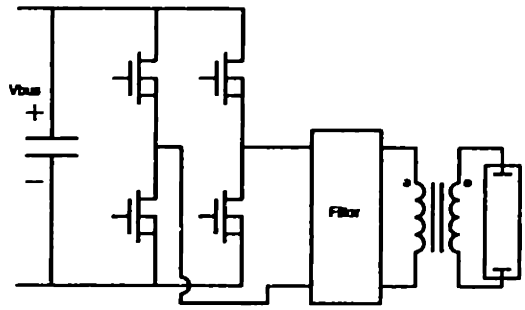

Figure 4-25: Full bridge

capacitor is required.

In situations demanding higher power, a full bridge topology may be used as shown in Figure 4-25. Here, the filter receives the full bus voltage positively and negatively. The main disadvantage of the full bridge is the extra switches required [70]. A dc blocking capacitor may be needed to correct for situations where the duty ratio is not exactly 50%.

Filters

The filter is used to shape the lamp waveforms by filtering out the higher harmonics of the switching frequency so the lamp sees essentially sinusoidal waveforms at the

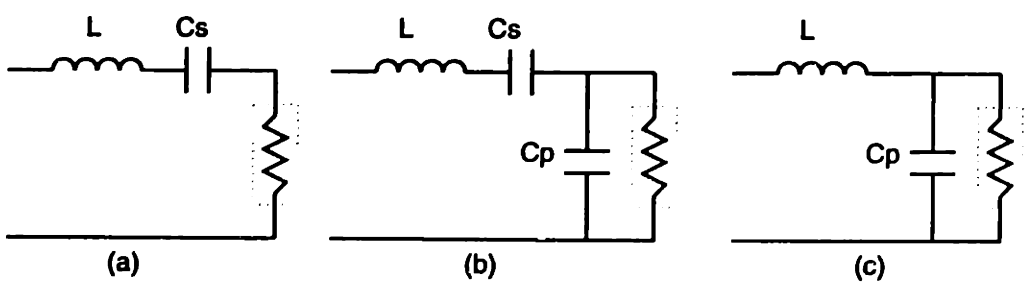

Figure 4-26: Filters (a) series LC (b) series parallel LCC (c) parallel LC

fundamental of the switching frequency. The filter may also be an integral part of the ignition of the lamps. There are many different possible filter implementations, and each has certain advantages and disadvantages.

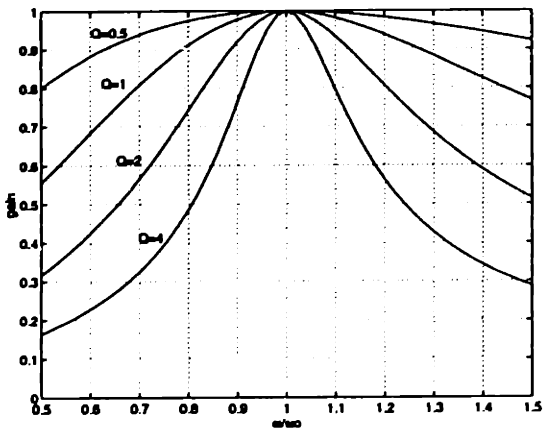

Figure 4-27: Gain versus frequency for series LC filter

A series loaded LC filter is shown in Figure 4-26a. Here the inductor and capacitor are connected in series with the lamp. The voltage gain of the filter as a function of switching frequency is shown in Figure 4-27 with changing values of Q. Near resonance, the gain of the filter is one. This characteristic makes this filter advantageous in free-running inverters where the converter operates near the resonant frequency of the filter. With changes in load impedance, the circuit will still operate around unity gain. A transformer must be used to generate the necessary starting voltages.

Figure 4-26b shows a series/parallel loaded filter. Figure 4-28 shows the gain of the filter versus frequency for different values of Q. The curves shown are for Cs equal to Cp. Unlike the series loaded case, this filter can achieve voltage gain, so it is possible to generate ignition without requiring the turns ratio of a transformer. The achievable voltage gains are not that high, however, and they decrease with increasing Q. There is also a substantial shift the in the resonant peak with varying Q. The gain near resonance changes substantially with varying load impedance, so this filter is not a good choice for free-running inverters.

Figure 4-26c shows a parallel loaded LC filter. Unlike the previous two filters

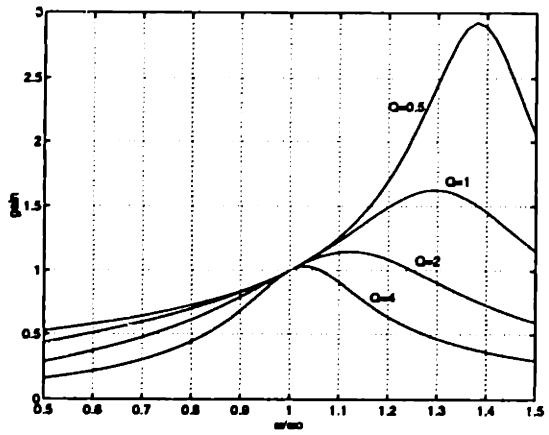

Figure 4-28: Gain versus frequency for series parallel LCC filter

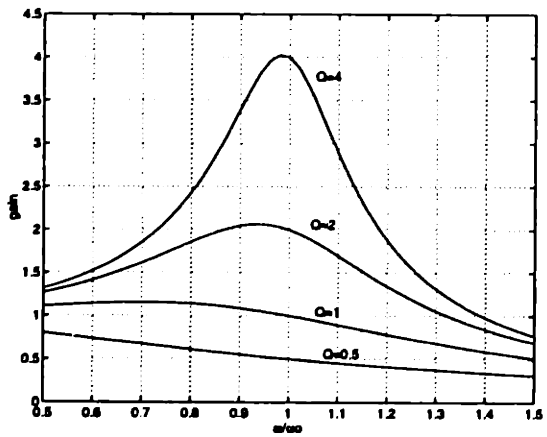

Figure 4-29: Gain versus frequency for parallel LC filter

which were band-pass filters, this one is a low-pass filter. High voltage gains near resonance are possible as can be seen in Figure 4-29. A ballast incorporating this filter can use the filter gain to ignite the lamp, so the transformer can be designed for steady state operation and would not be required to generate higher voltages. For this reason, the parallel loaded filter is a popular choice for electronic ballasts [20, 21, 71]. This filter also has poor regulation near resonance with changing load conditions, so it is not particularly well-suited for free-running inverters.

For controlled resonant inverters, the parallel loaded LC filter is almost ideal. When starting in a rapid start scenario, the electrodes must be preheated prior to

ignition. It is easy to operate the converter at a frequency higher than the resonant frequency to preheat the electrodes. At a high enough frequency, the gain of the filter is low and the lamp will not ignite. After sufficient preheat time, the frequency can be swept down towards the resonant frequency, where the resonant peak of the filter provides the voltage gain necessary to ignite the lamp.

For all these filters, operation above the resonant frequency is preferred. Above resonance, the filter looks inductive and the current to the filter lags the voltage. This allows the switching losses in the inverter at turn-on to be eliminated. Furthermore, fast recovery diodes are not needed. This is explained in greater detail in Section 7.5.

Control

The inverter topologies for electronic lamp ballasts can be divided into two classes, free-running and controlled. Free-running inverters are self-oscillating circuits that run at the resonant frequency of the circuit. The control is simple and relatively inexpensive, but the regulation of such circuits is poor since the frequency is essentially fixed. Lamps have changing impedance characteristics over their lifetime, so free-running inverters may operate the lamps at the wrong conditions since they have no explicit way to regulate the power.

Controlled inverters use current and/or voltage sensing to explicitly control or regulate the output to the desired conditions. This is generally achieved by varying the switching frequency of the converter to control the voltage gain of the resonant filter. With a varying switching frequency, the inverter is referred to as a quasi-resonant inverter. The main drawback of the controlled inverter is the cost and complexity associated with the control circuitry. The controlled inverter topology is becoming more and more the topology of choice for electronic ballasts because dimming of fluorescent lamps is possible by varying the output power of the inverter [13].

The basics of a half bridge (asymmetrical) free-running inverter are shown in Figure 4-30 [72, 73]. A feedback current transformer with its primary driven by the filter current controls the switches to turn on and off alternately. When the current

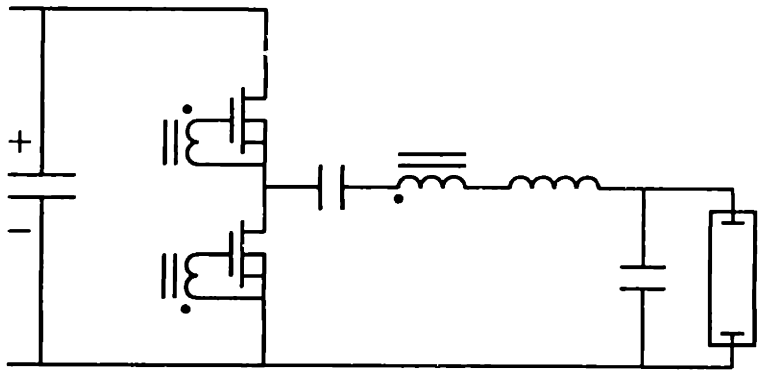

Figure 4-30: Half bridge (asymmetrical) free-running inverter

to the filter is positive, the high side gate capacitance is charged and the switch turns on. When the current to the filter is negative, the low side switch is turned on. A circuit like this is not self starting and must be pulsed by a diac to start the lower switch. Before the lamp is ignited, the Q of the circuit is very high and there is enough voltage gain to ignite the lamp. After the lamp is ignited, the Q of the circuit collapses and steady state operation ensues. A transformer may be required to match the lamp impedance to the inverter in order to insure the proper operating characteristics.

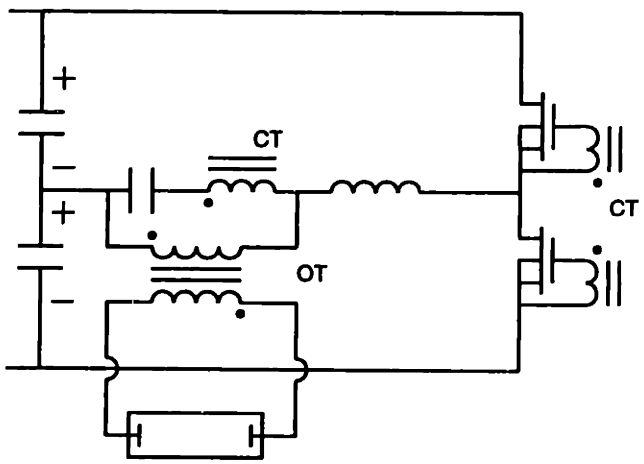

Figure 4-31: Half bridge free-running inverter

Figure 4-31 shows another free-running inverter described in US patent number 5124619 [74]. This one uses a true half bridge. A current feedback transformer CT uses the capacitor current to alternately turn on and off the two switches. An output transformer OT couples the load to the filter. Voltage gain for ignition is provided by the filter.

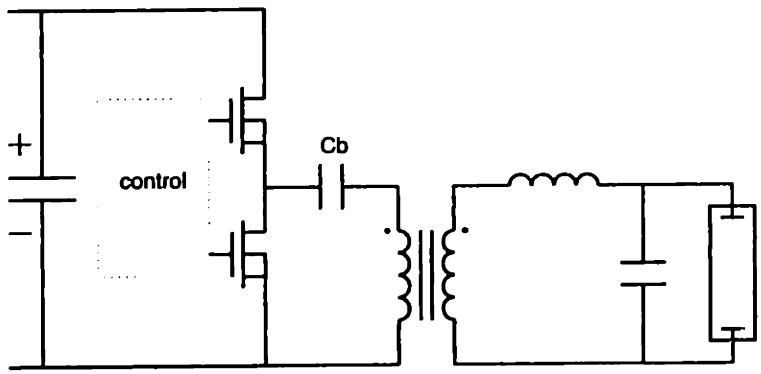

Figure 4-32: Half bridge (asymmetrical) controlled inverter

Figure 4-32 shows a half bridge (asymmetrical) controlled inverter [75]. This is similar to the resonant inverter topology presented in the basic electronic ballast of Figure 4-17. A blocking capacitor Cb blocks dc components from the transformer. The filter supplies the voltage gain for ignition and the transformer is used to match the load to the inverter circuit in the steady state. The switching frequency can be varied in order to take advantage of the varying voltage gain with frequency response of the filter. Thus the power to the lamp can be regulated to the desired operating conditions. The inductance of the filter can be implemented as a leakage inductance in the transformer, as in the electromagnetic autotransformer ballasts.

Summary of Inverter Types

Free-running or self-oscillating inverters have the advantage of low cost and simplicity of control. Performance-wise the regulation of power to the load is not good. They cannot be used for dimming since the power cannot be controlled. Manufacturing such inverters is relatively difficult, since a feedback transformer is required.

Controlled inverter topologies are generally favored over free-running inverters because of the ability to regulate the lamp power. This also makes the controlled inverter the topology of choice for applications where dimming of the lamps is desired. The main disadvantage is the cost and complexity of the control, although the control may be more easily manufactured if it consists of integrated circuits and semiconductor components.

4.3.5 Energy Storage Capacitor

The energy storage capacitor of the electronic ballast is a very important component. It has two functions which are somewhat related. First, it must provide a stable dc voltage to feed the input of the inverter. Second, it must balance the cyclic energy flow between the load and the utility. This is called load balancing energy storage and is illustrated in Figure 4-33.

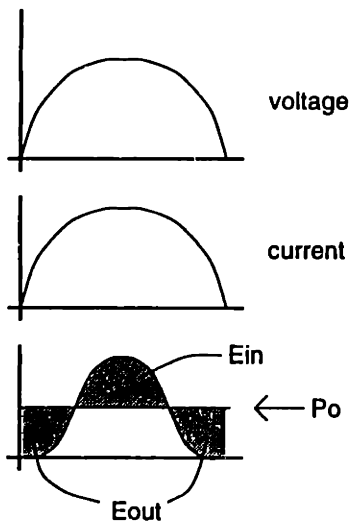

Figure 4-33: Load balancing energy storage

With a sinusoidal voltage and current drawn from the utility, the power input to the circuit varies as shown at twice the frequency of the utility (120 Hz). The power delivered to the load, however, is essentially constant at the average of the input power waveform. During periods of time where the utility is delivering less

power than the load is consuming, the energy storage capacitor must deliver energy to the load. When the utility is delivering more power than the load is consuming, the capacitor must store the extra energy. This is known as 120 Hz load balancing energy storage. The minimum energy storage required of the capacitor when the utility voltage and current waveforms are sinusoidal is

$$E_{min} = \frac{P_o}{\omega_{60}} \tag{4.6}$$

where P_o is the average power and ω_{60} is the radian frequency of the utility.

The capacitor which stores the load balancing energy must have a voltage that ripples at 120 Hz as the energy is delivered to and taken from the capacitor. Resonant inverter topologies require a fixed dc voltage for input. Any 120 Hz ripple at the input will appear as an undesirable 120 Hz modulation of the output voltage of the inverter unless the switching frequency is modulated to compensate for the ripple. For this reason, the energy storage capacitor must have a high value of capacitance so that the load balancing energy is a small fraction of the total energy stored in the capacitor at the desired dc bus voltage.

This capacitance cannot be reduced in size by changing the switching frequency or any other such methods since its size is solely a function of the power of the ballast circuit, and the frequency of the utility, which are both fixed for a given application. The dc bus voltage may be increased so that for a given capacitance more energy is stored and the load balancing energy is a smaller fraction of the total energy. This will result in a smaller voltage ripple, but the higher dc voltage will require semiconductor devices to handle the increased voltage stress. The switching losses in the converter will also increase.

4.4 Ballast Markets

This section provides a brief history of the ballast market. Data are presented for the quantity and value of United States shipments of both electromagnetic and electronic

ballasts over roughly the past decade. The current state of the market for electronic ballasts is discussed.

4.4.1 Market History

In 1982, the United States ballast market was exclusively electromagnetic ballasts with a quantity of 50 million units per year with a value of 300 million dollars ($6 per unit). In 1983, electronic ballasts entered the market with sales around 0.3 million units per year (at close to $30 per unit) [76]. By 1986, unit sales of electronic ballasts were up 30% to 0.4 million units which was less than 1% of the total number of ballasts sold (70 million units with a value of 400 million dollars).

In 1987, electronic ballast sales were spurred by rebate offers from utilities [76]. Sales of electronic ballasts rose to nearly 1.5 million units per year by 1989 for a total value of 25 million dollars.

In 1990, the National Appliance Energy Conservation Act was enacted which eliminated the old and inefficient electromagnetic ballasts by requiring that all units sold in the United States have a minimum efficiency equivalent to or better than energy efficient magnetic ballasts [77]. Demand for electronic ballasts exceeded supply since at the time there were only two manufacturers of electronic ballasts.

After 1990, many companies began to enter the electronic ballast market. From 1990 to 1992, annual unit sales of electronic ballasts rose from 3 million units to 13 million units. By 1993, even more companies entered the electronic ballast market, increasing competition and driving the price of electronic ballasts down. Unit sales rose to 25 million units in 1993 with a total value of 450 million dollars (about 46% of the total market in dollars).

4.4.2 Current Market

Figure 4-34 shows the quantity of United States shipments of fluorescent lamp ballasts for the years 1986 to 1995 [78, 79]. The data is separated into quantity of electronic ballasts, uncorrected power factor electromagnetic ballasts, power factor

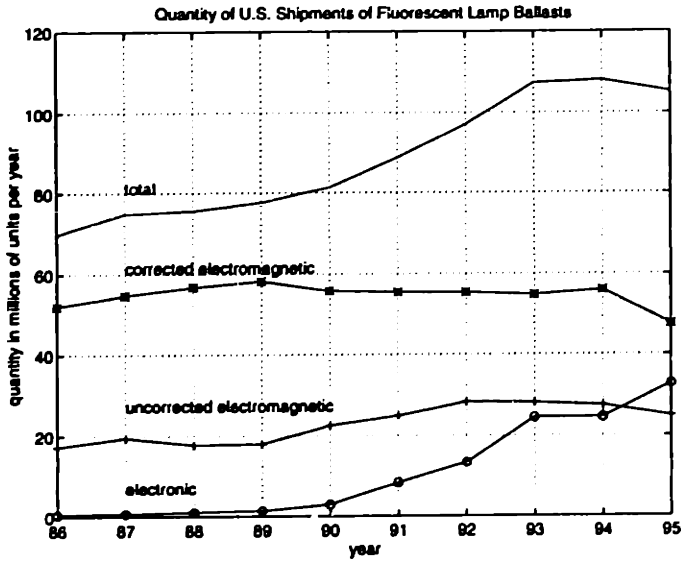

Figure 4-34: Quantity of U.S. shipments of fluorescent lamp ballasts

corrected ballasts, and the total ballasts. Figure 4-35 shows the value of United States shipments for the same ballast classes in Figure 4-34. Currently, the U.S. Market for ballasts is about 100 million units per year with a value of 1 billion dollars. Electronic ballast sales are 500 million dollars annually which represents a 50% market share in terms of dollars. The total number of electronic ballasts sold in 1995 was about 30 million units, which is 30% of the 100 million total ballast units sold.

Figure 4-36 shows the per unit value of power factor corrected electromagnetic ballasts and electronic ballasts for the years 1986 to 1995. It is interesting to note that the price of an electronic ballast has fallen from 27 dollars in 1986 to about 15 dollars in 1995, while electromagnetic ballast prices have risen from 7 dollars in 1986 to 9 dollars in 1995.

At this point, the gap in costs between the electronic and electromagnetic ballasts is closing. The payback time for a 40 watt lamp operated on an electronic ballast can be estimated as follows [80]. The yearly cost of operating a 40 watt lamp is roughly

$$40\,watts \times \frac{3000\,hours}{year} \times \frac{\$0.10}{kilowatt\,hour} = \$12\,per\,year\,operating\,cost \qquad (4.7)$$

For a given light output, a high frequency electronic ballast can operate the lamp

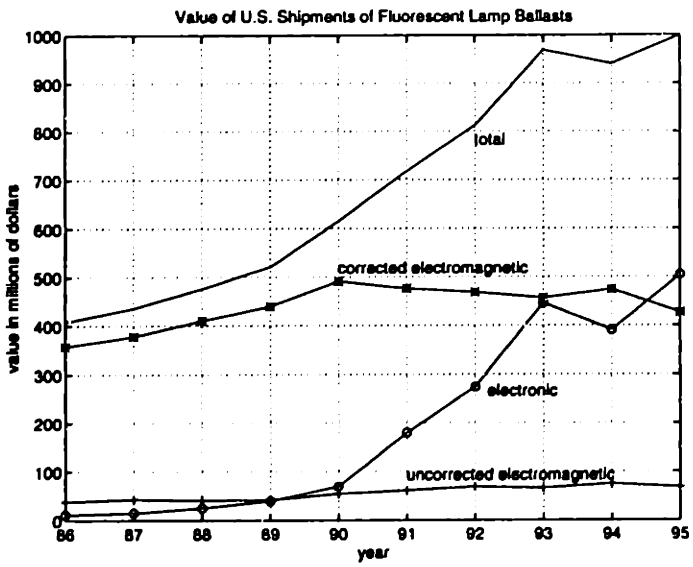

Figure 4-35: Value of U.S. shipments of fluorescent lamp ballasts

with reduced ballast losses and increased lamp efficacy for a total energy savings of around 15 to 20%, resulting in about $2 savings per year in energy costs. With a difference in cost of $6 between electronic and electromagnetic ballasts, the electronic ballast will pay back the difference in just three years (slightly more with interest factored in).

The previous case illustrated the obvious economic advantages of purchasing an electronic ballast over an electromagnetic ballast. However, the payback will be longer in the case of retrofitting old existing ballasts with new electronic ballasts. Since the old ballasts had poor efficiencies, the energy savings per year is greater (about $3 per year). But a major cost factor is the added labor costs for reinstallation which can range from $10 to $20 per ballast [59]. The older electronic ballasts were also much cheaper – about $3 per ballast. So payback is much more difficult to estimate, but a general figure is around 10 years. Government and utility incentives can help motivate the change to electronic ballasts in the future.

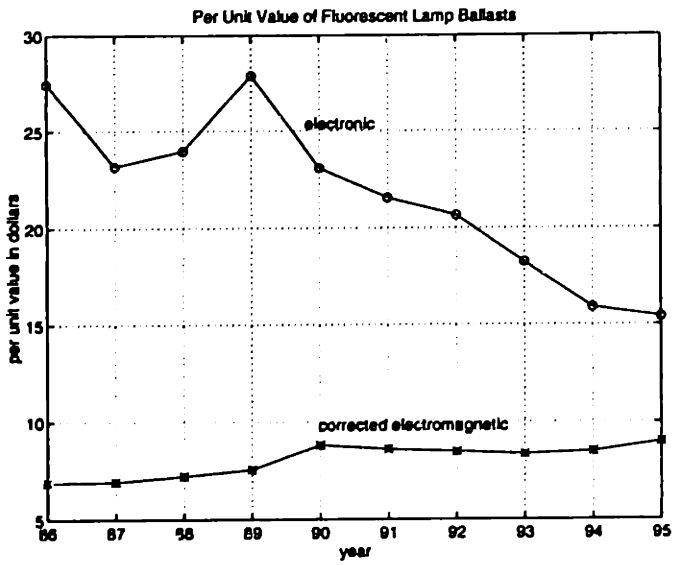

Figure 4-36: Per unit value of U.S. shipments of fluorescent lamp ballasts

4.4.3 Assessment

As the price gap between electronic and electromagnetic ballasts continues to close, electronic ballasts will surely dominate the market. Further advancement in reducing costs in the electronic ballast will be the most important factor driving the market. Additional concerns will involve the reliability of electronic ballasts, although electronic ballasts manufactured today are presumed to be very reliable. There may not be enough economic incentive to replace existing ballasts with new electronic ballasts. But ballast lifetimes are in the order of 20 to 30 years maximum, so the old electromagnetic ballasts already in service will have to replaced eventually. By reducing the cost of electronic ballasts and still further improving efficiencies and performance, the economic advantage of electronic ballasts will be impossible to ignore. Already sales of electromagnetic ballasts are waning, while sales of electronic ballasts are still increasing. Future domination of the ballast market by electronic ballasts is assured.

4.5 Summary

This chapter has described the requirements of the lamp ballast and the various lamp ballast circuits. Because all discharge lamps have a negative voltage to current relationship, ballasts are required to interface the lamp to the utility. The main purpose of the lamp ballast is to limit the lamp current to the desired operating value. The ballast must also provide for lamp ignition.

Electromagnetic ballasts are simple and relatively inexpensive, but tend to be inefficient and bulky. Electronic ballasts offer many advantages over electromagnetic ballasts, such as improved ballast efficiency, improved lamp efficacy, and smaller ballast size. The major disadvantage of electronic ballasts is their high cost.

Most electronic ballasts that exist today are based upon the resonant inverter. It is generally desirable to reduce the size of the ballast for space reasons, as well as to decrease the cost. The size of the filter components can be reduced by raising the switching frequency of the converter. However, the size of the energy storage capacitor cannot be reduced. This represents a fundamental size limitation of the resonant inverter ballast. The resonant inverter ballast also has many series switches and elements that degrade the efficiency of the converter.

The remaining chapters in this thesis describe a completely different approach to the electronic lamp ballast problem. An array of circuit topologies, each with different features and characteristics, is presented. The topologies are evaluated to determine their merits relative to existing ballast topologies.

Chapter 5

Introduction to a New Ballast Approach

A great deal of time was spent studying background material for this thesis. The topic of discharge lamps is a complicated subject that is not well-defined quantitatively. In fact, the invention of the discharge lamp came before much of the understanding of how the invention actually worked. But enough background of the discharge lamp has been presented here to give the reader a good foundational knowledge of the relevant concepts.

Besides the effort made to understand the lamps themselves, a lot of time was spent understanding the ballast technology. This involved understanding the electromagnetic ballasts, and also the electronic ballasts. This in itself is a very broad subject field, and this thesis has attempted to summarize the most important points.

Through knowledge of all this background material, the requirements of the ballast were understood. Initial work in this project involved investigating incremental improvements in existing ballast topologies in terms of efficiency, size, cost, and manufacturability. It became somewhat clear that the existing topologies had been developed quite thoroughly and that small improvements would lead to mediocre gains. Competition is keen in the current electronic ballast market, so the products that have already been developed are well-designed and effectively optimized.

With this in mind, the focus of the project shifted towards inventing totally new

and radically different approaches to the electronic lamp ballast. The ballast industry has focused almost exclusively on the resonant inverter approach. The resonant inverter is itself a very elegant solution to the electronic ballast problem, but it is not without its limitations. Developing new solutions and evaluating their merits relative to existing technology thus became the main focus of the project.

This chapter presents an introduction to the basic concepts behind our approach to the electronic lamp ballast problem. Most of the effort was concentrated on developing circuit topologies for the steady state operation of discharge lamps. The approach is very different than current ballast technology, so inevitably some issues and concerns must be addressed. The following chapters deal with the actual topologies and comparisons to existing ballast topologies.

5.1 Lamp Drive

In formulating a new approach to the electronic lamp ballast problem, it was necessary to both understand current ballast technology, and to *ignore* current ballast technology. By going back to the absolute basics and determining the fundamental requirements of the ballast, a general strategy for the lamp drive was developed which opened up many possibilities for unique circuit implementations.

The main purpose of the ballast is to limit the lamp current to the desired operating value. Furthermore, the radiation efficiency in the lamp discharge is highest for a given power at a constant current. That is, there is an optimum current with which to drive the lamp that yields the highest lamp efficiency. A dc current drive is desirable, but not practical in implementation because of the need for a periodic polarity reversal of the lamp. For these reasons, a square wave of current was selected as the basis for the new ballast topologies.

The frequency of the square wave current drive was selected to be 60 Hz synchronized to the utility. As will be shown in the following chapters, choosing this current drive allows the converter circuitry to be based upon dc-dc conversion techniques. The internal switching frequency of the converter can then be raised as high as possi-

ble to minimize the physical size of the filter elements, while the output at the lamps remains 60 Hz. This is in contrast to the resonant inverter approach where the lamp output is at the fundamental of the converter switching frequency. The resonant inverter switching frequency is then ultimately limited by the tolerable radiated EMI from the lamp.

Having the ballast based upon a dc-dc converter opens up an array of power conversion techniques for optimization. For instance, though the topologies presented here are implemented using basic square-wave converters, at high switching frequencies quasi-resonant conversion can be used [81]. It may be possible to use several interleaved converters operating in parallel, but out of phase, to reduce filter element size and improve efficiency [82]. As a final example, active EMI filtering could be employed to further reduce the filter element size [83]. The main point is that the field of dc-dc converters is rich with techniques for improving converter performance, and our ballast topologies can benefit directly from this knowledge now and in the future.

The 60 Hz square wave of current lamp drive does raise some concerns. Certainly, the 60 Hz square wave drive yields significantly greater lamp efficacy than 60 Hz sinusoidal drives. The 60 Hz square wave achieves the polarity reversal of the lamp while driving the lamp at the optimum value of current. At the optimum dc or square wave current, the efficacy of the arc radiation is at its highest, which is 5 to 10% greater than 60 Hz sinusoidal operation. With fast transitions in polarity, the electron density will not decay, as in the case of 60 Hz sinusoidal operation. There will be no flicker, loss of efficacy, or reignition problems with a suitable square wave drive. However, the question remains as to the efficacy of 60 Hz square wave versus high frequency sinusoidal drive.

The increase in lamp efficacy attributed to high frequency sinusoidal operation is due primarily to the reduction of the anode potential as described in Section 2.3.3. This is heavily dependent upon the type of lamp used. For longer lamps, where the electrode losses are already a small fraction of the total power, the gain in efficacy at high frequencies is slight. For shorter lamps, the gain in efficacy can be substantial

because the electrode potentials represent a significant fraction of the total arc voltage. A square wave at 60 Hz will not be as efficient as a high frequency sinusoidal drive, in general. The absolute difference will depend on the specific application.

In the case of HID lamps, the 60 Hz square wave drive is in many ways the ideal drive. HID lamps do not benefit as dramatically in efficacy, as fluorescent lamps do, from a high frequency drive. The high frequency drive tends to excite acoustic resonances in the arc tube as explained in Section 3.3, which makes high frequency operation of HID lamps extremely difficult. The 60 Hz square wave drive improves the lamp efficacy without compromising the stability of the arc.

5.2 Energy Storage

In the resonant inverter ballast case, the energy storage capacitor must provide a stiff dc voltage for input to the resonant inverter. Any 120 Hz ripple of the capacitor voltage will produce a 120 Hz modulation of the lamp voltage and current unless the ripple is corrected for. The consequence of this requirement is that the capacitor stores a peak energy which is much greater than the energy required for load balancing. For example, a 60 watt converter drawing sinusoidal current from the utility requires a minimum energy storage

$$E_{min} = \frac{P_o}{\omega_{60}} \tag{5.1}$$

$$E_{min} = 160mJ \tag{5.2}$$

With a $40\mu F$ capacitor storing this energy at a nominal voltage of 240 volts, the capacitor voltage will ripple from a minimum of 232 volts to a maximum of 248 volts for a ripple of $\pm 3\%$. The peak energy storage on the capacitor is

$$E_{peak} = \frac{1}{2} C(V_{peak})^2 \tag{5.3}$$

$$E_{peak} = 1.23J \tag{5.4}$$

which is more than 7.5 times the minimum energy storage required for load balancing. This capacitor tends to be physically large and cannot be reduced in size, since the energy storage is essentially just a function of the nominal power of the converter.

There are ancillary issues regarding the sizing of the energy storage capacitor. The capacitor is usually chosen to be an electrolytic capacitor for its capacitance per volume, and must be sized for long lifetime. The lifetime of the capacitor is determined by the drying out of the liquid electrolyte, and is mainly a function of the temperature. So the capacitor must have a low equivalent series resistance (ESR) to minimize the i^2R heating caused by the capacitor ripple currents. But the primary size concern for the capacitor is to minimize the 120 Hz ripple voltage.

As will be seen in the following chapters, this issue of reducing the size of the energy storage capacitor is addressed by our new topologies. This is an important feature of the new topologies because the energy storage capacitor represents a fundamental size limitation of the resonant inverter ballast.

5.3 Isolation

The transformer turns ratio in most electronic ballasts is used in matching the lamp impedance to the inverter impedance. A secondary benefit is the safety isolation provided by the transformer. This transformer represents a significant part of the ballast in terms of size, and also contributes to the losses in the ballast. Our approach to the ballast does not inherently require the use of a transformer, thereby eliminating the need for this component. The question remains as to the safety requirements of the ballast concerning the risk for electric shock.

It has become a popular notion in the ballast industry that transformer isolation is required in a ballast. But this is not the case. In fact, none of the millions of autotransformer-type ballasts in service today are isolated. The Underwriters Laboratories (UL) specification *UL935 Fluorescent-Lamp Ballasts Standard* outlines risk of electric shock measurements [84]. It is possible to design suitable electronic shock protection circuitry in the ballast which meets these specifications without resorting

to the addition of an isolation transformer. Several patents already exist that have employed such electronic protection means [85]. Nevertheless, the elimination of the isolation transformer in our designs remains a concern in the area of tubular fluorescent lamps. Compact fluorescents and HID lamps do not require safety isolation.

5.4 Power Integrated Circuit

A general feature of our approach has been the reduction of the filter element size perhaps at the expense of more semiconductor area and/or a higher number of semiconductor components. These new topologies were developed while keeping in mind the possibility of implementing the ballast as a power integrated circuit (PIC) chip employing both the power semiconductor switches and the associated control circuitry on a single die. For such a PIC solution to be feasible, the semiconductor device losses must be low enough such that the heat generated on the chip can be effectively dissipated. Increasing the converter efficiency is therefore important to the viability of a PIC implementation.

5.5 A Look Ahead

This chapter has presented a general introduction to the basic concepts and motivations for our new ballast approach. These ideas will be more clearly explained in context in the following chapters, which describe the new circuit topologies. Two basic families of circuits are presented. Chapter 6 describes the "series capacitor" type circuit topology, and Chapter 7 describes the "autotransformer" type circuit topology. Chapter 8 describes a topology called the auto UDII which offers the most potential for a viable commercial product.

Chapter 6

Series Capacitor Ballast

This chapter presents a new ballast topology that we have called the series capacitor ballast topology. It is first presented as a simple "black box" so that the basic concepts can be illustrated. Then the circuit implementation is described along with the basic control strategies. The basic topology is given in Section 6.2, and an improved topology is described in Section 6.6. Simulations and prototype results are given. Additional topological forms are presented and ancillary issues and concerns are discussed.

6.1 The Concept

6.1.1 Basic Waveforms and Features

The concept of the series capacitor ballast is presented in Figure 6-1, along with the basic waveforms. As the figure shows, the ballast is simply a "black box" which sits in series between the utility and the lamp. The ballast operates to regulate the lamp current to a 60 Hz square wave synchronized to the utility. Thus for each half cycle, the lamp current and voltage are a constant dc value. Driving the lamp with a square wave of current yields efficacy gains equivalent to dc operation, which are significantly better than 60 Hz sinusoidal operation.

Because there is no shunt path, the lamp current is also the utility current, which

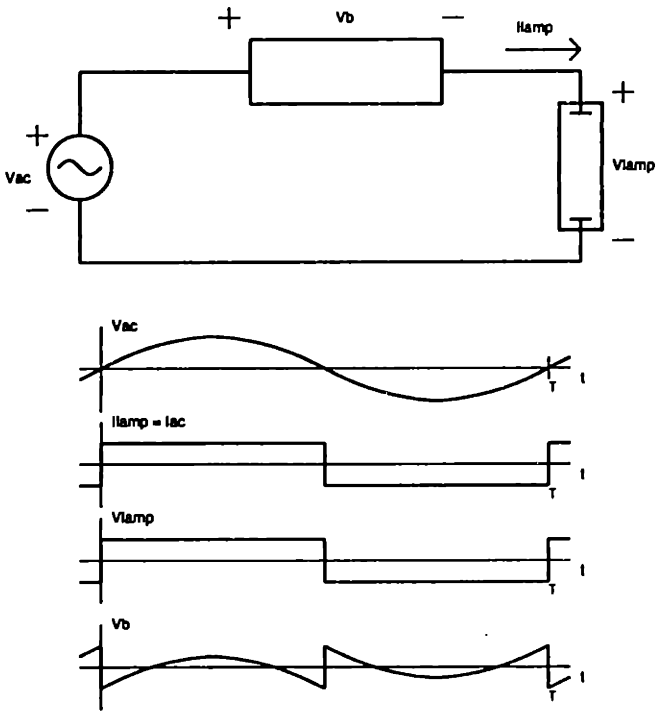

Figure 6-1: Series capacitor ballast basics

means that the utility current is a square wave. This has distortion, but might be acceptable in some applications.

For there to be no net energy storage in the ballast, the average ballast voltage for each half cycle of the 60 Hz waveform must be zero. This requires the lamp voltage to be the average of the utility voltage over a half cycle. (Note that since the ballast designs presented here are in general half cycle symmetric, "averages" refer to averaged values over the half cycle, not the whole 60 Hz cycle.) For a 115 V_{rms} utility, the average over a half cycle is $(2/\pi)\, V_{acpeak}$, which is approximately 100 volts. So this topology is most directly applicable to lamps that operate around 100 volts. Most discharge lamps are designed to have an arc voltage of around 100 volts. The series capacitor ballast design presented here is suitable for driving, for example, a high intensity discharge (HID) lamp since a typical 100 watt HID lamp operates at around 100 volts and 1 amp. Furthermore, the 60 Hz operation avoids the troublesome acoustic resonances encountered at higher frequency drives. But this topology is

certainly not limited to this application.

6.1.2 Load Balancing Energy Storage

The ballast voltage V_b is both positive and negative over one half cycle. Since the current is constant over a half cycle, the ballast is both storing and delivering energy. When the power delivered by the utility is less than that dissipated at the lamp, the ballast must supply the power to the lamp. Similarly, when the utility is supplying more energy than is dissipated at the lamp, the ballast must store the extra energy. This is the concept of load balancing energy storage. Simply stated, something must store or deliver energy to balance the mismatch between the load and utility energies.

Figure 6-2 is a comparison of load balancing requirements for different utility current profiles. The first shows a power factor corrected sinusoidal utility current and the resulting power waveforms. The minimum energy storage required can be seen as E_{in} or E_{out}. This can be calculated to be

$$E_{min_{sin}} = \frac{P_o}{\omega_{60}} \tag{6.1}$$

Where P_o is the average power of the utility (the power delivered to the load) and ω_{60} is the radian frequency of the 60 Hz utility. This is the minimum energy storage for load balancing for sinusoidal utility current. Typical electronic ballasts store eight times this energy or more in the dc bus capacitor. The energy flowing in and out of the capacitor must be a small fraction of the total energy stored in the capacitor in order for the voltage ripple to be small.

The second utility current profile in Figure 6-2 is a square wave current, which is a constant value over a half cycle. Again, the minimum energy storage is E_{in} or E_{out}. This can be calculated as

$$E_{min_{sq}} = \frac{P_o}{\omega_{60}} \left[\pi(\cos(\sin^{-1}\frac{2}{\pi}) - 1) + 2(\sin^{-1}\frac{2}{\pi}) \right] \tag{6.2}$$

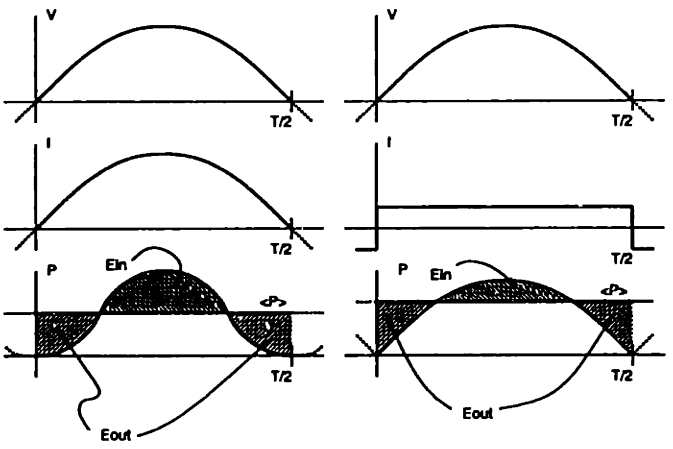

Figure 6-2: Load balancing energy storage — sinusoidal versus square wave current

Evaluating the expression gives

$$E_{min_{sq}} = 0.66 \frac{P_o}{\omega_{60}} \tag{6.3}$$

The minimum energy storage requirement of the square wave current profile is roughly two thirds the minimum required in the sinusoidal case. As will be seen in the following sections, the series capacitor topology can achieve the absolute minimum energy storage, which is even less than the minimum for power factor corrected waveforms. This is a great advantage over electronic ballasts based on the resonant inverter, where the energy storage in the capacitor can be eight times $E_{min_{sin}}$ or more.

6.2 Implementation

Up until now, the series capacitor ballast has only been shown as a "black box". Figure 6-3 begins to show what is required in the black box. A capacitor C_e is used for the energy storage element and is used as the input to a high frequency dc-dc converter. The high frequency dc-dc converter shapes the current to the desired value and is also needed because the ballast voltage V_b will not, in general, be equal to the capacitor voltage. So a voltage converter interface is required between the

energy storage capacitor and the rest of the circuit. The high frequency converter consists of two switches operated at high frequency and a single filter inductor.

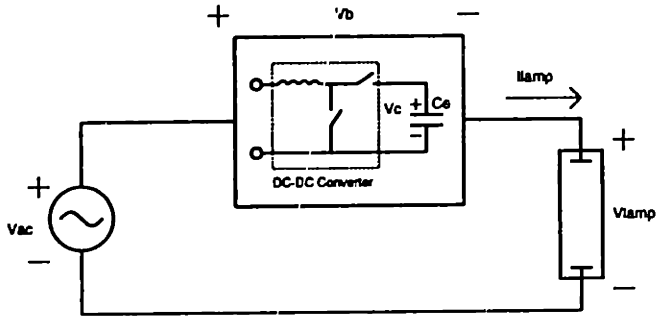

Figure 6-3: First step in implementing the series capacitor ballast

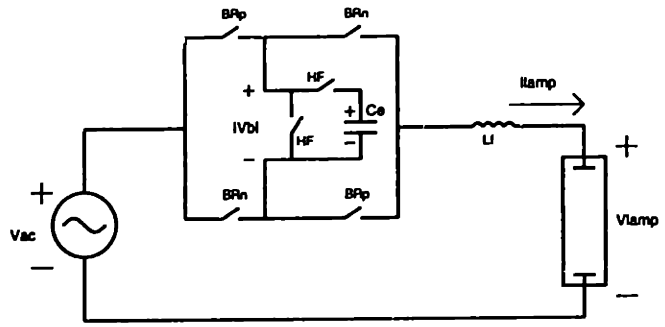

Figure 6-4: Series capacitor final topology

The next step in implementing the series capacitor topology is shown in Figure 6-4. Since the energy storage capacitor will typically be implemented with an electrolytic capacitor (which can support voltages of only one polarity), the output of the high frequency dc-dc converter will be limited to positive voltages. The required ballast voltage has both positive and negative voltages over a half cycle, so a low frequency bridge with four switches is needed for polarity reversal of the dc-dc converter output. Thus, the high frequency dc-dc converter has an input that is the energy storage capacitor voltage C_e, and two high frequency switches each labeled HF which work to regulate the lamp current to the desired value. Four low frequency bridge switches

are used to change the polarity of the dc-dc converter output. The dc-dc converter, which can generate only positive voltages, produces the absolute value of the ballast voltage V_b, and the four bridge switches change the polarity with respect to the lamp and utility as required. If the two switches labeled BRp are on, the output of the converter is positive, and if the two switches labelled BRn are on, the output of the converter is negative. Here the polarity of the ballast voltage is defined with the positive end connected to the utility, and the negative end connected to the filter inductor as shown in Figure 6-3. The filter inductor Lf for the dc-dc converter is placed outside the bridge in series with the lamp, since changes in the direction of the bridge during a half cycle force the inductor current to undergo step changes if the inductor is inside the bridge. All switches must carry bidirectional current and support unipolar voltage.

Some important waveforms are shown in Figure 6-5 over a half cycle. The ballast voltage V_b is the difference between the utility voltage and lamp voltage, the absolute

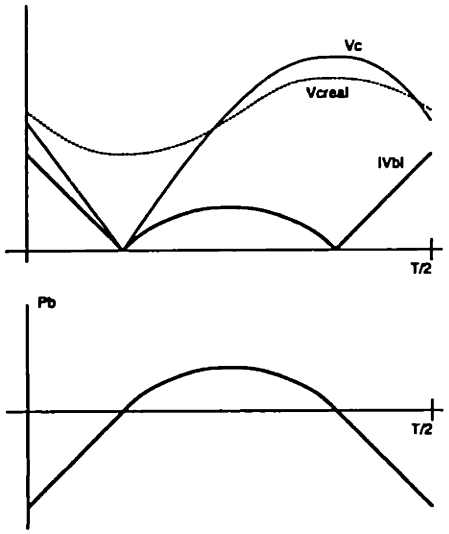

Figure 6-5: Series capacitor waveforms

value of which is shown on the first graph. The ballast power P_b is the product of the ballast current (same as the lamp current and a constant value over a half cycle) and the ballast voltage and is shown on the second graph. The capacitor voltage can be

calculated from the load balancing energy storage relationships as follows. The power delivered to the lamp P_o is the average of the utility voltage times the constant lamp current.

$$P_o = \frac{2}{\pi} V_{acpeak} I \tag{6.4}$$

The difference between the utility power and lamp power is defined as Δp.

$$\Delta p = V_{acpk} I \sin(\omega_{60} t) - \frac{2}{\pi} V_{acpeak} I \tag{6.5}$$

$$\Delta p = \frac{\pi}{2} P_o \sin(\omega_{60} t) - P_o \tag{6.6}$$

The ballast power is equal to Δp.

$$P_b = \Delta p \tag{6.7}$$

The load balancing energy can be found by integrating Δp,

$$E(t) = \int \Delta p \, dt \tag{6.8}$$

$$E(t) = -\frac{\pi}{2} \frac{P_o}{\omega_{60}} \cos(\omega_{60} t) - P_o t + K \tag{6.9}$$

where K is a constant of integration accounting for non-zero initial energy at $t = 0$.

The load balancing energy is stored in the capacitor, so the capacitor voltage may be calculated.

$$E(t) = \frac{1}{2} C V_c^2 \tag{6.10}$$

$$V_c(t) = \sqrt{\frac{2}{C} E(t)} \tag{6.11}$$

$$V_c(t) = \sqrt{\frac{2}{C} (-\frac{\pi}{2} \frac{P_o}{\omega_{60}} \cos(\omega_{60} t) - P_o t + K)} \tag{6.12}$$

If, at the beginning of the cycle, the energy on the capacitor is one half $E_{min_{sq}}$ and the starting voltage is $V_c(0)$, then the capacitor voltage waveform will look like V_c on the first graph in Figure 6-5. For the first portion of the cycle when P_b is negative,

half of $E_{min_{sq}}$ is taken out of the capacitor and V_c reaches zero. For the next portion of the cycle when P_b is positive, $E_{min_{sq}}$ is stored on the capacitor, bringing V_c to a peak voltage of $\sqrt{2}$ times $V_c(0)$. For the last portion of the cycle when P_b is negative, again half of $E_{min_{sq}}$ is taken out of the capacitor bringing V_c back $V_c(0)$. The peak energy storage is exactly the minimum required for load balancing, $E_{min_{sq}}$.

If the starting voltage of the capacitor is greater than $|V_b(0)|$ then V_c is greater than $|V_b|$ for the entire half cycle. Under this condition, down conversion from V_c to $|V_b|$ is all that is required of the high frequency dc-dc converter. So the down converter generates $|V_b|$ from V_c and the bridge does the necessary unfolding so the circuit sees V_b.

Using the starting voltage $V_c(0)$ or the peak voltage $\sqrt{2}\,V_c(0)$ as a design parameter, the minimum capacitance required can easily be determined. The peak capacitor voltage will be limited by the voltage rating of the switches. As an example, for a 100 W lamp with $V_{lamp} = 100$ V and $I_{lamp} = 1$ A,

$$E_{min_{sq}} = 0.66\,\frac{100}{\omega_{60}} = 175\,mJ \tag{6.13}$$

Choosing the peak capacitor voltage to be 200 V for 200 V devices, the capacitor will store exactly $E_{min_{sq}}$ at its peak voltage.

$$V_{cpeak} = \sqrt{\frac{2}{C_{min}}175\,mJ} = 200\,V \tag{6.14}$$

$$C_{min} = 8.75\,\mu F \tag{6.15}$$

And $V_c(0)$ is 141 V which is greater than $V_b(0)$ ($V_b(0) = 100$ V).

In actual designs, the capacitor voltage should have some safety margin so that V_c does not go below zero or above the device rating. This is achieved in practice by using a capacitance larger than the minimum and/or starting the cycle with greater than one half $E_{min_{sq}}$ in the capacitor. The actual capacitor waveform, V_{creal}, will be something like that illustrated in Figure 6-5.

6.3 Control Strategy

The general control strategy for the series capacitor ballast is shown in Figure 6-6. A fast feedback loop regulates the lamp current to a desired value. A unique requirement of this control is that the correct value of the desired current must be determined. Because of the series topology, the lamp must be driven with the specific value of current such that there is no net energy stored or dissipated in the ballast. The desired current is that which makes V_{lamp} equal to the average of the utility voltage, and is determined by the slow feedback loop.

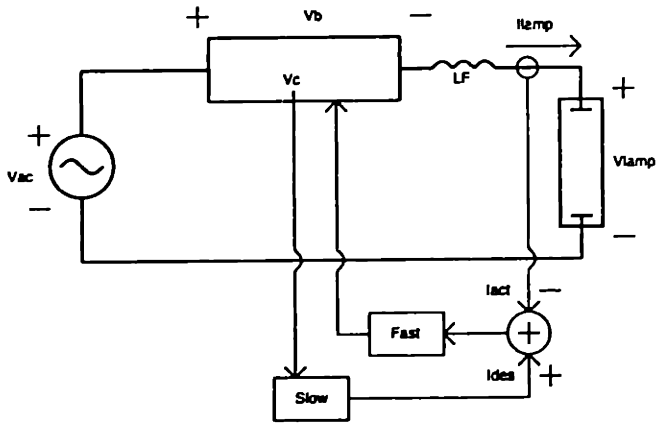

Figure 6-6: Series capacitor control strategy

6.3.1 Fast Feedback Compensation

Compensation of the fast feedback loop is relatively straightforward. At the loop cross-over frequency, the capacitor is essentially a constant source. Let the continuous duty ratio d indicate the on time of the high frequency switch in series with the capacitor. Furthermore, allow d to vary from $+1$ to -1 with a change of sign indicating a change in the direction of the bridge so that $d \times V_c = V_b$. The entire bridge and dc-dc converter can be replaced by a single voltage source equal to the continuous duty ratio times the capacitor voltage. By looking at incremental quantities, the incremental linearized averaged model can be derived as shown in Figure 6-7 for a

single filter inductor. R_o is the magnitude of the negative impedance of the lamp evaluated around its dc operating point. For a 100 watt HID lamp, this impedance is around 25 to 50 ohms. The input is shown as $\tilde{d}V_c$, the incremental continuous duty ratio times the capacitor voltage V_c. V_c varies at 120 Hz, but can be considered a constant for purposes of analysis. The range of variation of V_c must be taken into account for stability analysis since the loop gain will vary proportionally with variations in V_c. Because the fast feedback will be implemented with pulse width modulation control, techniques can be used to compensate for this variation in gain.

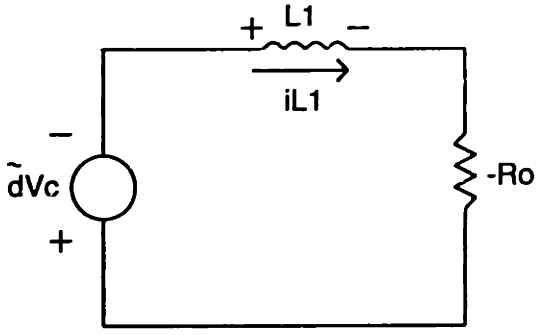

Figure 6-7: Series capacitor incremental linearized averaged model

Without any feedback, the transfer function from duty cycle to inductor current is

$$\frac{iL_1}{\tilde{d}} = \frac{-V_c}{sL_1 - R_o} \tag{6.16}$$

This has a pole at

$$s = \frac{R_o}{L_1} \tag{6.17}$$

which is in the right half plane and the system is unstable. This can be stabilized by adding a term to $\tilde{d}$ proportional to iL_1. If $\tilde{d}$ is replaced by $\tilde{d} - K_1 iL_1$ then transfer function becomes

$$\frac{iL_1}{\tilde{d}} = \frac{-V_c}{sL_1 - R_o - V_c K_1} \tag{6.18}$$

For stability, the pole must be in the left half plane.

$$s = \frac{R_o + K_1 V_c}{L_1} < 0 \tag{6.19}$$

$$K_1 < -\frac{R_o}{V_c} \tag{6.20}$$

By appropriate choice of K_1 the system can be stabilized at the desired control loop bandwidth, providing regulation of the lamp current to a desired value.

The use of higher order filters can result in an overall reduction of the filter size. However, this comes at the price of more complexity in the control loop compensation. For a third order LCL-type filter, it is generally necessary to feedback on more than one state variable to achieve regulation and stability.

6.3.2 Slow Feedback Compensation

If the bandwidth of the slow loop is much smaller than that of the fast loop, both loops can be compensated independently. The slow loop must determine the desired current such that there is no net energy stored or lost in the ballast, i.e., the power delivered by the utility is the same as the power dissipated in the lamp.

The strategy of the slow loop is to sample V_c at the beginning of every cycle (either 120 Hz or 60 Hz) and compare it to a nominal value. If the sampled V_c is larger than the nominal, then there is a net storage of energy in the capacitor and the desired value of current should be adjusted accordingly. If there is net storage, this implies that V_{lamp} is less than $<V_{ac}>$ and I_{lamp} should be decreased, resulting in an increase in V_{lamp} due to the negative impedance of the lamp. Conversely, if the sampled V_c is smaller than the nominal value, then the lamp current should be increased.

Since the change in desired current will be proportional to the difference between the sampled capacitor voltage and a nominal voltage, all relevant quantities for analysis are discrete. All information must be examined on a cycle by cycle basis (or half cycle, whichever is the sampling interval). A quick derivation of feedback analysis for the slow loop is presented here.

On a cycle by cycle basis, we can deal with averaged power. If the lamp and utility current is a constant I, then

$$< P_{ac} > = < V_{ac} > I \tag{6.21}$$

$$< P_{lamp} > = < V_{lamp} > I = V_{lamp} I \tag{6.22}$$

In the region of interest, the lamp v-i characteristic can be described as a straight line

$$V_{lamp} \approx I_{lamp}(-R_o) + V_o \tag{6.23}$$

where V_o is the voltage axis intercept at zero current. Since the model is being linearized around the dc operating point, V_o can be calculated to be

$$V_o = V_{nom} + I_{nom} R_o \tag{6.24}$$

where V_{nom} and I_{nom} are the nominal dc operating voltage and current for the lamp. The average lamp power as a function of the lamp current is then

$$< P_{lamp} > = I_{lamp}^2(-R_o) + I_{lamp} V_o \tag{6.25}$$

$$< P_{lamp} > = I^2(-R_o) + I(V_{nom} + I_{nom} R_o) \tag{6.26}$$

The energy quantity of interest is the difference between the energy delivered by the utility and the energy dissipated in the lamp.

$$\Delta E(t) = E_{ac}(t) - E_{lamp}(t) \tag{6.27}$$

The utility and lamp energies are the integral of the power.

$$\Delta E(t) = \int \Delta P(t)\, dt \tag{6.28}$$

$$\Delta E(t) = \int (< P_{ac} > - < P_{lamp} >)\, dt \tag{6.29}$$

$$\Delta E(t) = \int \{ < V_{ac} > \ I - [I^2(-R_o) + I(V_{nom} + I_{nom}R_o)] \} \, dt \tag{6.30}$$

Since averaged quantities are being used for power, equation 6.30 is only valid at discrete intervals at each sampling instant. This will be taken into account later in the analysis.

Since the controlling parameter is the current I, we replace I with $I + \tilde{i}$ to model the changes in energy in response to incremental perturbations in current. Looking again at the power,

$$\Delta P + \Delta \tilde{p} = < V_{ac} > \ (I + \tilde{i}) - [(I + \tilde{i})^2(-R_o) + (I + \tilde{i})(V_{nom} + I_{nom}R_o)] \tag{6.31}$$

expanding this expression,

$$\Delta P + \Delta \tilde{p} = < V_{ac} > \ (I + \tilde{i}) - [(I^2 + 2I\tilde{i} + \tilde{i}^2)(-R_o) + (I + \tilde{i})(V_{nom} + I_{nom}R_o)] \tag{6.32}$$

and finally linearizing,

$$\Delta \tilde{p} = < V_{ac} > \ \tilde{i} - [2I\tilde{i}(-R_o) + \tilde{i}(V_{nom} + I_{nom}R_o)] \tag{6.33}$$

we arrive at the final linearized expression for $\Delta \tilde{p}$ as a function of $\tilde{i}$.

$$\Delta \tilde{p} = \tilde{i} [\underbrace{< V_{ac} > \ + 2IR_o - (V_{nom} + I_{nom}R_o)}_{constant\ A}] \tag{6.34}$$

$$\Delta \tilde{p} = A\tilde{i} \tag{6.35}$$

The constant A is a function of the iamp parameters, the utility voltage, and the driving lamp current.

Now the effects of incremental perturbations in current to the system energy can be modeled.

$$\Delta \tilde{e}(t) = \int A\tilde{i} \, dt \tag{6.36}$$

A simple system diagram is shown in Figure 6-8. Since all system variables are

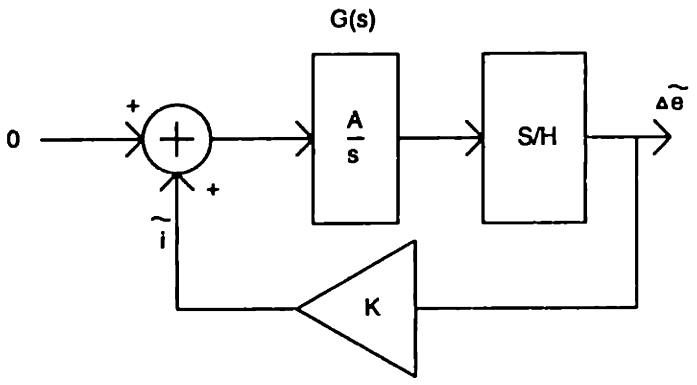

Figure 6-8: Slow loop continuous energy model

step functions, we perform a step invariant transform on the continuous time system to convert it to a discrete time system. This is done by sampling the continuous time system step response. The continuous time step response to the system in the frequency domain is given by

$$Y(s) = G(s)\frac{1}{s} \tag{6.37}$$

$$Y(s) = \frac{A}{s}\frac{1}{s} \tag{6.38}$$

In the time domain the response is

$$y(t) = tA \tag{6.39}$$

Sampling this with period T gives

$$y(nT) = nTA \tag{6.40}$$

Taking the z-transform, the plant transfer function can be found.

$$Y(z) = \frac{TAz^{-1}}{(1-z^{-1})^2} = G(z)\frac{1}{1-z^{-1}} \tag{6.41}$$

$$G(z) = \frac{TAz^{-1}}{1-z^{-1}} \tag{6.42}$$

This discrete time system is shown in Figure 6-9. However, the discrete time system

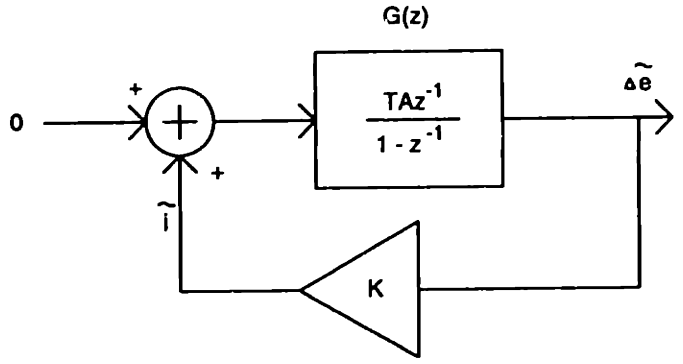

Figure 6-9: Slow loop discrete energy model

shown in Figure 6-9 models the effects of changing current on energy. Since the slow loop gathers energy information directly from sampling the capacitor voltage, a linearized relationship between energy and capacitor voltage must be found in order to complete the system model.

In the control loop, the change in energy is represented as

$$\Delta e = \underbrace{(E_{ac} - E_{lamp})}_{E_{act}} - E_{nom} \tag{6.43}$$

This is the change in energy from a nominal reference point as a function of the utility and lamp energies. Defining a change in capacitor voltage as

$$\Delta V_c = V_{cnom} - V_c(nT) \tag{6.44}$$

the linearized relationship between energy and capacitor voltage expressed as deviations from a nominal reference can be found.

$$\Delta e = E_{act} - E_{nom} \tag{6.45}$$

$$\Delta e = \frac{1}{2} C(V_c(nT)^2 - V_{cnom}^2) \tag{6.46}$$

$$\Delta e = \frac{1}{2} C \underbrace{(V_c(nT) + V_{cnom})}_{\approx 2V_{cnom}} \underbrace{(V_c(nT) - V_{cnom})}_{-\Delta V_c} \tag{6.47}$$

The constant relating changes in energy to changes in capacitor voltage is

$$\frac{\Delta e}{\Delta V_c} = -CV_{cnom} \tag{6.48}$$

which obviously depends on the capacitance and the starting voltage. This scale factor can be included in the system model in Figure 6-9 by dividing $G(z)$ by $-CV_{cnom}$ and by multiplying K by $-CV_{cnom}$. The final system is shown in Figure 6-10 with the feedback gain represented as a new constant M. The final system transfer function is

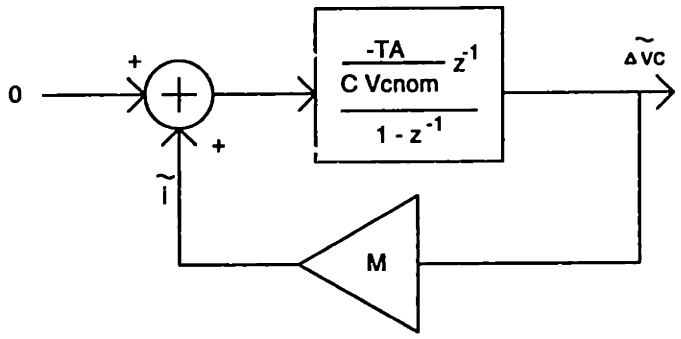

Figure 6-10: Slow loop discrete voltage model

$$\frac{v_c}{i} = \frac{(-\frac{TA}{CV_{cnom}})z^{-1}}{1 - [1 - M\frac{TA}{CV_{cnom}}]z^{-1}} \tag{6.49}$$

The pole is at

$$z = 1 - M\frac{TA}{CV_{cnom}} \tag{6.50}$$

The range of gain M which gives a damped response is given by

$$0 < M < \frac{CV_{cnom}}{TA} \tag{6.51}$$

Finally, an equivalent time constant can be found by examining the discrete impulse

response of the system.

$$\tau_{eff} = -\frac{T}{\ln(1 - M\frac{TA}{CV_{cvnom}})} \tag{6.52}$$

By appropriate choice of gain, the fast loop can be stabilized at a bandwidth higher than 60 Hz and lower than the switching frequency. The slow loop bandwidth should be much slower than the fast loop to allow for each loop to be compensated separately. With the addition of higher order filtering and a loop filter, stability becomes a much more complex problem.

6.4 Series Capacitor Simulations

This section presents some basic simulations of the series capacitor topology. Basic designs are presented and stability of the control loops are verified.

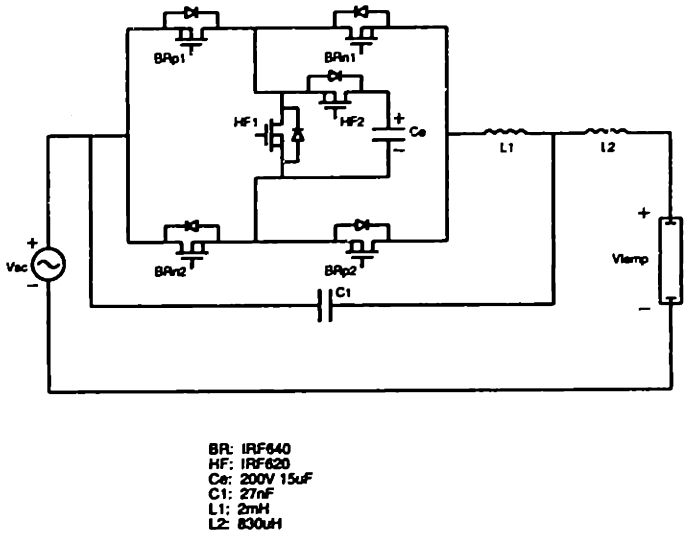

Figure 6-11: Series capacitor ballast with third order filter

A basic design of a series capacitor ballast is shown in Figure 6-11, with component values indicated. This particular design illustrates the use of a third order filter, instead of a single filter inductor. Note that the connection of the filter components is chosen so that high frequency currents are shunted away from the lamp and the

utility, and remain circulating through the converter. Switches with a voltage rating of 200 volts are used, and the energy storage capacitor is 15 μF.

The application chosen was for a 100 watt HID lamp that operates nominally at 100 volts and 1 amp. There have been attempts in the literature to model the terminal characteristics of discharge lamps, but the models have all been extremely complicated [86, 87, 88, 89, 90]. For purposes of these simulations, a 100 watt HID lamp was operated to determine the negative resistance around its nominal operating point. Then a dynamic model of the i-v characteristics was constructed from a fifth order polynomial that included this nominal operating point and negative resistance. To complete the model, it was assumed that the lamp would have a positive resistance characteristic during polarity changes. The i-v plot of the 100 watt HID lamp model is shown in Figure 6-12.

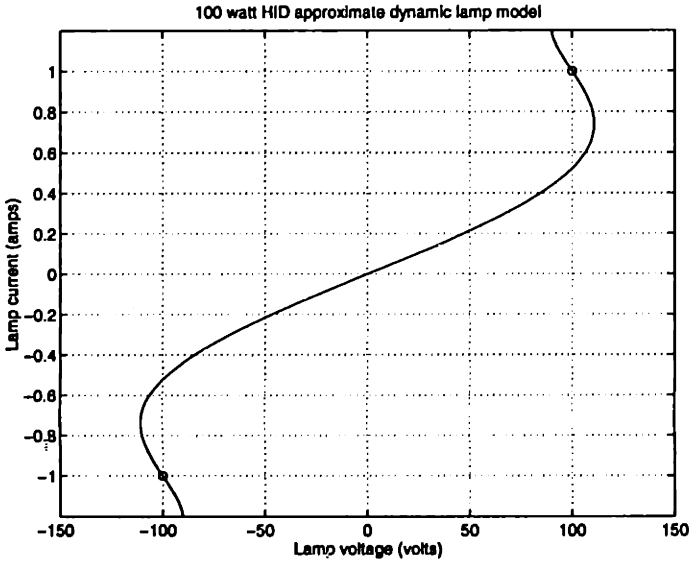

Figure 6-12: Approximate dynamic model of 100 watt HID lamp

The results of large signal averaged model simulations performed on *Simulink* are shown in Figures 6-13– 6-15. The third order filter requires additional feedback for stability, compared to the single inductor filter case. Two feedback gains are used on the two inductor currents to modify the duty cycle in the fast loop. The voltage on the energy storage capacitor is sampled at the beginning of every 60 Hz cycle and

compared to a nominal reference of 150 V. The difference is multiplied by a gain and added to a nominal reference of 1 A to generate the desired lamp current in the slow feedback loop. The filter is designed to limit the output current switching frequency ripple to $\pm$ 1%.

From the simulation results, it can be seen that the lamp is driven with a 60 square wave of current. The capacitor voltage is chosen to be a nominal 150 volts, about which the voltage ripples from a minimum of 104 volts to a maximum of 185 volts. The peak energy storage in the capacitor is only 1.5 times the theoretical minimum of $E_{min_{sq}}$ for square wave current. And in fact, the peak energy storage is equivalent to $E_{min_{sin}}$, which is the minimum for sinusoidal current.

The power profile in the lamp is essentially dc, which is desirable for HID lamp operation. With significant ac power components, acoustic resonances can be excited in the arc tube, causing arc instability. These simulations verified the stability of the control loop compensation. Of particular importance is the ability of the slow loop control to determine the proper operating current so that the ballast stores zero net energy.

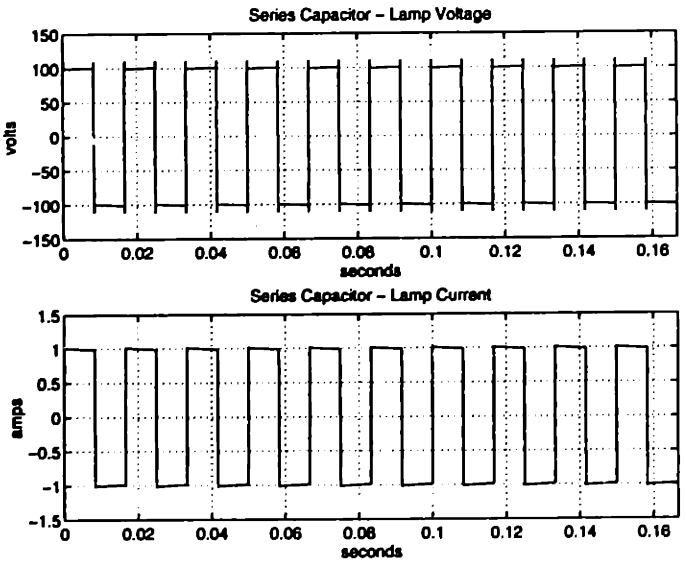

Figure 6-13: Averaged model simulations of series capacitor ballast— lamp voltage and current

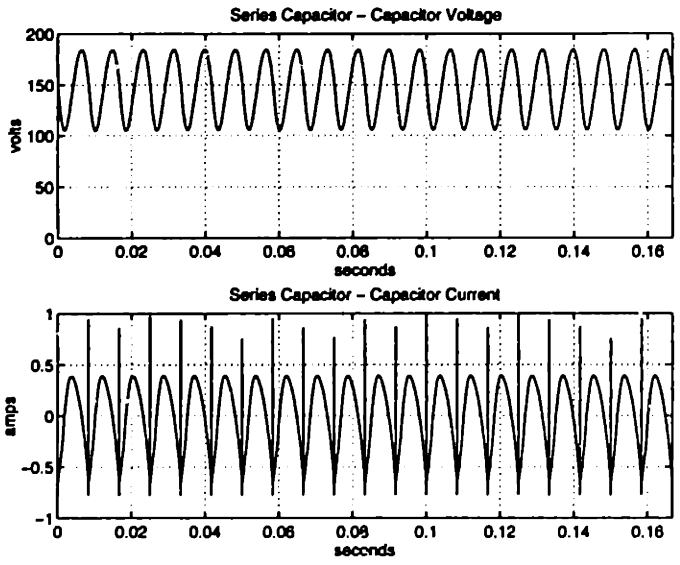

Figure 6-14: Averaged model simulations of series capacitor ballast— capacitor voltage and current

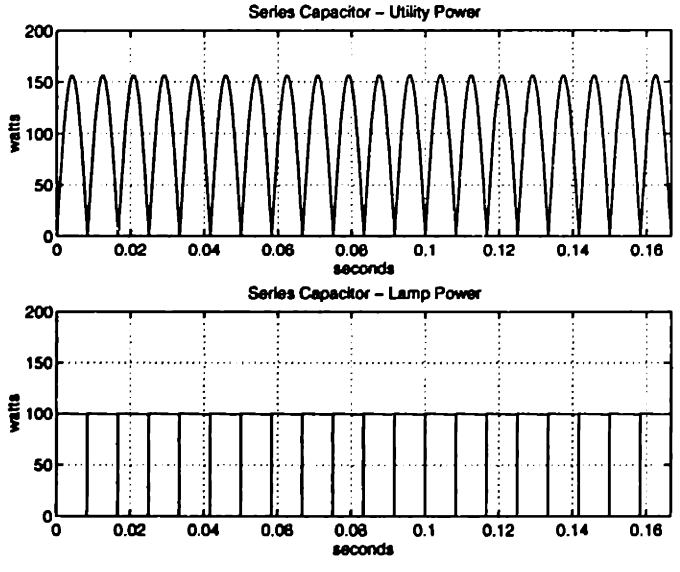

Figure 6-15: Averaged model simulations of series capacitor ballast— utility and lamp power

Some switching simulations are shown in Figure 6-16 and Figure 6-17. The converter switching frequency is 100 kHz. These simulations were done for a simplified series capacitor topology employing a single 20 mH filter inductor. The behavior of the switching simulations is similar to that of the averaged model simulations. Note that the capacitor voltage has a slight first order transient until the proper steady state lamp current value is determined to balance the power at the lamp and at the utility. The high frequency ripple current is approximately ±2%.

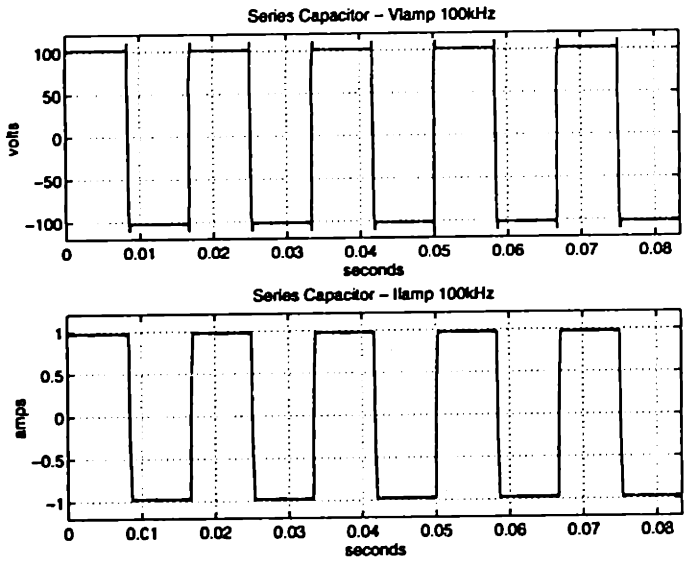

Figure 6-16: Switching frequency simulations of series capacitor ballast— lamp voltage and current

6.5 Series Capacitor Prototype Implementation

This section describes the series capacitor prototype that was built and evaluated. Comparisons between predicted efficiency and measured efficiency are given.

6.5.1 Series Capacitor Circuit

A basic prototype was designed as shown in Figure 6-18. The main purpose of the prototype was to verify the circuit concept under steady state operation. This focused

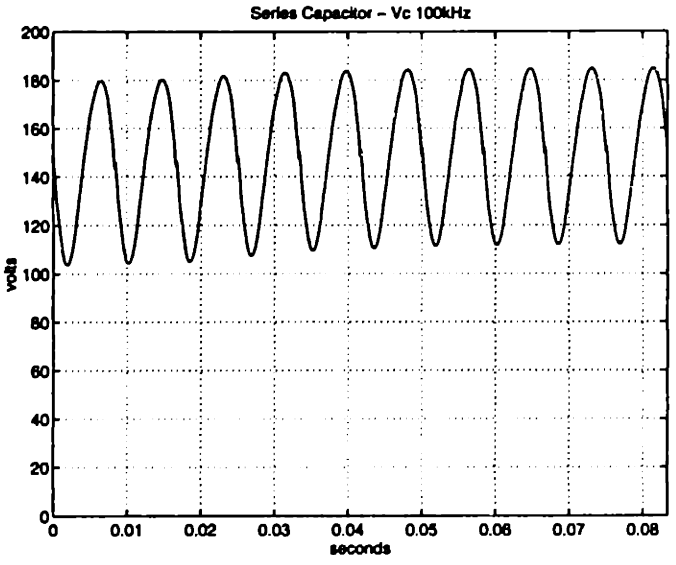

Figure 6-17: Switching frequency simulations of series capacitor ballast— capacitor voltage

on the verification of the analysis and design, including stability of the control loops and the prediction of efficiency. The other reason was simply to gain experience in building and operating a working topology.

The energy storage capacitor is a Philips 2222–118 electrolytic capacitor rated at 15 μF and 200 V. Two parallel capacitors were used in the prototype to limit excessive voltages during startup transients. The actual measured capacitance is 14 μF at 120 Hz, and 9.2 μF at 100 kHz. The ESR is 2.32 ohms at 120 Hz and 0.54 ohms at 100 kHz.

The inductor is a Magnetics D-44229-40 ferrite pot core gapped to an AL value of 400 (the gap is 0.034 inches). The inductance of 20 mH is obtained by 227 turns of AWG22 magnet wire. The dc resistance of the winding is 1.04 ohms.

Since the load voltage is fundamentally limited to the average of the utility voltage, a 250 ohm, 250 watt power potentiometer was adjusted to a value of 115 ohms to yield 100 watts at its operating voltage.

The high frequency dc–dc converter consists of two switches operating at 100 kHz. Each switch is an IRF620 power MOSFET (200 V, 0.8 ohms). Because the body

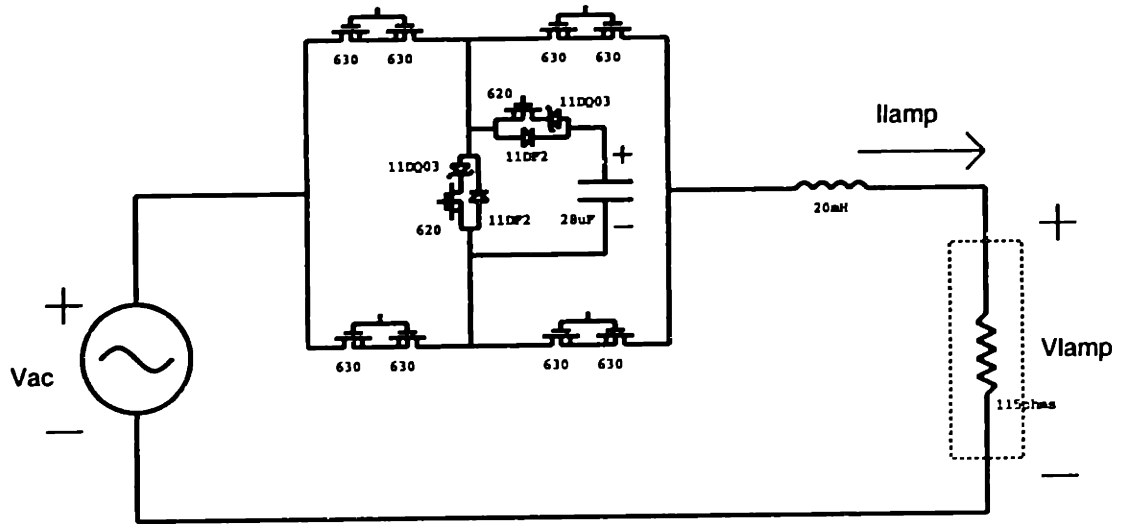

Figure 6-18: Series capacitor circuit prototype

diodes of these MOSFETs are too slow for this application, IRF11DF2 ultra-fast rectifiers (200 V_{off}, 1 A, 0.98 V_{on}, τ_{rr} = 35 ns) are connected antiparallel to the MOSFETs. To prevent reverse currents from conducting through the MOSFET body diode, IRF11DQ03 Schottky diodes (30 V_{off}, 1.1 A, 0.5 V_{on}) are connected in series with the MOSFETs.

Initially, the four bridge switches were intended to be implemented with IRF630 MOSFETs. However, because the MOSFETs have an inherent antiparallel body diode, a switch that is meant to be "off" is not really "off" unless there is a reverse bias on the body diode. During the times when the high side switch in the dc–dc converter is off, the capacitor is disconnected from the circuit and there is no reverse bias on the body diodes of the bridge switches. Current can flow through the bridge diodes of the "off" MOSFETs, instead of through the dc–dc converter. This causes problems with reverse recovery, since the body diodes of the MOSFETs are too slow for this application. Because of this, each bridge switch is implemented with two IRF630 MOSFETs with sources and gates connected together. When the switch is turned off, no current can conduct through the body diodes.

6.5.2 Series Capacitor Prototype Efficiency

Initially, the converter was operated in a dc mode. The was accomplished by shorting the utility voltage terminals and connecting a voltage source across the energy storage capacitor. The inductor current was sensed via a 0.5 ohm sense resistor placed inside the bridge in series with the dc-dc converter.

Figure 6-19 shows the output voltage across the load resistor with a dc input voltage of 150 volts. The output voltage is a 60 Hz square wave at approximately 111 volts amplitude. The high frequency current ripple is approximately $\pm$ 1%.

This operation verified the stability of the control loop regulating the load current to the desired value. It should be noted that the load is a positive resistance, instead of an actual discharge, and the stability of the control loops is easier to achieve. When driving an actual lamp, the control loops would have to be modified.

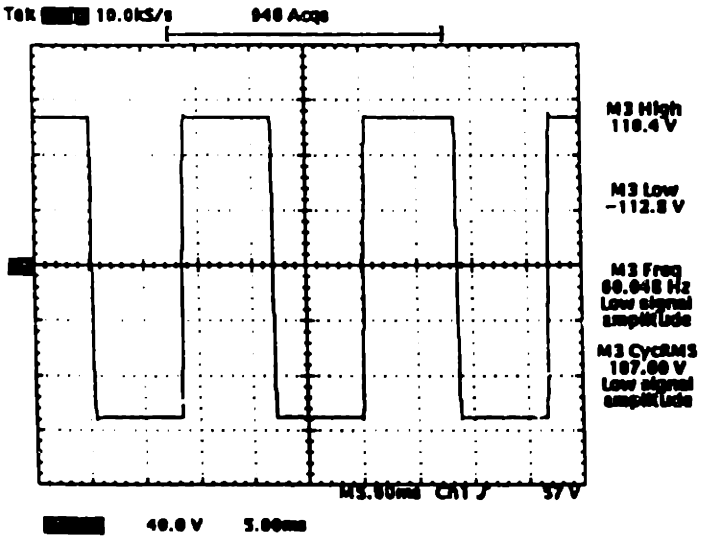

Figure 6-19: Output voltage — dc mode operation

The efficiency of the circuit was measured under various input voltages. The results are shown in Table 6.1. The measured losses are very close to the predicted losses considering the accuracy of the measurements. The predicted losses were obtained from calculations based upon results from the averaged model simulations.

The predicted losses break down as shown in Table 6.2. Numbers are shown for a variety of input voltages. There are a few components to the high frequency switching

Vin	130V	140V	150V	160V
Pin	101.4W	102.2W	105.0W	107.2W
Pdiss	4.1W	3.2W	4.3W	4.0W
Efficiency	**95.9%**	**96.9%**	**95.9%**	**96.3%**
Predicted dissipation	4.2W	4.4W	4.6W	4.7W
Predicted efficiency	**95.9%**	**95.8%**	**95.7%**	**95.7%**

Table 6.1: Measured versus predicted efficiencies

Vin	130V	140V	150V	160V
Pin	101.4W	102.2W	105.0W	107.2W
crossover	0.2444W	0.2688W	0.2940W	0.3168W
FET capacitance	0.0494W	0.0552W	0.0612W	0.0675W
diode capacitance	0.0988W	0.1104W	0.1225W	0.1349W
parasitic inductance	0.0012W	0.0012W	0.0012W	0.0012W
HF conduction	1.1334W	1.1592W	1.1838W	1.1926W
bridge conduction	1.2724W	1.3271W	1.3830W	1.4113W
EMI	0.8836W	0.9216W	0.9604W	0.9801W
reverse recovery	0.4277W	0.4704W	0.5145W	0.5198W
total dissipation	4.1109W	4.3142W	4.5206W	4.6242W
predicted efficiency	95.9%	95.8%	95.7%	95.7%

Table 6.2: Predicted losses

losses in the dc-dc converter. The first is a crossover loss at turn-on of the series switch:

$$E = \frac{1}{2} V_c I t_{on} \tag{6.53}$$

The voltage being switched is the capacitor voltage and the current being switched is the load current. The time t_{on} is a function of the ability of the gate drive to deliver the required charge to enhance the MOSFET. There is a loss associated with discharging the MOSFET parasitic capacitance at turn on:

$$E = \frac{4}{3} [\frac{1}{2} C_f \sqrt{V_f} (V_c)^{\frac{3}{2}}] \tag{6.54}$$

C_f is the MOSFET output capacitance defined at a voltage V_f. V_c is the voltage on the capacitance being discharged. There is a loss associated with charging the shunt (diode) switch capacitance:

$$E = \frac{8}{3}[\frac{1}{2} C_d \sqrt{V_d} (V_c)^{\frac{3}{2}}] \tag{6.55}$$

C_d is the diode capacitance defined at a voltage V_d. At turn off there is one loss due to the energy stored in the parasitic inductance formed by the capacitor, series switch, shunt switch loop:

$$E = \frac{1}{2} L_p I^2 \tag{6.56}$$

The other losses in the circuit include the gate drive energy of the high frequency switches:

$$E = Q_g V_s \tag{6.57}$$

Q_g is the gate charge, and V_s is the supply voltage of the charging circuit. There are two switches, so the energy per switching event is two times $Q_g V_s$.

These losses are energy losses at each switching event. To calculate the power loss, the energy must be multiplied by the switching frequency.

The other sources of loss in the switches include the i^2R conduction losses in the high frequency switches and the conduction losses in the bridge switches. Since the bridge switches are switching at low frequency, the switching and gate drive losses are small compared to the other losses in the circuit, and therefore can be ignored.

There are also losses associated with the energy storage capacitor and filter elements. The energy storage capacitor dissipates i^2R watts where i is the capacitor current and R is the ESR. The loss is predominantly due the the 120 Hz component of the capacitor current, since the ESR of the capacitor drops significantly at the switching frequency. The inductor losses are primarily due to the conduction losses through the dc winding resistance. The core losses are negligible.

Reverse recovery problems in the diode will contribute another source of loss:

$$P = V(I\,\tau_{rr})f \tag{6.58}$$

V and I are the voltage and current being switched, τ_{rr} is the reverse recovery time of the diode, and f is the switching frequency. If the MOSFET antiparallel diode is used, this loss is around 3 watts. For this reason, the high frequency switch implementation described earlier was used. An ultra-fast rectifier diode can be placed anti-parallel to the MOSFET. To restrict reverse current from flowing through the MOSFET, a Schottky diode can be placed in series with the MOSFET. With these additions, the power loss due to reverse recovery is around 0.5 watts. However, the high frequency conduction losses will increase due to forward conduction through the Schottky diode and conduction through the ultra-fast rectifier.

Under full ac operation, the actual losses will not differ significantly from the values measured in the dc case. The high frequency conduction losses will vary as the duty cycle varies, but the losses will remain somewhat constant. An additional loss will be the 120 Hz conduction loss through the equivalent series resistance of the capacitor. None of these losses include the power dissipated in the control circuitry.

6.5.3 Series Capacitor AC Mode Operation

AC mode operation consisted of operating the circuit directly off of the utility voltage. A Variac was used to vary the amplitude of the utility voltage.

Using the sense resistor to sense the inductor current did not work in ac mode operation because of the polarity changes within a half cycle. For ac mode operation, the current was sensed by sensing the (resistive) load voltage. This proved troublesome at the higher operating voltages due to the high frequency common-mode shifts.

Figure 6-20 shows the utility voltage, load voltage, and capacitor voltage. The peak utility voltage is 100 volts and the load voltage is about 64 volts. The capacitor voltage shows the 120 Hz ripple. This verifies the ability of the control to determine

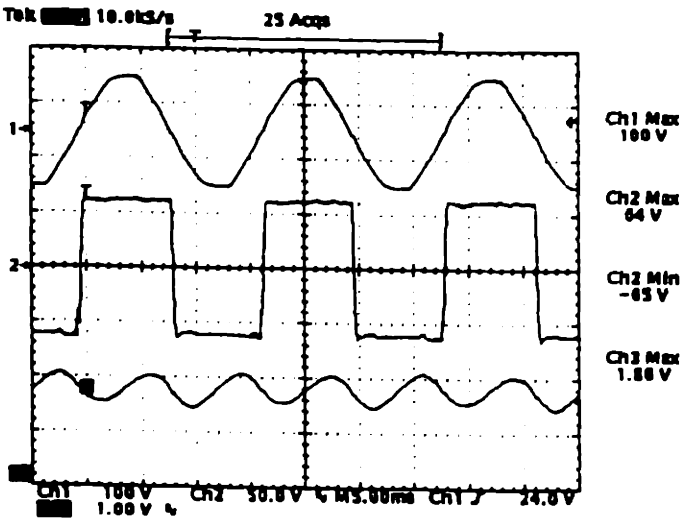

Figure 6-20: AC mode operation with peak utility voltage 100 V

the correct value of current to drive the load such that the load voltage is the average of the utility voltage over a half cycle.

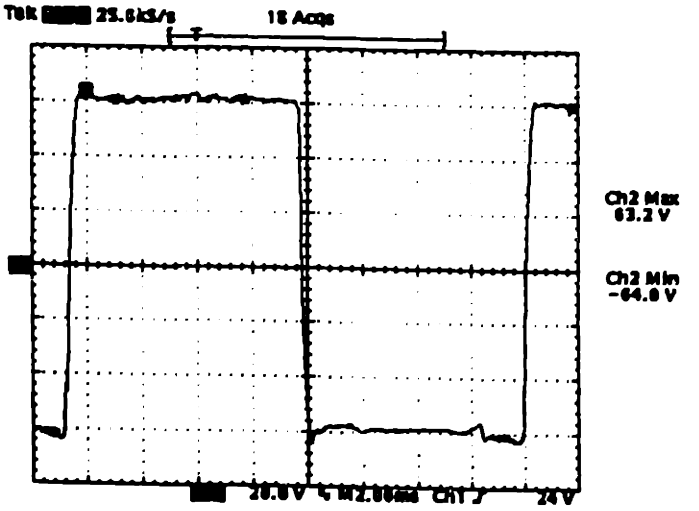

Figure 6-21: Load voltage with peak utility voltage 100 V

Figure 6-21 is a closeup of the lamp voltage. The noise on the waveform is due to the large high frequency common mode shifts in the control ground (negative side of the energy storage capacitor). During the periods where the control ground is

connected to the inductor, the output waveform is noisy. This is a consequence of the topology and the need to sense the load voltage in order to sense the current.

Figure 6-22 shows operation at full power (peak utility voltage of 160 V). Figure 6-23 is a closeup of one cycle of operation at full power. The noise due to the high frequency common mode shifts is obvious.

DC errors in nominal conditions, sensing, etc., caused deviations from the desired operation. Nominally, it was desired that the capacitor voltage begin each half cycle at around 150 V. In actuality, the capacitor voltage began each half cycle at around 120 V. It was difficult to tune parameters such that the correct operation was achieved. The feedback loops are compensated under proportional control only with high frequency roll off. Future implementations could incorporate integral control in addition to proportional control in order to improve performance.

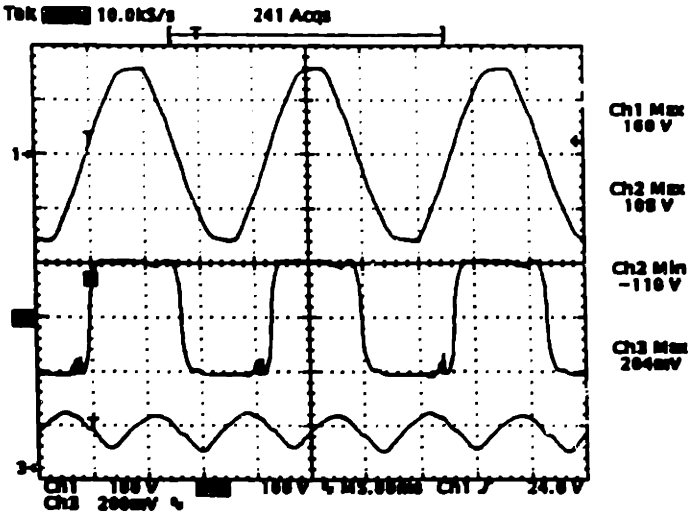

Figure 6-22: AC mode operation with peak utility voltage 160 V

6.6 Additional Topological Implementations

During the course of our research, the basic series capacitor topology was improved by using different switch implementations. The basic features of the improved topology are identical to the original topology. The main difference is that the efficiency is

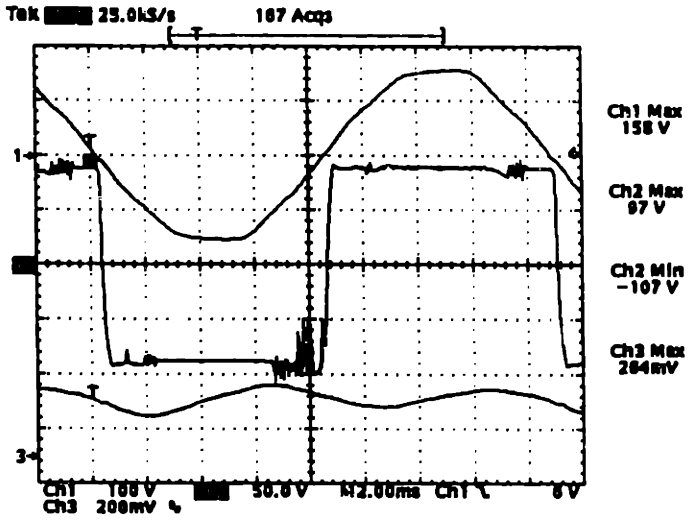

Figure 6-23: AC mode operation with peak utility voltage 160 V

improved by reducing the total switch count.

There is one major problem with the original series capacitor topology. If single mosfets are used for the bridge switches, high frequency currents can flow through the bridge antiparallel diodes instead of through the converter when the capacitor is disconnected from the circuit. This "freewheel" problem can be avoided by using two mosfets, sources connected, for each bridge switch as previously described. If a bridge switch is off, then currents cannot simply force the switch on by flowing through the antiparallel diodes.

An improved version of the series capacitor topology is shown in Figure 6-24. Like the original, it has two high frequency switches. However, it has only two bridge switches instead of four (or eight to remedy the "freewheel" problem). In this topology, the antiparallel diodes in the bridge switches are always reverse biased by the capacitor voltage, so there is no "freewheel" problem. All other features of this topology are identical to the original.

The main advantage of the improved topology versus the original is the reduced switch count. This also results in fewer conduction drops through the circuit. The improved topology has only two conduction drops through the converter, compared to the five drops through the prototype. The losses are then reduced from around 4.6

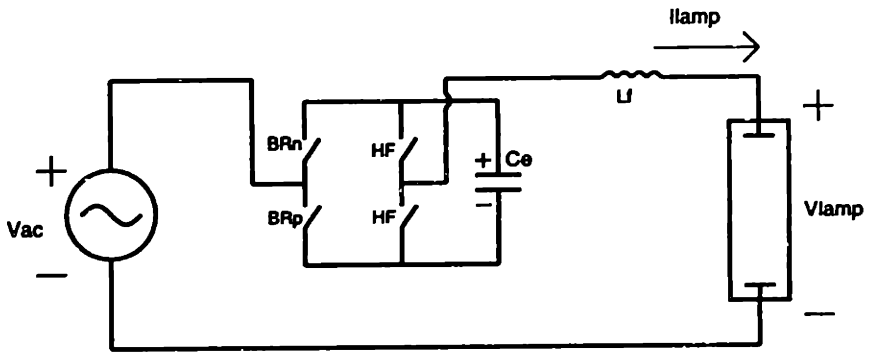

Figure 6-24: Improved series capacitor topology

watts in the prototype, to about 3.5 watts in the improved topology. This topology is roughly 1% more efficient than the original series capacitor topology for the same 100 watt application.

The four switch configuration in Figure 6-24 can be operated in many different ways, although the method already described is perhaps the optimal. All four switches could be operated at high frequency in a full bridge configuration. This would increase the switching losses significantly and also require more filtering at the load. Alternatively, one low side switch can be turned on, while the other pair of switches work at high frequency to generate one polarity of voltage. To generate the other polarity, the switch operation is reversed with the other low side switch being on, and the other pair of switches working at high frequency. In this case, all four switches are high frequency switches, but at any one time, one pair works at high frequency and the other works at low frequency.

Finally, it is possible to use only two high frequency switches as shown in Figure 6-25. The switch count reduction comes at the price of two energy storage capacitors, which ultimately makes this topology undesirable. Since the two switches are operated at high frequency and only the low frequency bridge conduction losses have been eliminated, the efficiency of this topology would not be much better than the improved series capacitor topology. Furthermore, operation is complicated and higher voltage switches would be required.

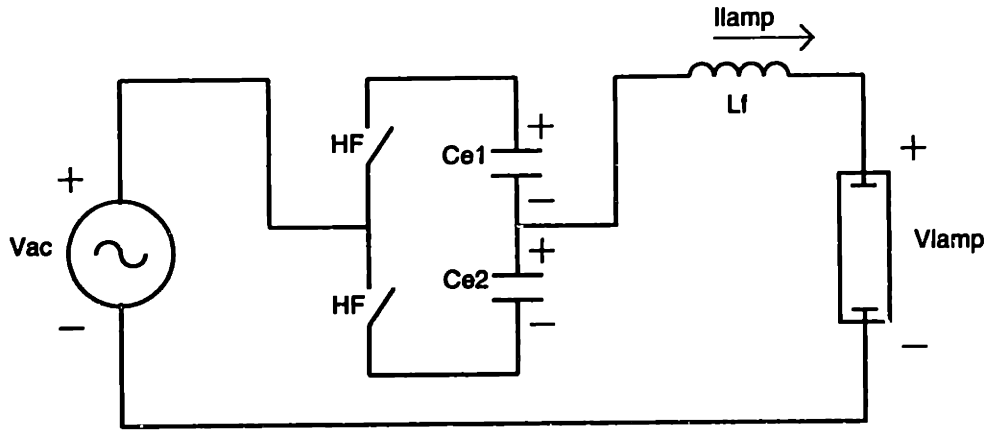

Figure 6-25: Two-switch series capacitor topology

6.7 Ancillary Issues

6.7.1 Waveform Distortion

While the simplicity of the series capacitor topology results in excellent efficiency and low component count, the topology is limited in controllability and features. The first major drawback of the series capacitor topology is the square wave of current drawn from the utility. Because the topology is a series element, no power factor correction on the utility current can be performed. The current then results in degraded power factor for the converter and high total harmonic distortion of the utility current. The real power can be calculated to be

$$Real\ Power = \frac{2}{\pi} V_{acpeak}\, I \tag{6.59}$$

where I is the dc value of current drawn from the utility during a half cycle of operation. The apparent power is

$$Apparent\ Power = \frac{V_{acpeak}}{\sqrt{2}}\, I \tag{6.60}$$

The power factor is then the ratio of the real power to the apparent power.

$$Power\ Factor = \frac{2\sqrt{2}}{\pi} = 90\% \tag{6.61}$$

This value of power factor is not due to any phase displacement of the utility current, but rather it is due to the waveform distortion of the utility current. The total harmonic distorton (THD) of the utility current is given by

$$THD = \sqrt{\frac{I_{rms}^2 - I_{1rms}^2}{I_{1rms}^2}} \tag{6.62}$$

where I_{rms} is the rms current and I_{1rms} is the rms value of the fundamental component of the current. The rms value of the fundamental component of a square wave current of amplitude I is

$$I_{1rms} = \frac{4}{\pi} I \frac{1}{\sqrt{2}} \tag{6.63}$$

Plugging this value into the expression for THD yields a THD of 48.3%. This high value of THD is a concern. However, non-power factor corrected ballasts with an input bridge rectifier to the energy storage capacitor draw currents only at the peaks of the utility, resulting in much greater current distortion and poorer power factor than the square wave case.

6.7.2 Voltage Control

Again because the series capacitor topology does not have a shunt path, the lamp voltage is constrained to be the average of the utility voltage. For a 120 V_{rms} utility, the lamp voltage must be around 108 volts, which is actually very close to the nominal operating voltage of most commercial lamps. If more precise regulation of the lamp voltage is required, it is possible to employ phase control of the converter. By introducing a phase lag α between the utility current and the utility voltage, the average power drawn from the utility becomes

$$< P_{ac} > = < V_{ac} > I \cos\alpha \tag{6.64}$$

where I is again the amplitude of the square wave current drawn from the utility. Because the ballast must not store or dissipate any net energy, the lamp voltage must be such that the power drawn from the utility is equal to the power delivered to the lamp. Keeping in mind that the utility current and the lamp current are the same, the average power delivered to the lamp is simply

$$< P_{lamp} > = V_{lamp}\, I \tag{6.65}$$

and then the lamp voltage must be

$$V_{lamp} = < V_{ac} > \cos\alpha \tag{6.66}$$

So by creating a phase displacement between the utility current and the utility voltage, the lamp voltage can be controlled to a value less than the average of the utility. Unfortunately, the power factor becomes

$$Power\ Factor = \frac{2\sqrt{2}}{\pi} \cos\alpha \tag{6.67}$$

One simple way to compensate for the decreasing power factor with phase angle α is to borrow the idea from the lead-lag ballast. That is, one can operate two lamps, one phased positively and one phased negatively, so that the sum of the currents cancel the phase displacement. The total current drawn from the utility will not have a phase angle. The THD of the total input current will decrease with increasing α for phase angles less than about 30 degrees, due to the reduction of the third harmonic. Beyond 30 degrees, the THD will increase.

Ignition

The series capacitor topology does not have any inherent mechanism for igniting the lamps. In an HID application, the ignition voltages are on the order of kilovolts, so a separate electronic ignitor circuit is typically used. This is then not necessarily a disadvantage of the topology. The true comparison between HID ballasts is between

the circuits used in steady state operation of the lamps, since all would require a similar ignition circuit.

6.8 Summary

The series capacitor topology uses high frequency dc-dc conversion techniques to generate a 60 Hz square wave of current to drive the lamp. The topology is extremely simple, and has a low component count. A basic topology consisting of four low frequency switches and two high frequency switches was presented to explain the concept, but an improved version uses only two low frequency switches and two high frequency switches. In its simplest form, the topology requires only one energy storage capacitor and one filter inductor. The simplicity of the topology makes very high efficiencies possible.

The switching frequency can be increased to minimize the size of filter elements, while the lamp will always be driven with 60 Hz waveforms. The energy storage capacitor represents a fundamental limitation in current ballast topologies, but in the case of the series capacitor topology, the load balancing energy storage capacitor can also be minimized. In fact, this topology can achieve a peak energy storage of only the minimum required for load balancing. The capacitor voltage must be greater than the magnitude of the ballast voltage for down conversion, and the peak of the capacitor voltage must not exceed the voltage rating of the switches.

Of course, other issues must be considered when reducing the size of the energy storage capacitor. As the capacitance decreases, the ESR increases, so that the increased dissipation in the capacitor ESR will be a concern. The efficiency of the converter will be affected somewhat, and the lifetime of the capacitor will decrease. However, in certain applications, the energy storage capacitance can be reduced to the point where capacitor technologies other than electrolytic can be considered. If a ceramic capacitor could be used instead of an electrolytic, the lifetime issues associated with the liquid electrolyte would no longer be a concern.

Because of the series topology, the lamp voltage must be the average of the utility

over a half cycle. A slow feedback loop is used to determine the correct value of lamp current to meet this criterion while the fast loop performs the actual regulation of lamp current. If the nominal lamp characteristics do not permit lamp operation around a lamp voltage of $< V_{ac} >$, phase control can be used for adjustment. To compensate for the degrading power factor, two units, phased positively and negatively, can be operated in parallel to drive two lamps. The square wave current drawn from the utility does raise some concerns as to the relatively high values of total harmonic distortion.

A prototype was constructed and evaluated, which was a valuable introductory learning experience. The prototype did not work so well at high power levels, which was a consequence of the current sensing. However, the prototype worked well enough to verify the concept, the control loop compensation, and the efficiency calculations.

Chapter 7

Autotransformer Ballast

This chapter presents the autotransformer ballast topology. It is an extension of the ideas from the previous chapter in that a shunt element is added to the series element of the series capacitor topology. This topology is meant to address the issue of power factor correction, which was not a feature of the series capacitor topology. The topology is first explained in terms of concepts, and then in terms of a circuit implementation. Simulations and additional topological forms are described along with general issues and concerns.

7.1 The Concept

7.1.1 Basic Waveforms

The basic structure of the autotransformer ballast is shown in Figure 7-1 along with basic waveforms. The ballast consists of two blocks, a series block and a shunt block, which interface the utility to the lamp. This topology is the logical extension of the series capacitor topology, which consisted of a single series block. Like the strategy of the series capacitor topology, the strategy of the autotransformer topology is to drive the lamp with a 60 Hz square wave of current synchronized to the utility. This yields increased lamp efficacy and allows the ballast to be based on dc-dc conversion techniques. Figure 7-2 shows the voltage, current, and power relationships for the

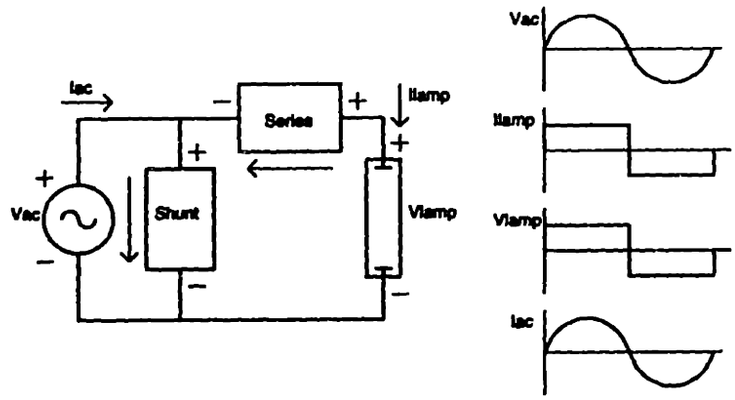

Figure 7-1: Autotransformer ballast basics

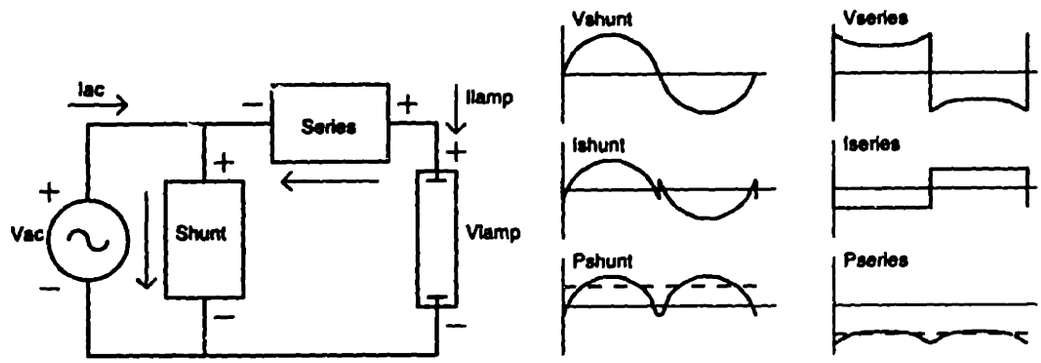

Figure 7-2: Autotransformer block waveforms

shunt and series blocks.

The addition of a shunt path means that the utility current is no longer constrained to be equal to the lamp current, as in the case of the series capacitor topology. The utility current may then be power factor corrected. The lamp voltage is not limited as it was in the series capacitor topology, but the autotransformer topology still does not provide absolute freedom of control of the voltage. The basic topology and placement of the series and shunt blocks dictate that only up conversion from the utility to the

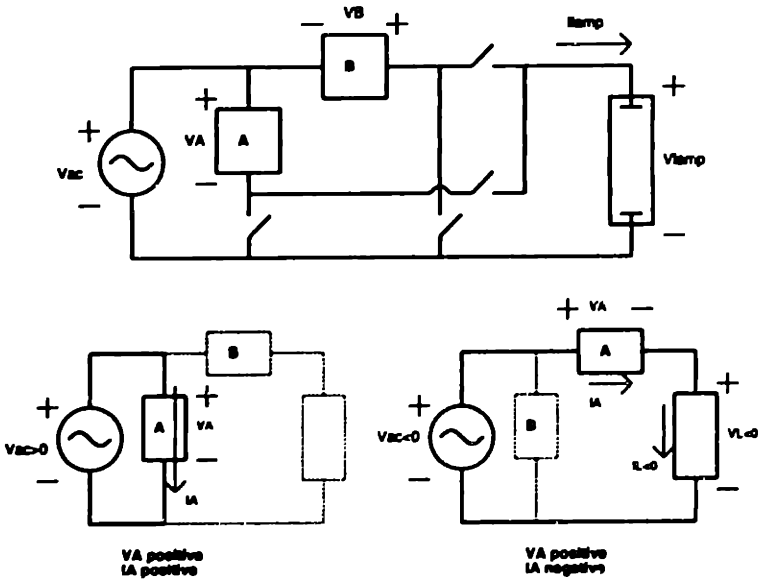

Figure 7-3: Autotransformer bridge implementation

lamp is possible. So the constraint on this topology is that the lamp voltage must be greater than the peak of the utility voltage. Since a 32 watt T8 lamp operates at around 150 V and 200 mA, an application for this topology might be driving two 32 watt T8 lamps in series.

The name of this topology comes from the similarity of the topology to an autotransformer. That is, the source is placed across one element, or "winding," and the output is taken across the series combination of two elements, or "windings." Energy is placed into the shunt element and taken out of the series element. In this way, the topology can be considered to be a type of electronic autotransformer. Keep in mind that the autotransformer topology does not actually contain a transformer.

From the waveforms in Figure 7-2, it can be seen that over a 60 Hz cycle, the shunt element always stores net energy while the series element always gives net energy. Some means must be provided to exchange the block positions every half cycle. At this point, the circuit implementation must be described in order to further explain the features of the topology.

7.1.2 Implementation

The bridge required to relocate the blocks every half cycle is shown in Figure 7-3. In particular, the path of block A is shown in detail. In the shunt position, block A sees

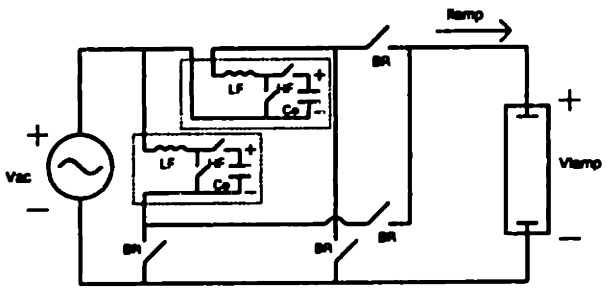

Figure 7-4: Autotransformer implementation

positive voltage and primarily positive current and thus stores a net energy. At the end of a half cycle, block A is switched to the series position where it sees positive voltage and negative current. In this position, block A loses energy. It can be seen that each block stores energy in the shunt position and then loses energy to the load in the series position. What is important to note is that the bridge enables the blocks to have unipolar voltage at their terminals (although the current is bipolar).

Since each block sees only positive voltage, each can be implemented as a dc-dc converter as shown in Figure 7-4. There are four low frequency bridge switches and four high frequency switches. Two capacitors are required for the load balancing energy storage. However, a much more clever implementation is shown in Figure 7-5. Here, there is only one capacitor and three high frequency switches. All switches, including the four low frequency bridge switches, must be bidirectional current and unipolar voltage. Furthermore, the capacitor voltage must be greater than the lamp voltage at all times. As mentioned before, the lamp voltage must be greater than the utility voltage.

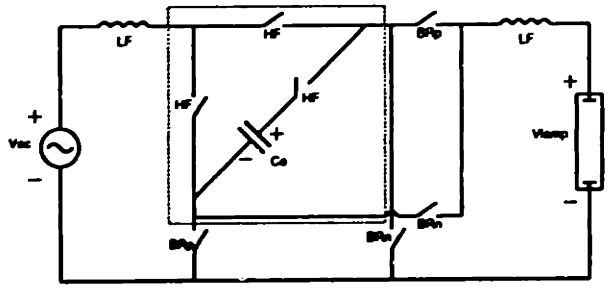

Figure 7-5: Autotransformer final implementation

7.1.3 Load Balancing Energy Storage

Since the autotransformer has power-factor-corrected utility current, the minimum energy storage is $E_{min_{sin}}$ as calculated in equation 6.1. Figure 7-6 shows the power and capacitor waveforms for a half cycle. The minimum capacitor voltage is the lamp voltage, and the maximum capacitor voltage is limited by the voltage rating of the switches. The power delivered to the lamp P_o is the average of the utility power.

$$< P_{ac} > = P_o = \frac{V_{acpeak} I_{acpeak}}{2} \tag{7.1}$$

The difference between the utility power and lamp power is defined as Δp where

$$\Delta p = -P_o \cos(2\omega_{60} t) \tag{7.2}$$

The load balancing energy is found by integrating Δp,

$$E(t) = -\frac{P_o}{2\omega_{60}} \sin(2\omega_{60} t) + K_1 \tag{7.3}$$

where K_1 is a constant of integration accounting for non-zero initial energy at $t = 0$. The capacitor voltage can then be calculated from $E(t)$ to be

$$V_c(t) = \sqrt{-\frac{P_o}{C\omega_{60}} \sin(2\omega_{60} t) + K_2} \tag{7.4}$$

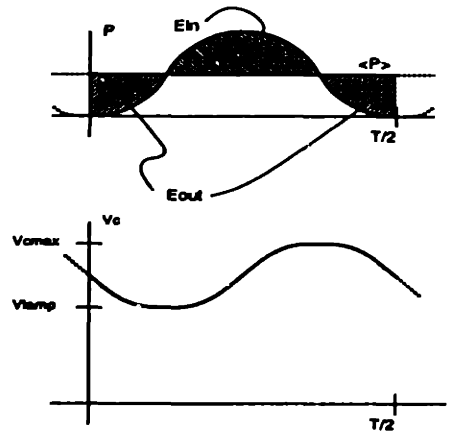

Figure 7-6: Autotransformer power and capacitor waveforms

where K_2 is equal to the initial capacitor voltage squared.

$$K_2 = V_c^2(0) \tag{7.5}$$

While the exact expression for the capacitor voltage is given in Equation 7.4, it is sometimes more convenient to derive a more intuitive approximate expression. The capacitor voltage can be expressed as a dc voltage plus a 120 Hz ripple component if the ripple is small enough. An approximate expression for the capacitor voltage is

$$V_c(t) \approx V - \underbrace{\frac{P_o}{2\omega_{60}CV}}_{\Delta v} \sin(2\omega_{60}t) \tag{7.6}$$

where V is the dc component of V_c and Δv is the amplitude of the ripple component. This approximation is valid under the condition

$$2V \gg \Delta v \tag{7.7}$$

From the approximate expression for V_c, it is easy to pick V and Δv and solve for the approximate capacitance.

$$C \approx \frac{P_o}{2\omega_{60}V\Delta v} \tag{7.8}$$

As an example, consider the autotransformer ballast driving two lamps (V_{lamp} =150 V and I_{lamp} =200 mA) in series. The power delivered to the lamps is 60 watts and the capacitor voltage must be greater than the sum of the two lamp voltages, 300 volts. If 400 volt switches are used, a capacitance can be chosen so that the capacitor voltage ripples between 300 volts and 400 volts. This capacitance is approximately 5 μF. Under these conditions, the peak energy storage in the capacitor is only 2.5 times $E_{min_{sin}}$. Within the parameters of the application, the energy storage in the capacitor can be minimized by allowing the maximum possible voltage ripple.

7.2 Control Strategy

The control strategy for the autotransformer ballast is shown in Figure 7-7. Two fast feedback loops regulate the lamp current to a nominal value and perform the power factor correction at the utility. The utility current is controlled to be a sinusoid of peak amplitude such that the utility power and lamp power are matched. The slow feedback loop sets the desired utility current amplitude by examining the energy information from the capacitor voltage.

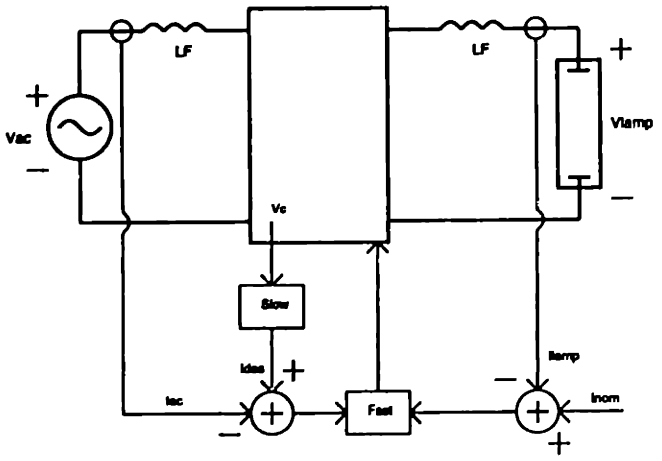

Figure 7-7: Autotransformer control strategy

7.2.1 Fast Feedback Compensation

To compensate the fast feedback loop, an incremental linearized averaged model must first be developed. This requires a closer look at the operation of the circuit. In order for the circuit to operate in continuous conduction, two of the high frequency switches must be closed at all times. Figure 7-8 is a picture of the circuit during the first half of the cycle with the three high frequency switches labeled shunt, series, and cap. If two switches are required to be on at all times, there are only three possible switching

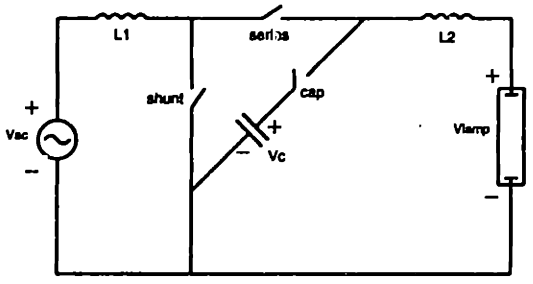

Figure 7-8: Autotransformer circuit during positive half cycle

states. By closing the cap switch and the series switch, V_c is placed across the shunt switch. Call this fraction of the switching cycle d_{ser}, where d_{ser} is a continuous duty ratio. In the averaged model the shunt switch can be replaced by a voltage source $d_{ser}V_c$, since during this part of the switching cycle the shunt switch sees V_c while in the other two switching states the shunt switch is closed. Likewise, with the cap and shunt switches closed, V_c appears across the series switch. This can be represented as a voltage source $d_{shu}V_c$ in the averaged model. Finally, the remaining fraction of the switching cycle must have the series and shunt switches closed, placing V_c across the cap switch. Again, this can be represented a voltage source $d_{cap}V_c$ in the averaged model. Since these averaged switch voltages form a voltage source loop with the capacitor, the constraint on the duty cycles is clear.

$$d_{shu}V_c + d_{ser}V_c + d_{cap}V_c = V_c \tag{7.9}$$

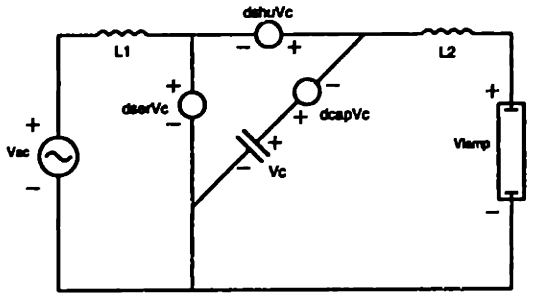

Figure 7-9: Large signal averaged model during positive half cycle

$$d_{shu} + d_{ser} + d_{cap} = 1 \tag{7.10}$$

The large signal averaged model is shown in Figure 7-9. The inductor current, i_{L1}, is power factor corrected.

$$i_{L_1} = \frac{2P_o}{V_{acpeak}} \sin(\omega_{60} t) \tag{7.11}$$

The inductor voltage required to generate this current is

$$v_{L_1} = L_1 \frac{di_{L_1}}{dt} = L_1 \omega_{60} \frac{2P_o}{V_{acpeak}} \cos(\omega_{60} t) \tag{7.12}$$

Typically, if the inductance is small enough, v_{L_1} is very small compared to the utility voltage and need not be accounted for in generating the nominal duty ratios. A feedback loop will be enough to correct for the error. Ignoring v_{L_1}, the nominal duty ratios can be found.

$$d_{ser} = \frac{V_{ac}}{V_c} \tag{7.13}$$

$$d_{shu} = \frac{V_{lamp} - V_{ac}}{V_c} \tag{7.14}$$

$$d_{cap} = \frac{V_c - V_{lamp}}{V_c} \tag{7.15}$$

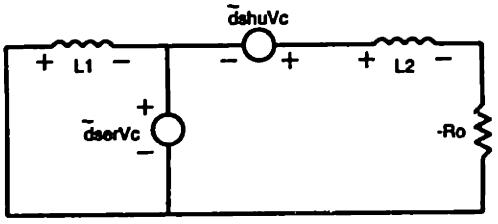

Figure 7-10: Incremental linearized averaged model

Since no duty cycle can be negative or greater than one, the following constraints exist:

$$V_{lamp} > V_{ac} \tag{7.16}$$

$$V_c > V_{lamp} \tag{7.17}$$

These constraints apply to all points in time in the half cycle.

Looking at the voltage source loop formed by the capacitor voltage and the averaged switch voltages, as long as V_c is greater than V_{lamp}, $d_{ser}V_c$ and $d_{shu}V_c$ can be generated independently. The voltage across the capacitor and cap switch combination will always be equal to the sum of the series and shunt switch voltages. The final incremental linearized averaged model is shown in Figure 7-10, where R_o is the magnitude of the negative impedance of the lamp and continuous duty ratios are replaced by incremental duty ratios.

The equivalent voltage $\tilde{d}_{ser}V_c$ operates independently to control the current through L_1, but the combination of $\tilde{d}_{ser}V_c$ and $\tilde{d}_{shu}V_c$ controls the current through L_2. This makes the combined system second order. It is sufficient to feedback on i_{L_1} to d_{ser} and to feedback on i_{l_2} to d_{shu} for control and stability. If the duty cycles are thus modified so that $\tilde{d}_{ser} = -K_1\, i_{L_1}$ and $\tilde{d}_{shu} = -K_2\, i_{L_2}$ then the characteristic equation of the system is

$$s^2 + (-\frac{R_o}{L_2} - \frac{K_1 V_c}{L_1} + \frac{K_2 V_c}{L_2})s + \frac{K_1 V_c (R_o - K_2 V_c)}{L_1 L_2} \tag{7.18}$$

where V_c is the capacitor voltage at the relevant point of the $60\,Hz$ cycle. Again,

the range of variation of V_c must be accounted for in determining the stability of the system. By appropriate choice of K_1 and K_2, the system can be stabilized with regulation on the utility current and lamp current. Using higher order filters can result in smaller filter size, but requires more complicated control feedback.

7.2.2 Slow Feedback Compensation

The slow loop analysis is similar to that of the series capacitor topology and is not explained in detail here. Once again, the strategy is to sample the capacitor voltage every cycle (or half cycle) and check against a nominal reference to determine the energy balance between the utility and the lamp. The controlling parameter is the peak of the utility current. Since the lamp current is independent of the utility current, the analysis is greatly simplified. The changes in energy of the system in response to changes in the peak utility current can be modeled by

$$\Delta\tilde{e}(t) = \int \frac{V_{acpeak}}{2}\tilde{i}_{acpeak}\,dt \tag{7.19}$$

which is a linearized incremental model. Performing a step invariant transformation to convert the continuous time system to a discrete system and applying the linearized relation of energy to capacitor voltage, the pole of the closed loop system can be found. The corresponding desired range of gain M for a damped response is

$$0 < M < \frac{2CV_{cnom}}{V_{acpeak}T} \tag{7.20}$$

This technique is described in detail in Section 6.3.2. Notice that in the series capacitor ballast, the constant A described the variation of energy in response to incremental changes in current (equation 6.34). This constant depended on both the lamp and utility characteristics since the lamp and utility currents were the same. Here the constant A is replaced by $V_{acpeak}/2$. Changing the peak of the utility current only affects the utility power, while the lamp power remains regulated to a nominal value.

By appropriate choice of gain, the slow loop can be stabilized at a bandwidth

smaller than the fast loop. The addition of higher order filtering makes the stability problem significantly more complex.

7.3 Autotransformer Simulations

This section presents some basic simulations of the autotransformer topology. Basic designs are presented and stability of the control loops are verified.

A basic design of the autotransformer ballast topology is shown in Figure 7-11, with component values labeled. This design uses third order filters at the utility and at the lamp. Switches with a voltage rating of 400 volts are used, and the energy storage capacitor is 10 μF.

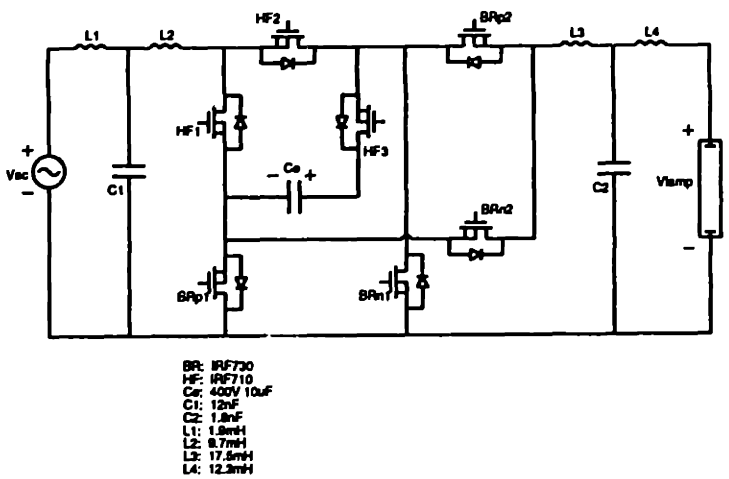

Figure 7-11: Autotransformer ballast with third order filters

The chosen load was two 32 watt T8 lamps in series. Each operates at 150 volts and 200 mA. To determine an appropriate dynamic model for the terminal voltage and current characteristics of the 32 watt T8 lamp, the static dc i-v characteristic of the lamp was measured. This is shown in Figure 7-12. From this static characteristic, the negative resistance around the operating point was determined. A dynamic model was then constructed from an 11th order polynomial and is shown in Figure 7-13.

The results of large signal averaged model simulations performed on *Simulink* are

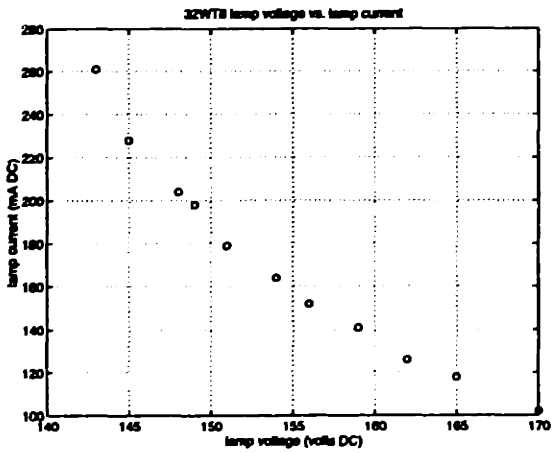

Figure 7-12: F32WT8 static lamp characteristic

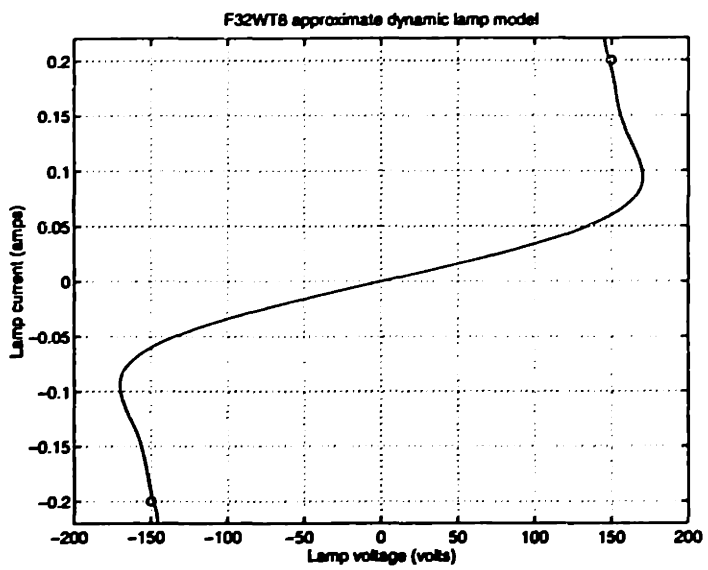

Figure 7-13: Approximate dynamic model of F32WT8 lamp

shown in Figures 7-14 – 7-17. The third order filters require additional feedback for stability, compared to the single order filter case. The load is two F32WT8 lamps in series, which results in a 60 watt load at 300 volts and 200 mA. Feedback is performed on all inductor currents to stabilize the filters. The voltage on the energy storage capacitor is sampled at the beginning of every 60 Hz cycle and compared to

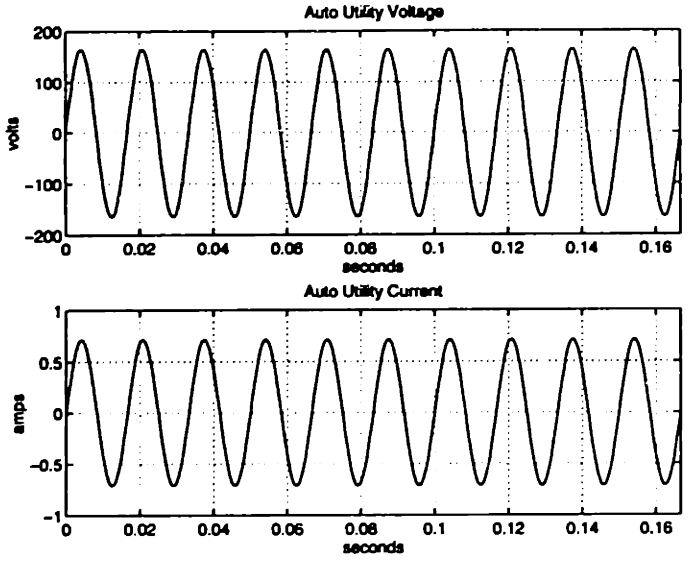

Figure 7-14: Averaged model simulations of autotransformer ballast— utility voltage and current

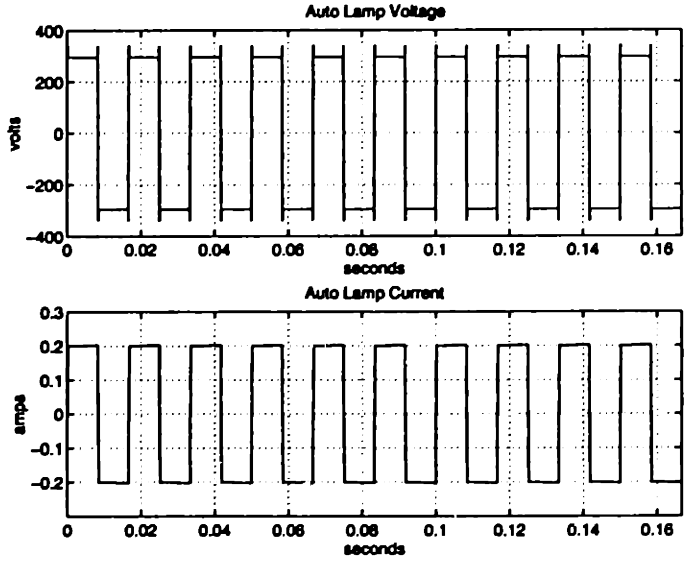

Figure 7-15: Averaged model simulations of autotransformer ballast— lamp voltage and current

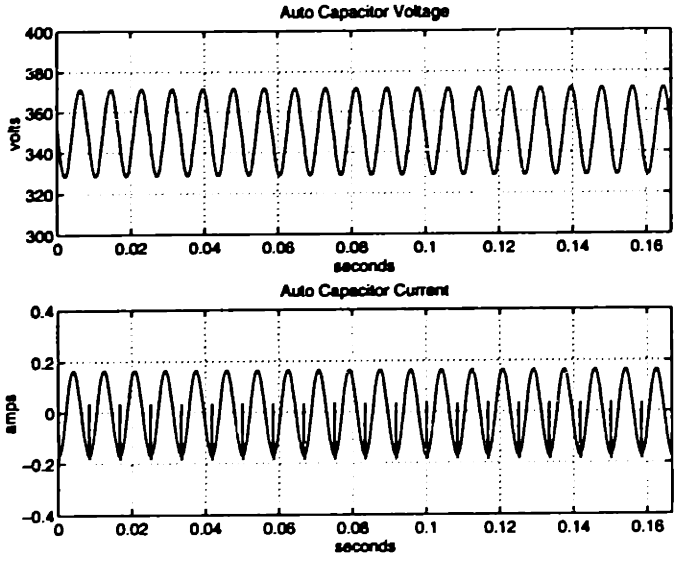

Figure 7-16: Averaged model simulations of autotransformer ballast— capacitor voltage and current

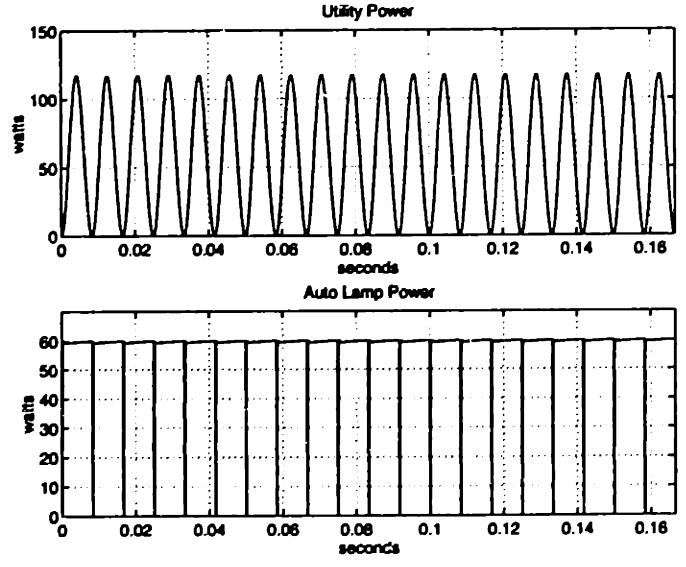

Figure 7-17: Averaged model simulations of autotransformer ballast— utility and lamp power

a nominal reference of 350 volts. The difference is multiplied by a gain and added to a nominal reference to generate the desired utility current amplitude. The filter is designed to limit both the utility current ripple and lamp current ripple to around +/- 1% of the average 60 Hz value.

From the simulation results, it can be seen that the lamp is driven with a 60 Hz square wave of current. The capacitor voltage is chosen to be a nominal 350 volts, about which the voltage ripples from a minimum of 326 volts to a maximum of 372 volts. The peak energy storage in the capacitor is about 4.3 times the theoretical minimum of $E_{min_{sin}}$.

7.4 Autotransformer Design Implementation

An actual prototype was designed, but not built. The components were specified so that an estimate of the converter efficiency could be obtained. These components and the efficiency calculations are described as follows.

7.4.1 Autotransformer Components

The energy storage capacitor is a Philips 2222-132-133 electrolytic capacitor rated at 10 μF and 400 V. The ESR is about 7.5 ohms at 120 Hz.

The input filter is comprised of three components. The inductor L_1 is made from a Magnetics D-42213-40 ferrite pot core gapped to an AL value of 400, which corresponds to a gap length of 0.006 inches. The value of inductance is 1.9 mH and is obtained from 60 turns of AWG24 yielding a dc coil resistance of 0.22 ohms. The second inductor L_2 is made from a Magnetics D-43019-40 ferrite put core gapped to an AL value of 400 (gap length 0.016 inches). The 9.7 mH of inductance is obtained from 152 turns of AWG24, which gives a dc resistance of 0.77 ohms. A capacitor C_1 is a 12nF Philips KP/MMKP-375 capacitor rated at 630 volts dc and 300 volts ac.

The output filter is also comprised of three components. The inductor L_3 is made from a Magnetics D-42213-40 ferrite pot core gapped to an AL value of 400 (gap length 0.006 inches). The inductance of 17.5 mH is obtained from 183 turns of

AWG28, resulting in a dc resistance of 1.73 ohms. The inductor L_4 is made from a Magnetics D-41811-40 ferrite pot core gapped to an AL value of 400 (gap length 0.005 inches). The 12.3 mH of inductance is obtained from 171 turns of AWG30, which gives a dc resistance of 2.13 ohms. A capacitor C_2 is a 1.8 nF Philips KP/MMKP-376 capacitor rated at 1600 volts dc and 500 volts ac.

The four low frequency bridge switches are each an IRF740 power MOSFET rated at 400 volts with an on state resistance of 1.0 ohm. The three high frequency switches are implemented with IRF710 MOSFETs which have a voltage rating 400 volts and an on state resistance of 3.6 ohms. Because the body diodes of these mosfets are too slow for this application, IRF11DF4 ultra-fast rectifiers (400 V_{off}, 1 A, 1.25 V_{on}, $\tau_{rr} = 30$ ns) are connected antiparallel to the MOSFETs. To prevent reverse currents from conducting through the MOSFET body diode, IRF11DQ03 Schottky diodes (30 V_{off}, 1.1 A, 0.5 V_{on}) are connected in series with the MOSFETs.

In this configuration, the topology will suffer from the same "freewheel" problem as in the series capacitor case. There is a switching state where the energy storage capacitor is disconnected from the circuit and currents can flow through the body diodes of switches that are meant to be off. This can be remedied by moving the lamp filter inductor inside the bridge. This is possible in the autotransformer topology case because the bridge switches change at each half cycle, and the current in the inductors is not interrupted.

7.4.2 Autotransformer Efficiency

The mechanisms for loss in the autotransformer high frequency dc-dc converter are similar to those described in the series capacitor topology. Consider the first switching state when the series and cap switches are on and the shunt switch is off. The transition to the next state involves turning on the shunt switch and turning off the series switch, while the cap switch remains on. The shunt switch is effectively a MOSFET and the series switch is effectively a diode. The switching losses incurred

here are due to the crossover loss switching a voltage of V_c and a current I_{ac}:

$$E = \frac{1}{2} V_c I_{ac} t_{on} \tag{7.21}$$

the loss in discharging the MOSFET capacitance:

$$E = \frac{4}{3} [\frac{1}{2} C_f \sqrt{V_f} (V_c)^{\frac{3}{2}}] \tag{7.22}$$

and the loss in charging the diode capacitance:

$$E = \frac{8}{3} [\frac{1}{2} C_d \sqrt{V_d} (V_c)^{\frac{3}{2}}] \tag{7.23}$$

In the next transition, the shunt switch remains on, while the series switch turns on and the cap switch turns off. In this case, the cap switch is effectively a MOSFET and the series switch is effectively a diode. The losses in this transition are due to the energy stored in the parasitic inductance of the loop where the current conducted in the cap switch is the lamp current:

$$E = \frac{1}{2} L_p I_{lamp}^2 \tag{7.24}$$

In the final transition, the cap switch turns on, the shunt switch turns off, and the series switch remains on. Here the shunt switch is effectively a MOSFET and the cap switch is effectively a diode. Again, the losses in this transition are due to the energy stored in the parasitic inductance of the loop where the current conducted in the shunt switch is the shunt current:

$$E = \frac{1}{2} L_p I_{shunt}^2 \tag{7.25}$$

The other losses in the circuit include the gate drive energy of the three high frequency switches, the conduction losses in the high frequency switches and the bridge switches, and the losses in the ESR of the energy storage capacitor and the dc winding resistance of the filter inductors. The core losses are minimal.

power	60 W
switching	0.37 W
HF conduction	1.31 W
bridge conduction	0.16 W
EMI filter	0.40 W
ESR C_e	0.10 W
reverse recovery	0.47 W
total	2.82 W
η	95.5%

Table 7.1: Autotransformer ballast loss predictions

However, these analyses do not account for reverse recovery. There is one transition where an effective diode is turned off (the series switch), and the recovery problems in the diode will contribute another source of loss:

$$P = V_c(I_{ac}\,\tau_{rr})f \tag{7.26}$$

If the MOSFET antiparallel diode is used, this loss is around 3 W. If ultra-fast rectifier diodes are used along with Schottky diodes, the loss due to reverse recovery can be reduced to about 0.47 W. However, this will add additional conduction losses. Using simulations, the efficiency of the autotransformer ballast can be estimated as shown in Table 7.1. The total losses in this case are around 2.8 W, which is an efficiency of 95.5%. This does not include the power dissipated in the control circuit.

7.5 Comparison to Existing Topologies

Because the autotransformer topology is suitable for driving two 32WT8 lamps in series, a logical comparison would be to an existing resonant inverter ballast for the same application. Although it is difficult to make one-to-one comparisons in most instances, it is still possible to make general comparisons. The autotransformer topology was already evaluated in the previous section. This section describes an example resonant inverter ballast so that comparisons may be drawn between the

two topologies.

7.5.1 Resonant Inverter Ballast

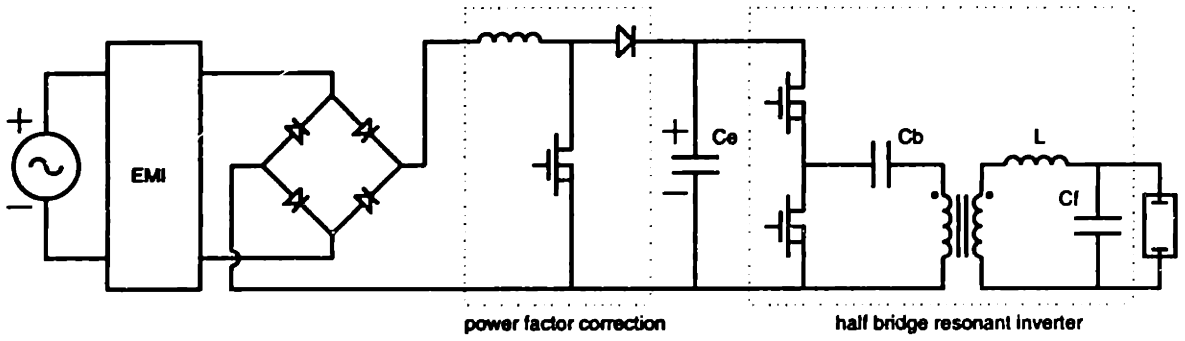

Figure 7-18: Resonant inverter electronic ballast

A basic electronic ballast based in the resonant inverter is shown in Figure 7-18. The utility is filtered through an EMI filter and then rectified by a full-wave bridge rectifier. A boost converter performs power factor correction on the input current while up-converting the rectified ac voltage to the dc bus voltage on the energy storage capacitor. The dc bus voltage is then inverted by the half bridge and filtered to drive the lamps. A transformer is used to match the load impedance to the inverter.

The main sources of loss in this ballast are as follows. There are losses in the EMI filter resulting mainly from conduction losses through inductor windings. The conduction losses through the diode rectifier bridge represent a major source of loss in the converter. The boost converter may be operated in a discontinuous or continuous mode. When operated in a discontinuous mode, there are losses associated with charging the diode capacitance and discharging the MOSFET capacitance at turn on. There are no crossover losses at turn on because the MOSFET is turned on at zero current. There are also no losses at the MOSFET turn off time. There are conduction losses through the diode, the MOSFET, and the inductor winding, as well as the gate drive losses for the MOSFET.

power	60 W
Input EMI Filter	0.5 W
Bridge Diodes	1.0 W
Boost Converter	1.0 W
Resonant Inverter	2.0 W
total	4.5 W
η	93.0%

Table 7.2: Resonant inverter ballast loss predictions

The resonant inverter operation is interesting. If the converter is operated at a frequency above the resonant frequency of the filter, then the filter looks inductive and there is a phase lag between the input current to the filter and the input voltage to the filter. If there is a suitable delay between turning one switch off and the other switch on, then the load current performs the charging or discharging of the parasitic switch capacitances, and there are no losses at turn on or turn off. There are still losses due to the conduction through the switch resistances and the gate drive losses for the MOSFETs.

The output filter losses are mostly due to the conduction losses through the inductor windings, and the transformer windings. There are also core losses in the transformer and inductor. The losses in the capacitors are mostly negligible. There are also losses due to the ESR of the energy storage capacitor.

Numerically for an example design, the predicted losses for the resonant inverter are shown in Table 7.2. These losses do not include the losses in the control circuitry. The total losses are around 4.5 watts, for a converter efficiency of around 93%. This example design used an inverter frequency around 40 kHz.

7.5.2 Comparison

From the numbers it can be seen that the autotransformer topology has losses around 2.8 watts, while the resonant inverter has losses around 4.5 watts. It is not sufficient to compare numbers without considering the proper context. However, one thing to note is that the efficacy of the lamp when operated on a 60 Hz square wave drive

is expected to be approximately 2–3% less than when operated on a high frequency sinusoidal drive. The improved efficiency of the autotransformer topology is expected to yield a system efficiency (ballast efficiency and lamp efficiency) that is roughly equivalent to the resonant inverter system efficiency.

Although the overall system efficiency of the autotransformer does not seem to offer any advantages over the resonant inverter, there are other fundamental advantages that result from the topological differences between the two. The autotransformer has three high frequency MOSFETs, while the resonant inverter has three high frequency MOSFETs plus a high frequency diode. The autotransformer has four low frequency bridge MOSFETs, while the resonant inverter has four low frequency bridge diodes. These bridge diodes represent a significant source of loss. In the case of the autotransformer, the topology has bridge synchronous rectification inherent to the topology. Active devices are used for the bridge switches which require drive energy, but can yield better efficiency by offering much lower conduction drops. Furthermore, two of the bridge switches carry only the shunt current, which is the difference between the utility current and the load current. The other two bridge switches carry the load current (which is only 0.2 amps for this application). The rectifier bridge in the resonant inverter ballast carries the full utility current, which has an average value around 0.5 amps.

Concerning the conduction losses in the converters, the autotransformer has lower semiconductor rms currents than the resonant inverter. This means that for a given die area, the conduction losses in the autotransformer semiconductor switches will be less than the losses in the resonant inverter semiconductor switches. For an equivalent die area, (both topologies use 400 volt switches), the conduction losses in the autotransformer will be half those of the resonant inverter.

One fundamental advantage of the autotransformer topology is that the lamp sees 60 Hz waveforms, regardless of the internal converter switching frequency. The resonant inverter drives the lamps at the fundamental of the switching frequency. This places limits on how high the resonant inverter switching frequency may be raised due to the radiated EMI from the lamps. The switching frequency of the autotransformer

may be raised as high as possible, within limits of acceptable efficiency, in order to reduce the size of the filter components.

7.5.3 Comparison of Energy Storage

Perhaps the most important advantage of the autotransformer topology is the freedom to allow as much 120 Hz ripple on the energy storage capacitor as possible in order to minimize the size of the capacitor. This is a general feature of all the new topologies presented in this thesis. The resonant inverter topology requires a fixed dc voltage on the capacitor, because any 120 Hz ripple on the capacitor will appear as 120 Hz modulation on the lamp waveforms. This ripple can be compensated by varying the frequency of the resonant inverter. The effectiveness of this strategy will depend heavily upon the quality factor of the resonant filter. This technique is patented in United States patent number 5,128,592 [91]. This patent specifically claims a method of varying the inverter frequency in the presence of varying (dc bus capacitor) source voltage such that the load current amplitude remains constant. The autotransformer does not use such methods to control the 120 Hz ripple on the load, and thus would not infringe upon this patent. The autotransformer can tolerate any amount of 120 Hz ripple and still drive the load with constant waveforms. The actual allowable ripple is constrained by the switch rating and the load voltage.

7.6 Additional Topologies

7.6.1 Autotransformer Up-Down Topology

One of the limitations of the autotransformer topology is that the load voltage is required to be greater than the utility voltage. This topology requires four bridge switches to "flip" the three switch dc-dc converter cell "vertically" every half cycle as shown in Figure 7-19. By exchanging the nodes indicated by the positive/negative arrow each half cycle, the converter can operate on both polarities of the utility. However, the topology is effectively limited to up conversion from the utility to the

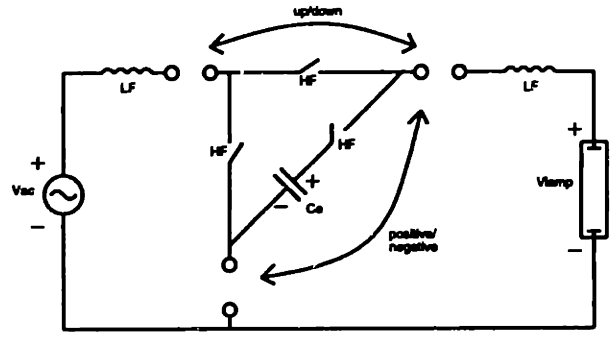

Figure 7-19: Autotransformer up/down concept

lamp. Therefore the lamp voltage must be greater than the utility.

In order to drive a load with a voltage less than the peak of the utility, down conversion from the utility to the lamp is required during a portion of each half cycle. This can be achieved by flipping the dc-dc converter cell "horizontally" as shown in Figure 7-19. By exchanging the nodes indicated by the up/down arrow, the converter can function as an up converter or a down converter from the utility to the lamp. The final implementation is shown in Figure 7-20. Four more bridge switches

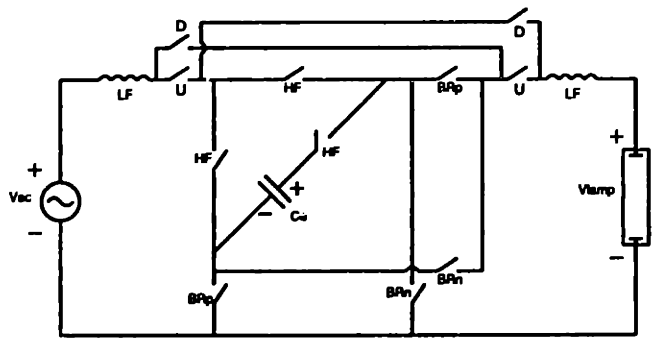

Figure 7-20: Autotransformer up/down final implementation

are added to accomplish the required topological changes. This autotransformer up-down topology is capable of driving virtually any lamp voltage while performing

power factor correction on the utility current. Although there are a large number of semiconductor switches, in the future these may all be implemented on a single power integrated circuit die with an integrated control.

7.6.2 Autotransformer Up-Down II Topology

A topological structure similar to the improved series capacitor topology can be utilized in the autotransformer up-down problem. The newest autotransformer topology is shown in Figure 7-21 and is henceforth referred to as the auto UDII topology. This

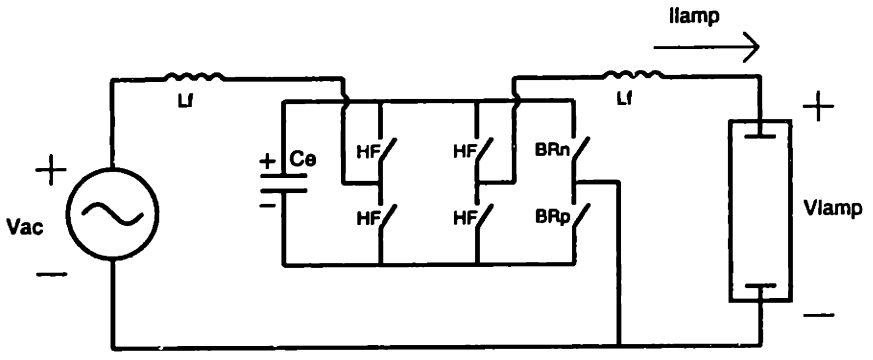

Figure 7-21: Autotransformer up-down II topology

topology replaces both previous forms of the autotransformer topology in terms of functionality. It consists of four high frequency and two low frequency switches. One high frequency pair works to control the utility current, while the other high frequency pair controls the lamp current. Like the other topologies, the lamp is driven with a square wave of current with power factor correction at the utility. There is no constraint on the lamp voltage, and no "freewheel" problem.

All the features of the auto UDII topology are identical to its topological counterparts. However, the total switch count has been reduced, resulting in fewer conduction drops through the converter. The original autotransformer topology has four drops, the first version of the autotransformer up-down topology has six, while the Auto UDII has only three. This topology is the subject of the next chapter.

7.7 Summary

The autotransformer topology uses high frequency dc-dc conversion techniques to generate a 60 Hz square wave of current to drive the lamp. Unlike the series capacitor topology, the autotransformer topology includes a shunt element which allows power factor correction on the utility current. While the first version of the autotransformer topology requires a load voltage higher than the utility, the subsequent up-down versions have no limitations on the load voltage. The final auto UDII topology requires only six total switches and is the subject of the next chapter.

Like the series capacitor topology, the switching frequency can be increased in order to minimize the size of the filter elements. The lamp always sees 60 Hz waveforms, so there is no fundamental concern of radiated EMI as in the case of the resonant inverter ballast where the output of the ballast is at the fundamental of the switching frequency. The switching frequency of the autotransformer ballast can be raised as high as possible within acceptable limits of efficiency.

The basic advantages of the autotransformer approach over the resonant inverter approach were described in Section 7.5. Perhaps the most important advantage is that the 120 Hz ripple on the energy storage capacitor can be maximized to reduce the size of the capacitor. Capacitor voltage ripple is not tolerable in the resonant inverter ballast due to the requirements of the topology. In the case of the autotransformer topology, the capacitor voltage can ripple between the switch rating and the load voltage. Within the parameters of the application, the energy storage capacitor can then be minimized.

Chapter 8

Autotransformer Up-Down II Ballast

This chapter focuses on the autotransformer up-down II ballast, henceforth referred to as the auto UDII ballast. It is perhaps the most commercially viable topology because there are no operation limitations. The basic circuit topology is explained and simulations are shown. A prototype is discussed and comparisons to other topologies are presented. The issue of the size reduction of the ballast with increasing switching frequency is addressed.

8.1 Auto UDII Topology and Implementation

8.1.1 Auto UDII Topology

The basic auto UDII topology was presented in the previous chapter, but is shown again here for convenience in Figure 8-1. The topology is similar in principle to all the other topologies presented previously. There are four high frequency switches and two low frequency switches. One pair of high frequency switches and the filter inductor on the utility work like a boost converter from the utility to the energy storage capacitor. The other pair of high frequency switches and the filter inductor on the load work like a down converter from the energy storage capacitor to the load.

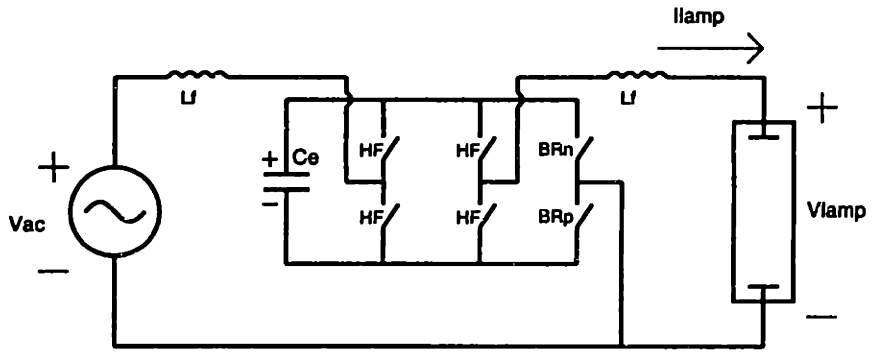

Figure 8-1: Autotransformer up-down II topology

The two bridge switches are switched alternately each half cycle. The unique bridge function provided by the two low frequency switches enables each converter stage to function on both polarities of the utility voltage.

The general strategy of the topology is the same as the other topologies. The lamp is driven with a 60 Hz square wave of current. This topology is capable of providing power factor correction on the input current. There is no "freewheel" problem with this type of circuit structure, since any switch (MOSFET) that is intended to be off will always have a reverse bias across the antiparallel body diode. There is no limitation on the lamp voltage that this topology can drive, unlike the series capacitor and autotransformer topologies. The only operational constraint is that the energy capacitor voltage must be greater than the utility voltage, and it must be greater than the lamp voltage. This is clearly evident from the up conversion from the utility to the capacitor, and from the down conversion from the capacitor to the load.

The basic topology in Figure 8-1 shows only a single filter inductor on the utility and a single filter inductor at the load. Higher order filters could be used. The operation of the converter is relatively simple. One pair of high frequency switches works to regulate the utility current to the desired shape and magnitude. For power factor corrected current, this shape is a sinusoid. The other pair of high frequency switches works to regulate the lamp current to the desired value, which is a 60 Hz square wave synchronized to the utility.

There are only three conduction drops through the converter, which can result in high converter efficiency. Furthermore, the bridge switches carry the shunt current, or the difference between the utility and lamp currents.

8.1.2 Synchronous Rectification

Bidirectional current switches are needed in all the topologies presented. MOSFETs are ideal choices except for the slow (200–300ns) reverse recovery characteristic of the body diode. For each high frequency switch, a series Schottky and an ultra-fast rectifier ($\tau_{rr} = 35$ns) can be used as shown in Figure 8-2. The disadvantages of this

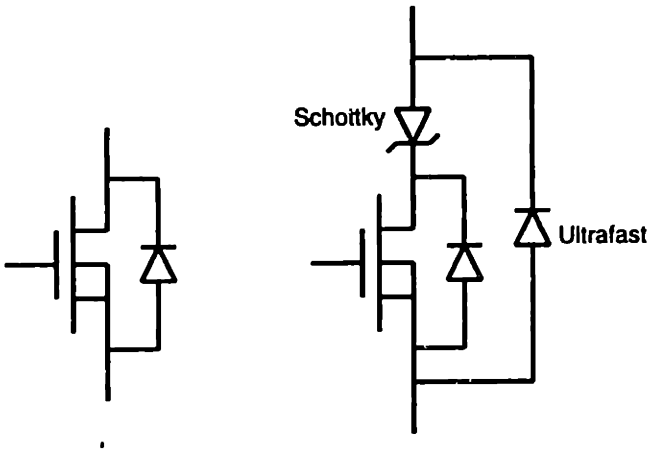

Figure 8-2: High frequency switch implementations

approach are obvious, increased conduction losses and high component count. This was the approach used in implementing the high frequency switches in both the series capacitor and autotransformer topologies.

For the auto UDII topology, a different approach to the high frequency switch was investigated. An alternative implementation for the high frequency switches is to use synchronous rectification as shown in Figure 8-3. For a typical dc–dc converter application, single MOSFETs can be used for each high frequency switch if certain criteria are met. If the MOSFET channel resistance is small, the current will flow through the channel and not through the body diode. When one switch channel is

turned off, the current will flow through the body diode until the other switch is turned on. If the switch timing is tight (30ns), only 30ns of charge will build up in the body diode.

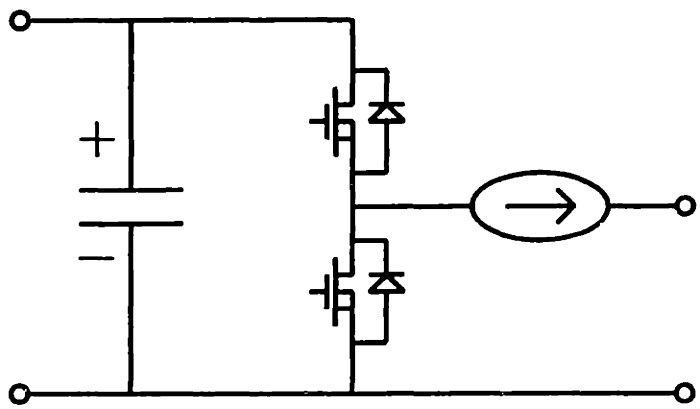

Figure 8-3: Synchronous rectification

Two circuits were constructed as shown in Figure 8-4. Each represents a different

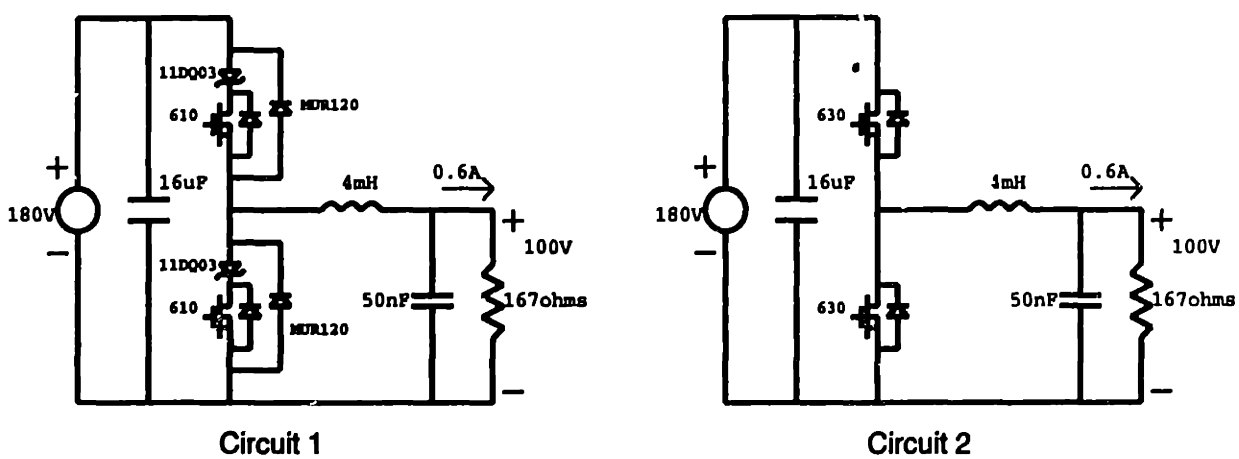

Figure 8-4: Synchronous rectification test circuits

implementation for the output stage of the auto UDII prototype driving a 60 watt (100 V, 0.6 A) load. The first circuit uses IRF610 MOSFETs with series Schottky

and antiparallel ultra-fast rectifiers. The predicted losses were 1.60 watts, and the observed losses were 1.59 watts. The second circuit uses only IRF630 MOSFETs for each switch. The calculated losses were 1.78 watts and the observed losses were 1.97 watts.

The differences in efficiencies between the two circuits are small and difficult to resolve accurately. The bottom line is that this study shows that synchronous rectification is a viable solution in certain applications. With properly sized MOSFETs and a suitable gate drive mechanism, each high frequency switch can be implemented with a single MOSFET. The chief benefit of this approach is the reduced component count. The efficiencies of the three-switch approach versus the single switch approach depend upon the application and switching frequency. The efficiency of the single switch approach is dominated by switching losses, since the MOSFET resistance is required to be small and the corresponding conduction losses are therefore small. Large MOSFETs are required to achieve the low on state resistance, which results in large parasitic device capacitances. At high switching frequencies, the efficiency of the single switch approach tends to be poor relative to an optimized three switch solution. In the case of the three switch solution, the MOSFET size can be optimized to balance switching losses and conduction losses, so the conduction losses through the various switch drops tend to dominate the efficiency. At high switching frequencies, the three switch solution can achieve better efficiency than the single switch solution. Again, the results will depend upon the specific application.

8.2 Simulations

A basic design of the auto UDII topology is shown in Figure 8-5. The application is driving a load at around 60 watts at 100 volts and 0.6 amps. A single 10 mH inductor filters the utility current, while a 5 mH inductor and a 50 nF capacitor filter the load. Each switch is a single International Rectifier IRF630 power MOSFET, with an on state resistance of 0.40 ohms and a voltage rating of 200 volts. This low value of switch resistance must be chosen so that the switches may operate as

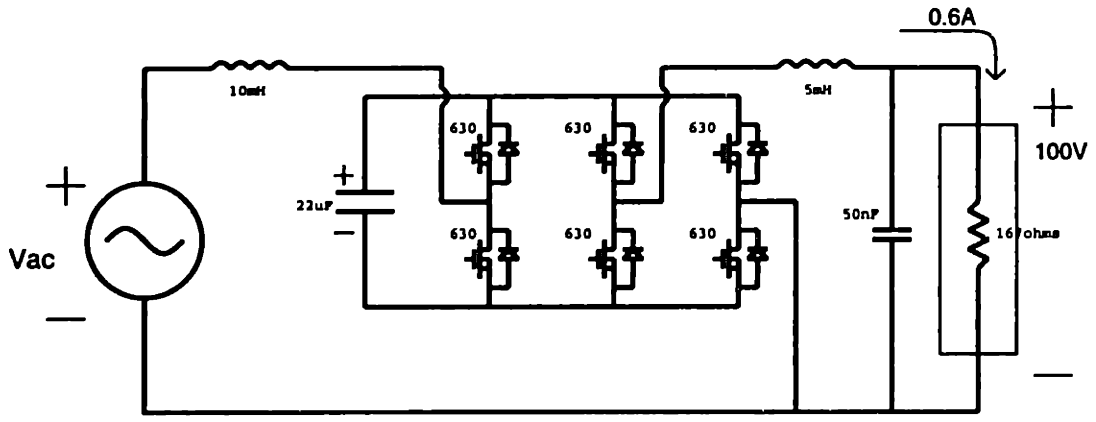

Figure 8-5: Auto UDII design with 200 volt switches

synchronous rectifiers as explained in the previous section. Because the switches are rated at 200 volts, the energy storage capacitor can only ripple between 200 volts and the peak of the utility, which is around 160 volts. With these constraints, the capacitance selected for the energy storage capacitor is 22 μF.

Waveforms from averaged model simulations are shown in Figures 8-6 and 8-7. The load is driven with a 60 Hz square wave of current at an amplitude of 0.6 amps. The resulting load voltage is a similar 60 Hz square wave of amplitude 100 volts. The utility current is power factor corrected. For a switching frequency of 100 kHz, the overall losses in this system are around 3.1 watts for a converter efficiency of around 95.1%. The peak energy storage in the capacitor is roughly 2.8 times the minimum energy required for load balancing.

Because 200 volt switches were used in this design, the capacitor voltage is tightly constrained between 200 volts and the peak of the utility. It would probably be desirable to use 250 volt switches to allow the capacitor to have more voltage ripple. In this case, the design would be as shown in Figure 8-8. This design is identical to the previous 200 V switch design except that the switches are now rated at 250 volts. The MOSFETs used are IRF634 which have an on state resistance of 0.45 ohms and a voltage rating of 250 volts. The main advantage of going to 250 volt switches is

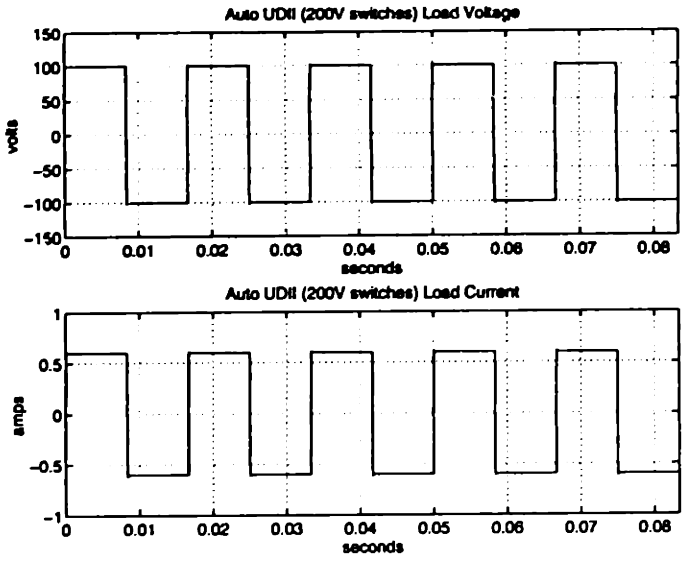

Figure 8-6: Averaged model simulations of auto UDII ballast— load voltage and load current

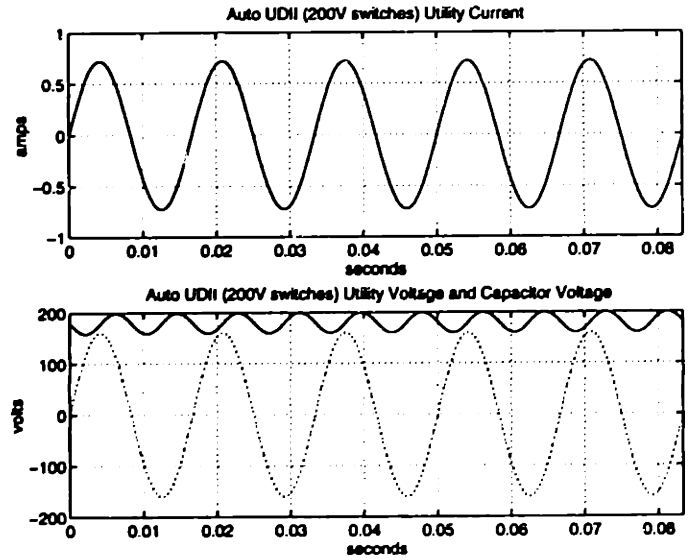

Figure 8-7: Averaged model simulations of auto UDII ballast— utility current and capacitor voltage

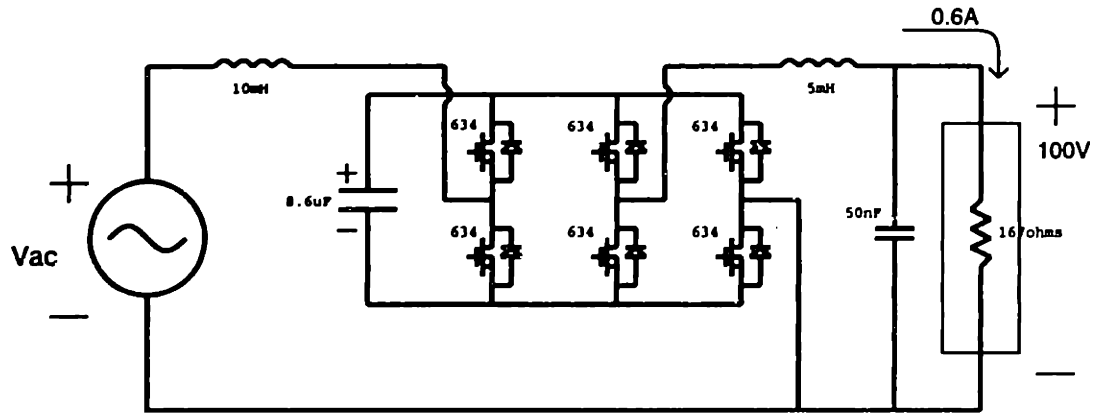

Figure 8-8: Auto UDII design with 250 volt switches

that the capacitor voltage has more range to ripple. In this case, the capacitor voltage can ripple from 160 volts up to 250 volts, and the capacitance may therefore be reduced from 22 μF in the 200 volt case, to only 8.6 μF. The simulated waveforms are all identical except for the capacitor voltage, which is shown in Figure 8-9. Now

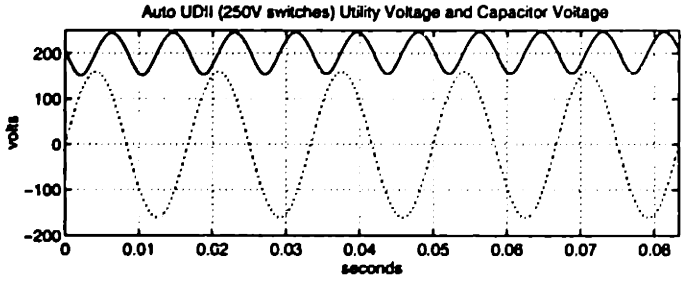

Figure 8-9: Averaged model simulations of auto UDII ballast (250 V switches)—capacitor voltage and utility voltage

the peak energy storage is only 1.7 times the minimum required for load balancing.

The only disadvantage of the 250 V switch design is the increased switching losses due to the greater energy being stored and dissipated in the parasitic capacitances. The difference is not that much greater than the previous 200 V design. The losses for this design are around 3.2 watts for an efficiency of 94.9%.

8.3 Prototype Results

This section describes the work done on an actual prototype of the auto UDII topology. The components and design are described. Measured results are compared to simulated results. A comparison between the auto UDII topology and an existing ballast topology is made.

8.3.1 Components

The final Auto UDII prototype is shown in Figure 8-10. Please note that the proto-

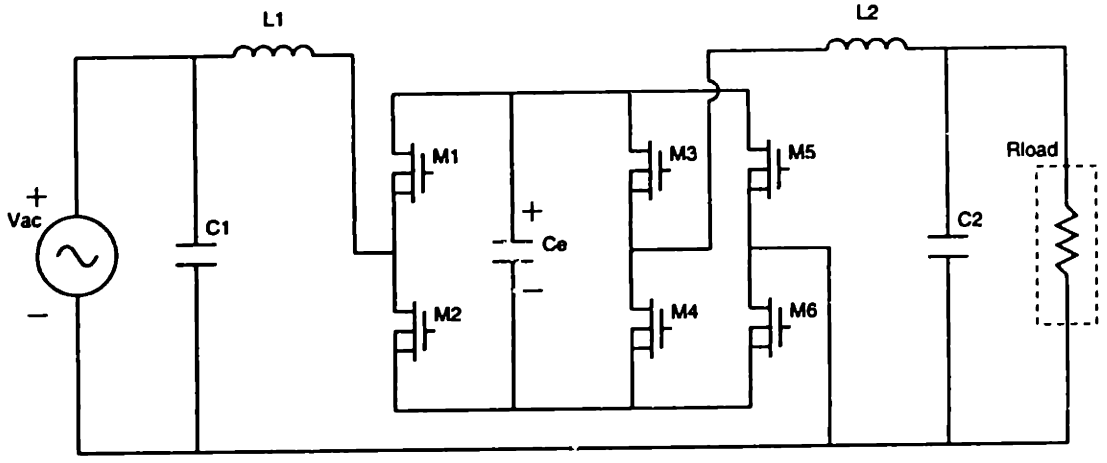

Figure 8-10: Final Auto UDII prototype

type was constructed with readily available components and is therefore not necessarily optimal in terms of size and performance. The goal of this phase of research was to demonstrate a working prototype (proof of concept) and to verify achievable performance and efficiency.

The prototype drives a 60 watt load (0.6 A, 100 V) with a 60 Hz square wave of current synchronized to the utility. The input current is power factor corrected. The load used for testing is a 167 ohm power resistor.

All MOSFETs are International Rectifier IRF630 power MOSFETs which have a voltage rating of 200 V and an on state resistance of 0.4 ohms. The switches

are operated as synchronous rectifiers, requiring a low on state resistance to avoid accumulating reverse recovery charge in the MOSFET antiparallel diodes. M1–M4 are operated at high frequency (100 kHz) while M5 and M6 are operated at low frequency (60 Hz).

The 120Hz voltage ripple on the energy storage capacitor C_e most not exceed the switch rating of 200 V and it must remain above the peak of the utility (approximately 160 V). The minimum capacitance that meets these requirements is 22 μF. The actual capacitor used is a Mallory TC57 aluminum electrolytic rated at 30 μF and 250 VDC. The ESR at 120 Hz is less than 4.09 ohms. C_e is also bypassed with two 50 nF ceramic disc capacitors. It should be noted that if 250V switches are used, the minimum capacitance can be reduced from 22 μF to 8.6 μF.

The utility side filter inductor L1 is 10 mH made from 155 turns of AWG24 on a Magnetics D-43019-40 ferrite pot core. The load side filter inductor L2 is 5 mH made from 110 turns of AWG24 on a Magnetics D-42616-40 ferrite pot core.

The utility side filter capacitor C1 is made of three 100 nF Sprague 715P10496L polypropylene capacitors rated at 600 VDC/200 VAC. The load filter capacitor C2 is a 47 nF Sprague 715P47396L polypropylene capacitor rated at 600 VDC/200 VAC. All capacitors have dissipation factors less than 0.1 percent.

The two inductor currents are each sensed with an LEM LA25-NP/SP11 current transducer. Note that isolated current sensing is not required for this topology. Sample and hold techniques may be used to sense switch currents instead of inductor currents.

8.3.2 Results

Waveforms of the prototype operating in full ac mode are shown in Figure 8-11. The top two traces are the utility and energy storage capacitor voltages at 100 V/div. Note that the capacitor voltage ripples at 120 Hz and is constrained between 200 V (switch rating) and 160 V (peak of utility). The third trace is the utility current at 0.5 A/div. It is power factor corrected with some noticeable crossover distortion. The bottom trace is the load current at 0.5 A/div. It is a square wave of current

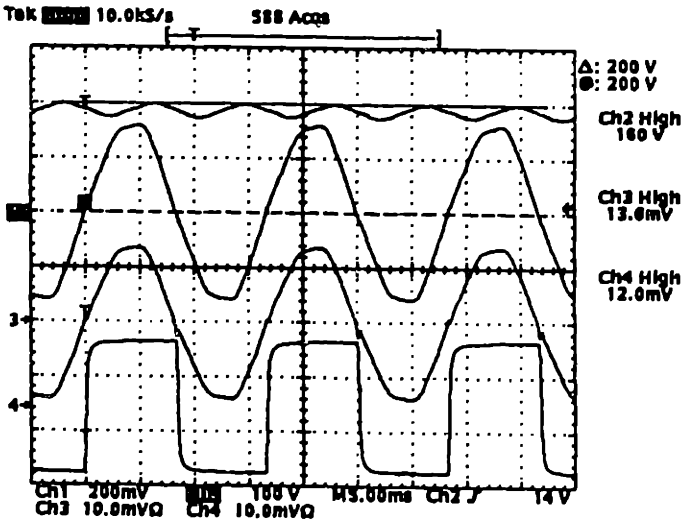

Figure 8-11: AC prototype waveforms – top two traces: utility voltage and capacitor voltage 100V/div, bottom two traces: utility current and load current 0.5A/div.

synchronized to the utility at 60 Hz.

The losses are summarized in Table 8.1. The measured losses are approximately

60 W load (100 V, 0.6 A)	losses
switching	1.9 W
conduction	0.4 W
reverse recovery	1.0 W
filter	0.4 W
ESR	0.3 W
total predicted losses	**4.0 W**
total measured losses	**4.5 W**
measured efficiency	**93.0%**

Table 8.1: Auto UDII prototype evaluation

4.5 watts which agrees well with predicted values. The overall prototype efficiency is 93%. The dominant loss mechanisms are the high frequency switching losses. Mosfets with low on state resistance are required for synchronous rectification in this application. So while conduction losses in the devices are small, the capacitive switching losses are substantial. Control circuit losses are not included since presumably in the final implementation the circuitry would be integrated onto a single control chip or

power integrated circuit.

The observed waveforms agree well with the averaged model simulations. The control loops are stable and function as predicted. The response of the fast loop regulating the load current differs slightly from the simulation results. This can mostly be attributed to inaccuracies resulting from the averaged model. Further differences arise from the nonidealities in the real circuit.

The output ripple current is ± 1% at 100 kHz. The input current ripple was not measured, but calculations suggest approximately 400 μV at 500 kHz into a 50 μH/50Ω LISN (Line Impedance Stabilization Network). Some small modifications to the input filter would be required to meet FCC part 18 subpart C specifications. The measured power factor is 0.999 and the current THD is approximately 2.9%.

The peak energy storage on C_e is 3.75 times the minimum required for load balancing. A 22 μF capacitor would have achieved 2.75 times the minimum. With 250 V switches, an 8.6 μF capacitor could have been used achieving a peak energy storage of 1.7 times the minimum.

The resistive load used for the prototype testing gives accurate efficiency results for a given operating point. The stability of the control is easier with a simple resistive load. For an actual lamp load, the control loops would need to be compensated to account for the negative resistance characteristic of the discharge.

8.3.3 Comparison to Other Topologies

The auto UDII topology is functionally identical to the three stage topology shown in Figure 8-12, which is an existing topology. Given the same switching frequency, both topologies require identically sized filters to achieve the desired specifications. Depending upon device ratings, both topologies can allow for identical 120 Hz ripple voltage on the energy storage capacitor. There is no fundamental difference in operation between the two topologies.

However, the topologies differ in device count. The auto UDII has four high frequency MOSFETs and two low frequency MOSFETs. The three stage has essentially four high frequency devices (two MOSFETs and two diodes) and eight low frequency

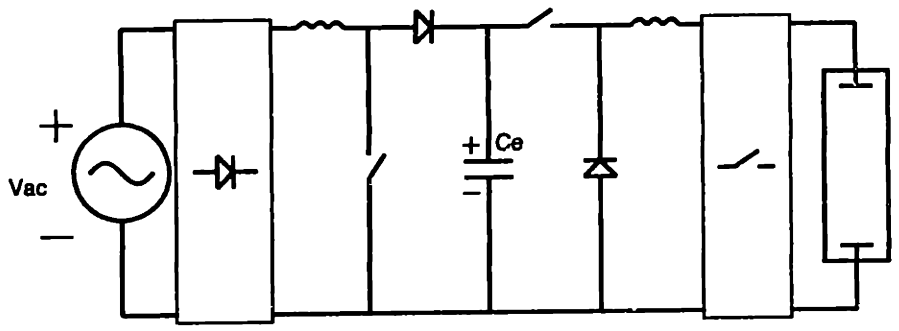

Figure 8-12: Three stage topology

switches. The efficiencies of the two topologies are similar except for the additional conduction losses in the three stage topology. For a 60 watt application, the three stage topology would dissipate approximately an additional 1.4 watts for a loss of over 1% in efficiency compared to the auto UDII. The auto UDII essentially combines input (synchronous) rectification, power factor correction, and output inversion into one stage. The auto UDII topology is then fundamentally more efficient than the three stage topology.

A further benefit of the Auto UDII topology is the option to use resonant techniques to ignite the load. The typical resonant frequency of the output LC filter of the auto UDII topology is around 10 kHz for a 100 kHz switching frequency. It would be possible to operate the output stage as a resonant inverter at 10 kHz during ignition. The lamp would be an open circuit prior to ignition, so the gain of the filter would be very high. Providing that the filter has a suitable quality factor, the output filter would provide the voltage gain to ignite the lamp. In order to use resonant ignition, the components in the output filter of the auto UDII would have to be properly designed to handle the increased voltages and currents during ignition. The three stage topology requires a separate ignition circuit since resonant techniques cannot be used to ignite the load. The final full bridge prohibits a resonant ignition approach. Being able to combine the ignition function into the inherent circuit topology represents an important topological advantage for the auto UDII ballast.

It is difficult to compare the auto UDII topology to the traditional resonant inverter approach. But in terms of energy storage, the Auto UDII can minimize the energy storage capacitor within the parameters of the system. Resonant inverter approaches demand very little capacitor ripple, thus requiring a large energy storage capacitor. The ripple cannot be arbitrarily large since 120 Hz ripple must be attenuated by output frequency control as explained in Section 7.5.2.

8.4 Ballast Size Versus Switching Frequency

This section presents a study concerning the minimum achievable physical size of the auto UDII topology as a function of the converter switching frequency. By increasing the switching frequency, the size of the filter inductors and capacitors can be reduced. At higher switching frequencies, however, the efficiency of the converter decreases. Ultimately it is desirable to raise the converter switching frequency to the point where the size is minimized but the losses are acceptable.

In the following sections, the specifications for the circuit design are outlined and the filter components are described. Various high frequency switch implementations are explored. The results for volume reduction and the effects on converter efficiency are given.

8.4.1 Specifications

Auto UDII circuits were designed for driving a 60 watt load (100 V, 0.6 A) with a 60 Hz square wave of current and input power factor correction. Designs were completed at several switching frequencies (20 kHz, 50 kHz, 100 kHz, 200 kHz, 500 kHz). At each switching frequency, designs were optimized to achieve the minimum volume of filter components.

The input filter was chosen to be an L-C-L type filter required to meet FCC Part 18 subpart C (250μV into a 50 μH/50 Ω LISN from 450 kHz to 30 MHz). The output filter was chosen to be an L-C type filter attenuating output current ripple to $\pm$ 2.5% at the switching frequency. This level of high frequency ripple is reasonable for a

commercial product. The primary concern is the excitation of acoustic resonances in HID type lamps by the high frequency components. For the level of attenuation chosen for these designs, these acoustic resonances will not be excited.

The choice of filter configurations is somewhat arbitrary. Generally speaking, a filter can be designed with smaller volume using higher order filters, up to a point. There are greater filtering requirements at the utility side due to the FCC regulations, so an L-C-L filter was chosen to meet those criteria. Smaller volume was achievable with an L-C-L filter compared to an L-C filter. For the load side filter, an L-C filter was deemed satisfactory.

8.4.2 Filter Elements

The filter elements required are inductors and capacitors. Certain specific types of inductors and capacitors were chosen for these designs based mainly on performance and volume. The data for the components described here can be found in the corresponding data books [92, 93, 94].

The designs used 200 V switches which constrained the energy storage capacitor to a value of 22 μF. Note that this value is solely a function of nominal capacitor voltage and converter power and does not change with switching frequency. The capacitor chosen is a Philips 2222-118 22μF 200V electrolytic with an ESR at 100 Hz of 3.17 ohms.

The filter inductors were chosen to be Philips ferrite pot cores with type 3F3 material. This material has low losses and can operate at frequencies as high as 750 kHz.

The filter capacitors are Sprague type 716P polypropylene film capacitors with 200 VDC/155 VAC rating. These have very low losses with dissipation factors less than 0.1%.

8.4.3 Semiconductor Devices

The main focus of this study is determining the minimum size achievable by raising the converter switching frequency. Ultimately, a power integrated circuit (PIC) implementation is the direction this project will most likely take. The vision is to have a single chip, integrating both the control circuitry and the power semiconductor devices. It was decided that for the purposes of this study, the MOSFETs used would behave like standard International Rectifier MOSFETs with half the device capacitances. Data for the International Rectifier MOSFETs was taken from [95]. It is assumed that a factor of two reduction in size for PIC technology devices compared to discrete transistors is possible.

Three different approaches to high frequency switch implementation were explored. The first approach was using a single MOSFET for each switch operated as a synchronous rectifier. That is, the device was chosen with small enough on state resistance such that the antiparallel diode did not conduct with reverse current flowing through the channel.

The second approach was using a MOSFET with a series Schottky diode and an antiparallel ultra-fast rectifier for each high frequency switch. This approach was expected to work better than the single MOSFET solution, in general, with increasing frequency because of the added degree of freedom in choosing the optimal MOSFET size to balance conduction and switching losses. The Schottky diodes were assumed to have a forward conduction drop of 0.5 V. The ultra-fast rectifiers were assumed to have a forward conduction drop of 1 V and a reverse recovery time of 35 ns.

Finally, the last approach was using a single "superfet" for each high frequency switch. As described before, the body diode in typical power MOSFETs is too slow for high frequency switching converter applications. There have been power MOSFETs developed with fast recovery body diodes, but the recovery times are only marginally improved over standard MOSFETs and still too slow for this application [96, 97, 98]. For example, a Siemens FREDFET BUZ205 device is rated at 400 volts and has an on state resistance of 1.0 ohm. The typical reverse recovery time for the body

diode of this device is around 180 ns, which is much too long compared to the 35 ns reverse recovery time of a discrete ultra-fast rectifier. Although commercial MOSFET body diodes are too slow, it may be possible in the future to manufacture power MOSFETs with very fast body diodes. These hypothetical MOSFETs are referred to as "superfets" and are assumed to be International Rectifier devices with half the capacitance and a 30 ns body diode.

8.4.4 Results

Figure 8-13 shows a plot of filter element volume versus frequency. The total volume

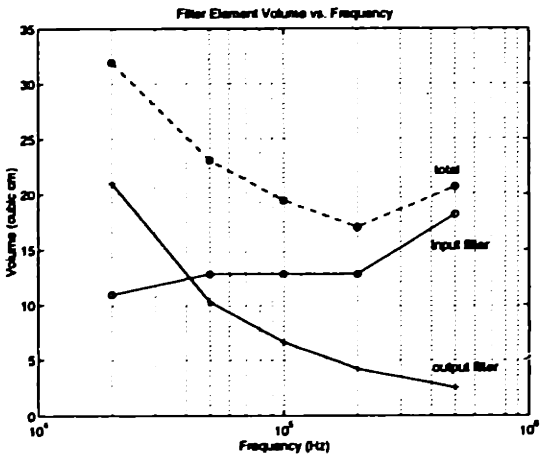

Figure 8-13: Filter element volume versus frequency

decreases with frequency up to 200 kHz. However, at 500 kHz the volume increases. This can be understood by examining the volume of the input filter elements. The input filter volume is roughly constant in frequency due to the increasing harmonics that fall into the regulated band of 450 kHz–30 MHz. The increase in the input filter volume at 500 kHz is because the fundamental of the switching frequency at 500 kHz is within the FCC regulated range of 450 kHz–30 MHz. The output filter volume decreases with frequency as expected, since the design specification was simply to attenuate to $\pm$ 2.5% at the switching frequency.

Figure 8-14 shows the normalized total volume of filter elements versus frequency. This figure is more useful than the absolute numbers given in Figure 8-13. As can be

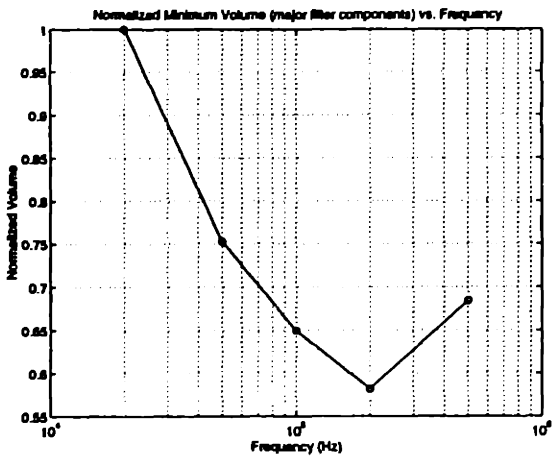

Figure 8-14: Normalized total filter element volume versus frequency

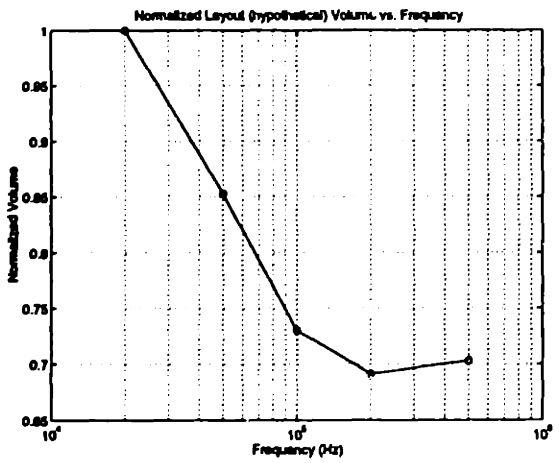

Figure 8-15: Normalized layout volume versus frequency

seen, the volume of the filter elements is reduced by over 40% at 200 kHz versus the 20 kHz solution. The volume reduction at 500 kHz is more than 30% relative to the 20 kHz solution. These numbers include the volume of the electrolytic energy storage capacitor, which is a significant fraction of the total volume, but is not affected by the switching frequency. For example, the energy capacitor represents 18% of the total component volume for the 200 kHz solution.

Since simply reducing the volume of the filter elements themselves does not necessarily result in a smaller total ballast package, hypothetical layouts were explored to gain an understanding of potential size reduction. Each layout was chosen to minimize volume. In Figure 8-15 the normalized hypothetical volume is shown versus frequency. There is a 30% reduction in layout volume at 200 kHz versus 20 kHz.

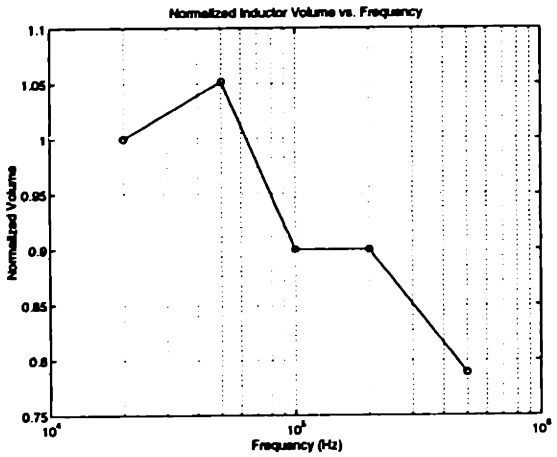

Figure 8-16: Normalized inductor volume versus frequency

Figure 8-16 shows the normalized inductor volume versus frequency. In general, the volume of the magnetics decreases with frequency. Presumably, the cost of the magnetics is therefore also decreasing with frequency. Similarly, in Figure 8-17 the normalized capacitor volume is shown and decreases with frequency until 200 kHz. The increase at 500 kHz is again due to FCC requirements.

Figure 8-18 shows the converter efficiency versus frequency for all three high frequency switch implementations. The single switch solution performs well at lower frequencies due to reduced conduction losses. However, at higher switching frequencies, switching losses quickly dominate resulting in poor converter efficiency. The multiple switch solution initially incurs greater conduction losses at low frequencies, thus the efficiencies are lower than the single switch solution. But at higher frequencies, smaller MOSFETs may be used to reduce switching losses. At 100 kHz, both single and multiple switch solutions are roughly equivalent in efficiency. But beyond 100 kHz, the multiple switch solution yields higher efficiency than the single switch

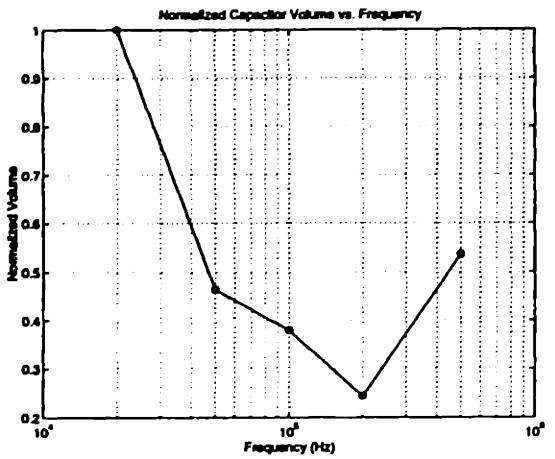

Figure 8-17: Normalized capacitor volume versus frequency

solution.

The superfet solution, of course, outperforms all solutions at all frequencies. At 200 kHz, efficiency with superfets is nearly 96% while the multiple switch and single switch solutions are approximately 93.5% and 93% respectively.

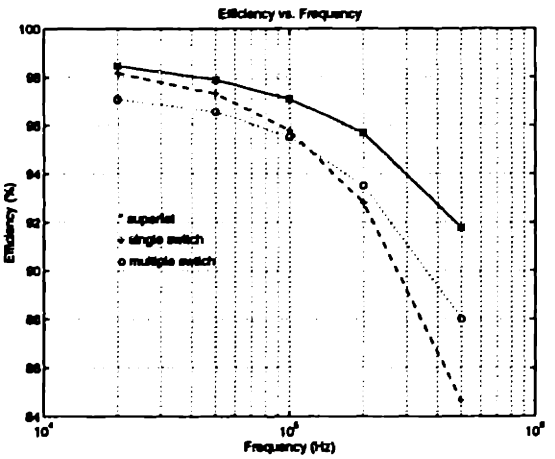

Figure 8-18: Converter efficiency versus frequency

8.5 Summary

The auto UDII topology has been presented as a refinement of the series capacitor and autotransformer topologies. The topology consists of four high frequency and two low frequency switches. The lamp is driven with a 60 Hz square wave of current with power factor correction on the input current. Unlike the series capacitor and autotransformer topologies, there is no constraint on the lamp voltage. The energy storage capacitor may be minimized within the parameters of the system.

When compared to an existing topology, the auto UDII demonstrates an improvement in efficiency of over one percentage point while maintaining precisely identical functionality. The combination of input synchronous rectification, power factor correction, and output inversion into one stage results in the improved efficiency. Perhaps a more important fundamental advantage of the auto UDII is the ability to use resonant ignition with the output filter already existing in the topology. A separate electronic ignition circuit would not be required. The existing three-stage topology requires an separate ignitor.

Hypothetical designs were explored at various switching frequencies to determine the possible size reduction of the auto UDII topology. In general, the minimum volume is reached at a switching frequency of 200 kHz. The layout volume can be reduced by 30% at 200 kHz versus the 20 kHz solution. All types of high frequency switch implementations yield good efficiencies at 200 kHz (93%–96%). The efficiency using superfets is almost 96% at 200 kHz compared to 98% at 20 kHz. Presumably, cost and size can be reduced with increasing switching frequency at the expense of converter efficiency.

Chapter 9

Summary and Future Work

9.1 General Summary

An array of topologies suitable for driving discharge lamps has been presented that are very different from the traditional resonant inverter ballast approach. The general strategy of these new ballast circuits is to drive the lamp with a 60 Hz square wave of current synchronized to the utility. The motivation for the 60 Hz square wave drive is for two basic reasons. The first reason is that the lamp is most efficient when operated at its optimal current. The second reason is that driving the lamp with a regulated current is inherently current limiting, which is the primary role of the ballast itself.

Using this general strategy for the lamp drive, the resulting circuit topologies can be based on dc-dc converters. This means that the switching frequency of the converter may be increased in order to reduce the size of the filter elements without concern of radiated EMI problems from the lamp. This is in contrast to the resonant inverter approach where the lamp is driven at the switching frequency, and therefore there are limits as to how high the frequency can be raised without generating significant radiated EMI. In our new topologies, the EMI is strictly a filtering problem as the lamp sees only 60 Hz waveforms. Beyond this advantage, the many techniques for optimizing dc-dc converter performance already present in the field can be applied directly to these new ballast topologies.

Perhaps the most ground breaking improvement in the new topologies is the ability

to minimize the energy storage capacitor. For example, the 40μF capacitor in the resonant inverter ballast can be reduced to less than 10μF by using the topologies in Chapters 7 and 8. In the resonant inverter approach, this capacitor represents a fundamental size limitation. It simply cannot be reduced in size since it must maintain a constant dc voltage for input to the resonant inverter. The capacitor size then is really just a function of the converter power. As was shown in this document, the new topologies can tolerate an arbitrary amount of capacitor voltage ripple, thus allowing a reduction in the size of the capacitor. In fact, in the series capacitor topology, the absolute minimum capacitance may be used. The resonant inverter may allow 120 Hz ripple on the capacitor, but the resulting ripple on the lamp must be attenuated by frequency control of the inverter. This technique has been patented in U.S. patent number 5,128,592. A value of our topologies is that 120 Hz ripple may be compensated without infringing on this patent.

Isolation is not provided in any of the proposed topologies, which may or may not be a concern. Elimination of the expensive and lossy isolation transformer is certainly an advantage from a cost and efficiency viewpoint. In the case of tubular fluorescent lamps, the issue of safety isolation is a problem. But in many applications, such as HID lamps and compact fluorescent lamps, safety isolation is not needed.

9.2 Topology Summary

The series capacitor topology was the first topology presented, and the simplest. It consists of two high frequency switches, two low frequency switches, a single filter inductor and an energy storage capacitor (in its simplest form). The basic nature of the topology allows high efficiencies. The most interesting feature of the series capacitor topology is that it can achieve the absolute minimum energy storage required for load balancing, a feature not present in any existing topologies today. However, the simple series nature of the topology results in some limitations. The lamp current is the same as the utility current, and is therefore not power factor corrected. The harmonics in the square wave current drawn from the utility will be a concern. The

lamp voltage is limited to the average of the utility voltage (around 100 volts), which is actually the arc voltage of most discharge lamps. The main problem is that there is no means of regulating the lamp voltage. It is possible to use phase control at the expense of the power factor. There is no inherent means for lamp ignition, but for HID applications, a separate ignition circuit is always used anyway.

The autotransformer topology expanded upon the series capacitor topology with the addition of a shunt element. This allows power factor correction on the utility current while allowing any lamp voltage to be driven. The basic structure of the topology, however, limits the lamp voltage to be greater than the utility voltage because only up conversion from the utility to the lamp is possible. The converter consists of a unique dc-dc converter cell consisting of three high frequency switches. Four low frequency switches are used for output polarity inversion. The energy storage capacitor can be minimized within the parameters of the system. An example reduction in the energy storage is a peak energy storage in the autotransformer topology of only one third the peak storage in the resonant inverter ballast. Like in all these new topologies, the 120 Hz ripple on the capacitor can be attenuated easily at the load because of the nature of the dc-dc conversion. This is in contrast to the frequency modulation control in the resonant inverter. The autotransformer topology can be converted for up-down conversion with an additional four bridge switches. This allows any lamp voltage to be driven.

The auto UDII topology is perhaps the most flexible of all the topologies presented in this document. It has no constraint on the lamp voltage and can provide for power factor correction, so it may have the most potential as a viable commercial product. The basic topology consists of four high frequency switches, two low frequency switches, two inductors, and an energy storage capacitor. The operation of the topology is relatively simple and straightforward. Again, the energy storage capacitor can be minimized within the parameters of the application. A combination of input synchronous rectification, power factor correction, and output inversion into one stage results in improved efficiency over an existing topology that is a functional equivalent of the auto UDII. This existing topology is called the three stage topology

and must use a separate ignition circuit. The auto UDII topology can use resonant techniques, using components in the output filter, to ignite the lamps without requiring any separate circuitry.

9.3 General Concerns

The chief concern of our approach is the efficacy of a 60 Hz square wave lamp drive compared to a high frequency sinusoidal drive. The 60 Hz square wave drive is expected to be more efficient than the 60 Hz sinusoidal drive, but not as efficient as the high frequency sinusoidal drive. The high frequency sinusoidal drive results in a reduction in the anode potential which yields higher lamp efficacy. This may factor into the possible applications for these new topologies. For HID lamps, the 60 Hz square wave drive is in many ways the optimal lamp drive, since it avoids the excitation of acoustic resonances. Furthermore, HID lamps do not exhibit the significant efficacy gains at high frequency that fluorescent lamps do.

Another concern is the elimination of lamp electrode heating. This is only an issue in the case of fluorescent lamps. Typically, the lamp electrodes are heated during starting to lower the breakdown voltage of the arc. The auxiliary heating of the electrodes is not necessary during operation as the lamp current heats the electrodes sufficiently. So removing the filament heating during steady state operation can result in improved efficiency. However, in applications where the lamp can be dimmed, electrode heating is required to maintain thermionic emission at low current levels. The electrode heating is usually accomplished with auxiliary windings on the transformer present in the resonant inverter ballasts. In the case of our topologies, it would be possible to use windings on a filter inductor to provide the necessary electrode heating.

A final concern is the elimination of the isolation transformer. If it is possible to eliminate the transformer from the ballast topology, then significant savings in cost and manufacturing can potentially be realized. In the resonant inverter ballast, the transformer serves a dual purpose. The first purpose is to match the load impedance

to the resonant inverter circuit. The second purpose is to provide safety isolation. Some means of providing suitable shock protection in the new topologies must be devised. There is already on-going research in the area of electronic ground fault detection and shock protection means in the ballast industry. This is not a concern in the area of compact fluorescents and HID lamps, where safety isolation is not needed.

9.4 Future Work

Most of the future work involved in this project revolves around making the ballast topologies viable as actual commercial products. Concerning the topologies themselves, future work should center on optimizing the dc-dc converters. This would involve examining tradeoffs in discontinuous conduction mode versus continuous conduction mode operation, for example. The topologies presented in this document are all operated in the continuous conduction mode. Advanced dc-dc conversion techniques could possibly be employed, such as interleaved power conversion and soft-switching. The switching frequency should be raised to minimize the size of the filter components within acceptable limits of efficiency. The filter designs should be optimized in terms of physical size and stability. It may be possible to use active EMI filter techniques to further reduce the physical size of the filter components.

The issue of current sensing has not been dealt with in this document. Hall effect sensors have been used in the auto UDII topology to provide the requisite current sensing. This approach is probably too expensive for a commercial product. In most of the topologies presented, it is simple enough to use a sense resistor and a sample and hold to sense the appropriate switch currents. This is somewhat difficult to do at high frequencies with discrete components, but certainly much easier to accomplish in an integrated circuit.

This work has focused on the operation of converters during the steady state. The ignition problem is certainly a challenging one, and is in many ways a separate problem. The ignition of fluorescent lamps is generally not a problem, since the voltages

required are around 500 volts peak. There is the issue of the electrode heating, however. In the case of ignition for HID lamps, the problem is very challenging. Usually a separate ignition circuit is used, so that does not affect the work presented here. But it has been proposed that the auto UDII topology can use resonant techniques to ignite the lamp. If the application is driving an HID lamp, then this issue of ignition should be addressed. The ignition of the HID lamp occurs in four phases. The first is the breakover phase which occurs at around 2.5 kV. The second is the glow phase where the arc voltage is high and the lamp current is low. During this phase, the electrodes are heated to thermionic emission temperatures. The third phase is the run-up phase where the lamp approaches a short circuit and operates at low voltage and high current. The final phase is, of course, nominal steady state operation. It would be possible to operate the auto UDII topology in a resonant mode to achieve the breakover and glow phases of ignition. Then the converter could be operated in a normal operation mode providing 60 Hz waveforms during run-up and steady state operation. Future work would involve designing and incorporating the ignition function into the topology.

As mentioned before, some work must be done to address the issue of shock protection in tubular fluorescent lamp ballast applications. An isolation transformer is not required in electronic ballasts as long as suitable means for safety protection are provided. It is possible to use some form of a ground fault detection circuit to sense shock situations and then open and close a suitable combination of switches in the topology to provide the shock protection.

A major area for future work will involve the development of power integrated circuit (PIC) solutions for these topologies. It will be important to develop a control integrated circuit for these topologies, since it is unlikely that a discrete control circuit can be cost effective. It then becomes natural to think of a single chip incorporating both the power semiconductor devices and the control circuitry. This PIC development would also address the issue of the current sensing mentioned previously. High converter efficiency will be vital to the viability of the PIC solution. A PIC can effectively dissipate only so much power, so low converter losses will be a key factor in

this area. The size versus frequency study of the auto UDII topology presented in the previous chapter was done with the PIC solution in mind. PIC implementations can achieve higher switching frequencies and possibly improved efficiencies by eliminating parasitics from the discrete device packages and interconnections.

Finally, suitable applications for these topologies must be found. Because the topologies are based on a 60 Hz square wave current drive, the natural application has been towards HID lamps. High frequency operation of HID lamps has been difficult to realize due to the acoustic resonances, and the efficacy gains at high frequency are not as dramatic as those achieved in fluorescent lamps. Because the 60 Hz square wave drive results in lower efficiency than high frequency sinusoidal drive in fluorescent lamps, these topologies may be excluded from fluorescent lamp applications. However, the difference in lamp efficacy will depend on the lamp type, and the improved converter efficiency may be able to compensate for the lower lamp efficacy. A possible application to explore is the area of compact fluorescent lamps, where the ballast efficiencies are typically poor. Furthermore, many compact fluorescent topologies have no power factor correction. The series capacitor topology might then be a possibility due to its low component count and inherent simplicity. There are many different lamp types and possible areas of application where the topologies presented in this document could be implemented.

Appendix A

Kinetic Theory of Gases

The mean energy for the electrons of a discharge can be determined from the kinetic theory of gases. The electrons (and ions) in the discharge move randomly and have a distribution of velocities. Note, there is a general drift movement due to the applied electric field, but the drift velocities are negligible compared to the random velocities. The kinetic energy K_e of a particle is given by

$$K_e = \frac{1}{2} m v^2 \tag{A.1}$$

where m is the particle mass and v is the particle velocity. To find the average, or mean energy, once must compute the average of the squared velocity,

$$< K_e > = \frac{1}{2} m < v^2 > \tag{A.2}$$

which can be expressed simply in terms of the root mean square velocity v_{rms}

$$< K_e > = \frac{1}{2} m v_{rms}^2 \tag{A.3}$$

James Clerk Maxwell determined the speed distribution of gas molecules to be

$$P(v) = 4\pi \left(\frac{M}{2\pi RT} \right)^{\frac{3}{2}} v^2 e^{-Mv^2/2RT} \tag{A.4}$$

where M is molecular mass in kg/mol, T is absolute temperature in degrees Kelvin, v is the velocity in m/s, and R is the gas constant $8.31 J/mol/K$. $P(v)$ is a probability distribution function that gives the fraction of molecules whose velocities lie between zero and infinity. The total area of $P(v)$ is one. To calculate the mean of the velocity squared, one must weight the quantity v^2 by the distribution function, and integrate from zero to infinity.

$$< v^2 > = \int_0^\infty v^2 P(v)\, dv \tag{A.5}$$

Solving this expression yields

$$< v^2 > = \frac{3RT}{M} \tag{A.6}$$

or

$$v_{rms} = \sqrt{\frac{3RT}{M}} \tag{A.7}$$

Substituting v_{rms} into Equation A.3, the mean kinetic energy is

$$< K_e > = \frac{3}{2} \frac{mRT}{M} \tag{A.8}$$

But the ratio M/m is Avagadro's constant N_A, which is $6.02 \times 10^{23} mol^{-1}$.

$$< K_e > = \frac{3}{2} \frac{R}{N_A} T \tag{A.9}$$

Finally, the ratio R/N_A is the Boltzmann constant k, which is $1.38 \times 10^{-23} J/K$ or $8.62 \times 10^{-5} eV/K$.

$$< K_e > = \frac{3}{2} k T \tag{A.10}$$

So the mean energy of particles in a gas is dependent only on the temperature. In the plasma discharge, the electron temperature is much greater than the ion temperature. The mean energy for the electrons is simply

$$< K_e >_{electrons} = \frac{3}{2} k T_e \tag{A.11}$$

where T_e is the electron temperature. For a T_e of 7737 K, the mean electron energy is 1 eV. The terms electron temperature and electron energy are often used interchangeably [99].

Appendix B

Ambipolar Diffusion

In a plasma discharge, the electrons and ions diffuse to the tube wall through a process called ambipolar diffusion. The electrons are lighter and have higher thermal velocities, and diffuse faster than the ions. This leaves an excess of ions in the plasma, which creates a radial electric field which slows the electrons down and accelerates the positive ions to the wall. The net effect is that both ions and electrons diffuse at the same rate, called the ambipolar diffusion rate. The ambipolar diffusion rate can be calculated from the particle transport equations

$$\Gamma_i = n_i \mu_i E - D_i \frac{dn_i}{dr} \tag{B.1}$$

$$\Gamma_e = -n_e \mu_e E - D_e \frac{dn_e}{dr} \tag{B.2}$$

where n is the particle concentration cm^{-3}, μ is the mobility in $cm^2/V/s$, E is the radial electric field in V/cm due to the ion space charge, and D is the diffusion coefficient in cm^2/s. These equations give the ion and electron fluxes in $particles/cm^2/s$. In the plasma, the electron and ion concentrations are approximately equal, $n_i \approx n_e = n$, and the electron and ion fluxes are also equal, $\Gamma_i = \Gamma_e = \Gamma$. So now Equations B.1 and B.2 can be combined and solved for Γ.

$$\frac{1}{\mu_i}\Gamma + \frac{1}{\mu_e}\Gamma = -\left[\frac{D_i}{\mu_i} + \frac{D_e}{\mu_e}\right]\frac{dn}{dr} \tag{B.3}$$

$$\Gamma = - \frac{\mu_e D_i + \mu_i D_e}{\mu_e + \mu_i} \frac{dn}{dr} \tag{B.4}$$

To simplify this expression, it is helpful to know that the diffusion coefficients are given by the Einstein relationship.

$$D_i = \mu_i \frac{kT_i}{q} \tag{B.5}$$

$$D_e = \mu_e \frac{kT_e}{q} \tag{B.6}$$

Here q is the electron charge $1.6 \times 10^{-19} coul$, T_i is the ion temperature in Kelvin, T_e is the electron temperature in Kelvin, and k is the Boltzmann constant $1.38 \times 10^{-23} J/K$. In this case, the ion mobility is much smaller than the electron mobility, $\mu_i \ll \mu_e$, and the ion temperature is also much less than the electron temperature, $T_i \ll T_e$. Equation B.4 can then be simplified to

$$\Gamma \approx - \mu_i \frac{kT_e}{q} \frac{dn}{dr} \tag{B.7}$$

and we now define the ambipolar diffusion constant D_a

$$D_a = \mu_i \frac{kT_e}{q} \tag{B.8}$$

To calculate the ionization frequency ν_i $(pairs/electron/s)$ to balance the ambipolar diffusion losses, we can start by stating that the flux of particles at a radius of $r + dr$ must equal the flux at a radius of r plus the particles generated by ionization within the space of dr as shown in Figure B-1.

$$2\pi(r + dr)\Gamma_{r+dr} = 2\pi r \Gamma_r + 2\pi r \, dr \, n \, \nu_i \tag{B.9}$$

Simplifying and substituting terms for Γ,

$$- (r + dr) D_a \left.\frac{dn}{dr}\right|_{r+dr} + r D_a \left.\frac{dn}{dr}\right|_r - r dr \, n \, \nu_i = 0 \tag{B.10}$$

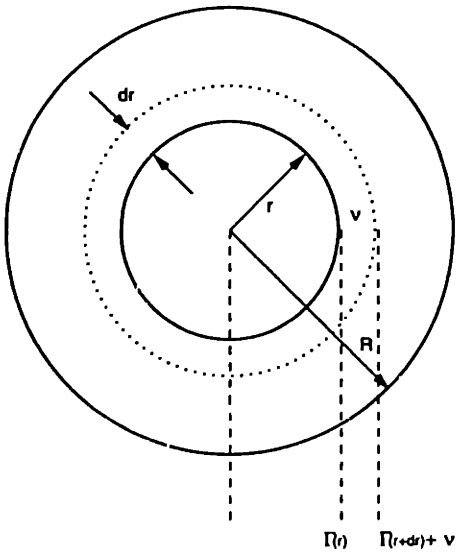

Figure B-1: Flux of ion-electron pairs and generation by ionization

Dividing through by dr and rearranging gives

$$\frac{1}{dr}\left[\left.\frac{dn}{dr}\right|_{r+dr} - \left.\frac{dn}{dr}\right|_{r}\right] + \frac{1}{r}\left.\frac{dn}{dr}\right|_{r+dr} + \frac{n\nu_i}{D_a} = 0 \tag{B.11}$$

To get a differential equation, we let dr approach zero and we get the following:

$$\underbrace{\frac{1}{dr}\left[\left.\frac{dn}{dr}\right|_{r+dr} - \left.\frac{dn}{dr}\right|_{r}\right]}_{\frac{d^2n}{dr^2}} + \frac{1}{r}\underbrace{\left.\frac{dn}{dr}\right|_{r+dr}}_{\approx \left.\frac{dn}{dr}\right|_{r}} + \frac{n\nu_i}{D_a} = 0 \tag{B.12}$$

The term on the left can be found from a Taylor series approximation, or by simply noting that it is the definition for the second order derivative of n with respect to r. Rewriting Equation B.12 we get

$$\frac{d^2n}{dr^2} + \frac{1}{r}\frac{dn}{dr} + \frac{n\nu_i}{D_a} = 0 \tag{B.13}$$

If we make a variable substitution,

$$x = r\sqrt{\frac{\nu_i}{D_a}} \tag{B.14}$$

then Equation B.13 becomes

$$x\frac{d^2n}{dx^2} + \frac{dn}{dx} + nx = 0 \tag{B.15}$$

Equation B.15 is Bessel's equation of order zero, with a solution for n that is $J_o(x)$, which is a Bessel function of order zero. $J_o(x)$ looks like an exponentially decaying sinusoid with a maximum at $x = 0$ and a first zero at $x = 2.4$. We know that at the tube wall the radius is R and the particle concentration must be zero. From our variable substitution we have

$$x = 2.4 = R\sqrt{\frac{\nu_i}{D_a}} \tag{B.16}$$

The ionization frequency ν_i is finally

$$\nu_i = \left(\frac{2.4}{R}\right)^2 D_a \tag{B.17}$$

$$\nu_i = \left(\frac{2.4}{R}\right)^2 \mu_i \frac{kT_e}{q} \tag{B.18}$$

This is the ionization frequency required to maintain the steady state plasma density [5, 100, 101, 102].

References

[1] Peter N. Wood. HEXFETs for use in electronic ballasts. *Vector*, pages 11–14, June 1990.

[2] John D. Paul. The electronic ballast. In *Power Conversion Proceedings*, pages 467–483, 1981.

[3] Thomas C. Jednacz. Power-quality design implications of high frequency lighting ballasts and control. In *IEEE Industry Applications Meeting*, pages 1853–1858, 1991.

[4] John E. Traister. *Principles of Illumination.* Howard W. Sans and Co., Inc., New York, 1974.

[5] John F. Waymouth. *Electric Discharge Lamps.* The M.I.T. Press, Cambridge, 1971.

[6] M. A. Cayless and A. M. Marsden, editors. *Lamps and Lighting.* Edward Arnold, Baltimore, Maryland, 1983.

[7] R. J. Haver. Electronic ballasts. *PCIM*, pages 52–56, April 1987.

[8] Dragan M. Vasiljevic. The design of a battery-operated fluorescent lamp. *IEEE Transactions of Industrial Electronics*, pages 499–503, November 1989.

[9] Charles L. Amick. *Fluorescent Lighting Manual.* McGraw-Hill Book Company, Inc., New York, 1960.

[10] W. Elenbaas, editor. *Fluorescent Lamps.* The Macmillan Press, LTD, New York, 1971.

[11] John E. Kaufman, editor. *IES Lighting Handbook 1984 Reference Volume.* Illuminating Engineering Society of North America, 1984.

[12] J. W. F. Dorleijn and A. G. Jack. Power balances for some fluorescent lamps. *Journal of the Illuminating Engineering Society*, pages 75–84, Fall 1985.

[13] Bob Christiansen. A comparison of magnetic and electronic ballasts: Part II. *Electrical Manufacturing*, pages 43–45, July 1990.

[14] Joseph R. Knisley. Understanding the use of new fluorescent ballast designs. *EC&M*, pages 67–73, March 1990.

[15] Rudolph R. Verderber, Oliver C. Morse, and Fracis M. Rubinstein. Performance of electronic ballast and controls with 34- and 40-watt f40 fluorescent lamps. *IEEE Transctions on Industry Applications*, pages 1049–1059, November/December 1989.

[16] Marian K. Kazimierczuk. Electronic ballast for fluorescent lamps. *IEEE Transactions on Power Electronics*, pages 386–395, October 1993.

[17] Dale E. Hitchcock. High frequency characteristics of 32 watt T8 lamps. *Journal of the Illuminating Engineering Society*, pages 26–35, October 1983.

[18] E. E. Hammer. Comparative starting-operating characteristics of typical F40 systems. *Journal of the Illuminating Engineering Society*, pages 63–69, Winter 1989.

[19] E. E. Hammer and Caio A. Ferreira. F40 fluorescent lamp considerations for operation at high frequency. *Journal of the Illuminating Engineering Society*, pages 63–73, Fall 1995.

[20] Melvin C. Cosby and R. M. Nelms. Designing a parallel-loaded resonant inverter for an electronic ballast using the fundamental approximation. In *Applied Power Electronics Conference*, pages 418–423, 1993.

[21] T. H. Yu, H. M. Huang, and T. F. Wu. Self excited half-bridge series resonant parallel loaded fluorescent lamp electronic ballasts. In *Applied Power Electronics Conference*, pages 657–664, 1995.

[22] Nanjou Aoike, Kouhei Yuhara, and Yorikiyo Nobuhara. Electronic ballast for fluorescent lamp lighting system of 100 lm/W overall efficiency. *Journal of the Illuminating Engineering Society*, pages 225–239, October 1984.

[23] Edward E. Hammer. Fluorescent lamp operating characteristics at high frequency. *Journal of the Illuminating Engineering Society*, pages 211–224, October 1984.

[24] E. E. Hammer. High frequency characteristics of fluorescent lamps up to 500kHz. *Journal of the Illuminating Engineering Society*, pages 52–61, Winter 1987.

[25] Sam Ben-Yaakov, Michael Gulko, and Alex Giter. The simplest electronic ballast for HID lamps. In *Applied Power Electronics Conference*, pages 634–640, 1996.

[26] W. H. Lake and J. M. Davenport. Low wattage metal halide lamps. *Journal of the Illuminating Engineering Society*, pages 66–72, January 1982.

[27] W. Elenbaas, editor. *High Pressure Mercury Vapour Lamps and Their Applications.* Philips Technical Library, 1965.

[28] S. Wada, A. Okada, and S. Morii. Study of HID lamps with reduced acoustic resonances. *Journal of the Illuminating Engineering Society*, pages 162–175, Winter 1987.

[29] William R. Alling. Important design parameters for solid-state ballasts. *IEEE Transactions on Industry Applications*, pages 203–207, March/April 1989.

[30] Koichiro Tanigawa and Hiroshi Nishimura. Latest trends in light source systems. Lighting Reseach and Development Laboratory in Matsushita Electric Works, Ltd.

[31] Hans-Juergen Faehnrich and Erhard Rasch. Electronic ballasts for metal halide lamps. *Journal of the Illuminating Engineering Society*, pages 131–139, Summer 1988.

[32] Laszlo Laskai, Prasad Enjeti, and Ira J. Patel. White-noise modulation of high-frequency high-intensity discharge lamp ballasts. In *IEEE Industry Applications Meeting*, pages 1953–1961, 1994.

[33] E. Rasch and E. Statnic. Behavior of metal halide lamps with conventional and electronic ballasts. *Journal of the Illuminating Engineering Society*, pages 88–96, Summer 1991.

[34] H. Nishimura, H. Nagase, K. Uchihashi, T. Shiomi, and M. Fukuhara. A new electronic ballast for HID lamps. *Journal of the Illuminating Engineering Society*, pages 70–76, Summer 1988.

[35] N. Fukumori, H. Nishimura, K. Uchihashi, and M. Fukuhara. A study of HID lamp life when operated by electronic ballasts. *Journal of the Illuminating Engineering Society*, pages 41–47, Winter 1995.

[36] T. M. Lemons, G. Obolensky, and M. J. McGovern. A new HID ballast concept. *Journal of the Illuminating Engineering Society*, pages 229–234, July 1976.

[37] R. Christiansen. Effects of high levels of harmonics from lighting equipment and systems. In *IEEE Industry Applications Meeting*, pages 1859–1862, 1991.

[38] Y. C. Liang. A novel electronic ballast for fluorescent lamps. *Lighting in Australia*, pages 14–17, June 1988.

[39] M. Gyoten, K. Ito, and N. Yoshikawa. Development of an electronic starter for fluorescent lamps. *Journal of the Illuminating Engineering Society*, pages 86–90, Summer 1995.

[40] William J. Roche and Howard W. Milke. Fluorescent lamp starting aids — how and why they work. *Journal of the Illuminating Engineering Society*, pages 29–36, October 1974.

[41] E. E. Hammer. Peak and RMS starting voltage procedure for standard/low energy fluorescent lamps. *Journal of the Illuminating Engineering Society*, pages 204–210, July 1981.

[42] R. Paraman. Energy saving in fluorescent tube lights. *Electricity Conservation Quarterly*, pages 10–13, October 1989.

[43] Meerten Luursema. Power conversion for fluorescent. In *International Power Conversion Proceedings*, pages 3A.2–1–3A.2–8, 1980.

[44] Bodo M. Wolffframm. Ballasts – past, present, and future, a review of the ballasts. In *IEEE Industry Applications Meeting*, pages 1288–1292, 1984.

[45] Bob Christiansen. A comparison of magnetic and electronic ballasts: Part I. *Electrical Manufacturing*, pages 45–47, May 1990.

[46] J. C. Engel, R. T. Elms, and R. E. Hanson. A new energy efficient fluorescent lamp ballast. *Journal of the Illuminating Engineering Society*, pages 130–133, April 1980.

[47] E. E. Hammer. Effects of changing line voltage with various fluorescent systems. In *IEEE Industry Applications Meeting*, pages 1674–1679, 1986.

[48] Pat Mann. A guide to electronic ballasts. *Lighting Design*, page 28, March 1992.

[49] E. E. Hammer and T. K. McGowan. Characteristics of various F40 fluorescent systems at 60 Hz and high frequency. In *Industry Applications Society Conference Record*, pages 1255–1261, October 1983.

[50] G. D. Garbowicz. An improved hybrid fluorescent lamp ballast. *Journal of the Illuminating Engineering Society*, pages 42–45, Summer 1992.

[51] G. D. Garbowicz. Hybrid ballasts II: high-efficiency-type ballasts for 32-W T8 and 34-W T12 lamp systems. *Journal of the Illuminating Engineering Society*, pages 22–30, Winter 1994.

[52] B. R. Collins and R. E. Wenner. Starting pulse tester for high pressure sodium systems. *Journal of the Illuminating Engineering Society*, pages 195–200, July 1976.

[53] P. O. Lauritzen, J. A. Jorgensen, S. D. Meyer, and J. G. Osborn. A dimmable (1000:1 range) fluorescent ballast for instrument panel lighting. *Journal of the Illuminating Engineering Society*, pages 86–90, January 1983.

[54] John K. Moriarty Jr. and Thomas E. Truax. Electronic ballast chip set with integral power FETs. In *IEEE Industry Applications Meeting*, pages 2090–2097, 1995.

[55] T. F. Wu, T. H. Yu, J. C. Hung, and H. P. Yang. Analysis and design of dimmable electronic ballasts for fluorescent lamps using fuzzy controller. In *Applied Power Electronics Conference*, pages 648–654, 1996.

[56] T. H. Yu, L. M. Wu, and T. F. Wu. Comparisons among self-excited parallel resonant, series resonant and current-fed push-pull electronic ballasts. In *Applied Power Electronics Conference*, pages 421–426, 1994.

[57] Kurt J. Nemer. One utility's experience with electronic ballast systems. In *Electronic Ballast Design and Control*, pages 26–30. High frequency Power Conversion Conference, 1994.

[58] Sujit K. Biswas and R. P. Dhanuka. Reliability of electronic ballasts in industrial fluorescent lighting applications. In *IEEE Industry Applications Meeting*, pages 1915–1919, 1992.

[59] Raul Abesamis, Paul Black, and Jeffrey Kessel. Field experience with high-frequency ballasts. In *IEEE Industry Applications Meeting*, pages 2358–2359, 1989.

[60] Karl Johnson and Robert Zavadil. Assessing the impacts of nonlinear loads on power quality in commercial buildings – and overview. In *IEEE Industry Applications Meeting*, pages 1863–1869, 1991.

[61] Anthony Lorusso and Kenneth B. Bowes. Harmonic and power characteristics of electronic ballasts for fluorescent lighting. In *Applications Power Quality/ASD Proceedings*, pages 146–159, October 1990.

[62] R. J. Scwabe and S. Zelingher. Interference between electronic lighting and other applications. In *IEEE Industry Applications Meeting*, pages 2076–2082, 1995.

[63] Shozo Kataoka and Kaoru Atagi. Prevention of IR interference from high frequency fluorescent lighting to IR remote-control systems. In *Applied Power Electronics Conference*, pages 677–683, 1995.

[64] Bob Christiansen. EMI and electronic ballasts. *Powertechnics Magazine*, pages 25–30, September 1990.

[65] Jim Spangler and Anup K. Behera. Power factor correction techniques used for fluorescent lamp ballast. In *IEEE Industry Applications Meeting*, pages 1836–1841, 1991.

[66] R. R. Verderber, O. C. Morse, and W. R. Alling. Harmonics from compact fluorescent lamps. In *IEEE Industry Applications Meeting*, pages 1853–1858, 1991.

[67] Bob Mammano and Lloyd Dixon. Choose the optimum topology for high power factor supplies. *Powerconversion and Intelligent Motion*, pages 8–18, March 1991.

[68] Chin S. Moo, Ying C. Chuang, and Ching R. Lee. A new power factor correction circuit for electronic ballasts with series-load resonant inverter. In *Applied Power Electronics Conference*, pages 628–633, 1996.

[69] Bob Christiansen. Correcting fluorescent lamp ballast power. *Powertechnics Magazine*, pages 33–36, May 1990.

[70] D. Tadesse, F. P. Dawson, and S. B. Dewan. A comparison of power circuit topologies and control techniques for a high frequency ballast. In *IEEE Industry Applications Meeting*, pages 2341–2347, 1993.

[71] R. M. Nelms, T. D. Jones, and Melvin C. Cosby Jr. A comparison of resonant inverter topologies for HPS lamp ballasts. In *IEEE Industry Applications Meeting*, pages 2317–2322, 1993.

[72] Peter N. Wood. Simplified ballast designs using high voltage mos gate drivers. In *Electronic Ballast Design and Control*, pages 49–59. High Frequency Power Conversion Conference, 1994.

[73] Yiyoung Sun. PSpice modeling of electronically ballasted compact fluorescent lamp systems. In *IEEE Industry Applications Meeting*, pages 2311–2316, 1993.

[74] Mihail S. Moisin and Kent E. Crouse. Circuit for driving a gas discharge lamp load, June 23, 1992. United States Patent Number 5,124,619.

[75] Urs Mader. Steady-state analysis of a voltage-fed inverter with second-order network and fluorescent lamp load. In *Applied Power Electronics Conference*, pages 609–615, 1996.

[76] R. R. Verderber. Analysis of past and future electronic ballast markets. In *Electronic Ballast Design and Control*, pages 2–8. High Frequency Power Conversion Conference, 1994.

[77] Yunfen Ji and Robert Davis. Starting performance of high-frequency electronic ballasts for 4-foot fluorescent lamps. In *IEEE Industry Applications Meeting*, pages 2083–2089, 1995.

[78] Bureau of the Census. Current industrial report, fluorescent lamp ballasts mq36c(95)-5, September 1996.

[79] Bureau of the Census. Current industrial report, fluorescent lamp ballasts mq36c(96)-3, November 1996.

[80] Jim Eyer and C. R. Stevens. Electronic lighting ballast technology for office equipment power supplies. In *Electronic Ballast Design and Control*, pages p31–40. High Frequency Power Conversion Conference, 1994.

[81] Martin F. Schlecht and Leo F. Casey. Comparison of the square-wave and quasi-resonant topologies. In *Power Electronics Specialists Conference*, pages 124–134, 1987.

[82] Brett A. Miwa. Interleaved conversion techniques for high density power supplies, May 1992. Doctor of Philosophy thesis, Massachusetts Institute of Technology.

[83] Thomas Farkas and Martin F. Schlecht. Viability of active EMI filters for utility applications. *IEEE Transactions on Power Electronics*, pages 328–337, May 1994.

[84] Underwriters Laboratories Inc. *Standard for Fluorescent-Lamp Ballasts UL935 Eighth Edition.* 1993.

[85] Richard C. Counts. Ground fault detector and associated logic for an electronic ballast, August 24, 1992. United States Patent Number 5,334,912.

[86] Edward L. Laskowski and John F. Donoghue. A model of a mercury arc lamp's terminal v-i behavior. *IEEE Transactions of Industry Applications*, pages 419–426, July/August 1981.

[87] Philip R. Herrick. Mathematical models for high-intensity discharge lamps. *IEEE Transactions on Industry Applications*, pages 648–654, September/October 1980.

[88] J. J. Lowke, R. J. Zollweg, and R. W. Liebermann. Theoretical description of ac arcs in mercury and argon. *Journal of Applied Physics*, pages 650–660, February 1975.

[89] Ning Sun and Bryce Hesterman. PSpice high frequency dynamic fluorescent lamp model. In *Applied Power Electronics Conference*, pages 641–647, 1996.

[90] U. Mader and P. Horn. A dynamic model for the electrical characteristics of fluorescent lamps. In *IEEE Industry Applications Meeting*, pages 1928–1934, 1992.

[91] Thomas E. Dean, Russel G. Greenwood, and Sylvan E. Irwin, IV. High frequency ballast for gaseous discharge lamps, July 7, 1992. United States Patent Number 5,128,592.

[92] 1994 North American Edition Philips Components Electrolytic Capacitors Data Handbook.

[93] Philips Components Ferrite Materials and Components Catalog.

[94] 1995 Sprague Ceramic, Film, and Aluminum Capacitor Catalog.

[95] International Rectifier 1993 HEXFET Power MOSFET Designer's Manual, Volume III.

[96] Arthur P. Connolly. The FREDFET - a new mosfet for motor speed control circuits. In *International Power Conversion Proceedings*, pages 105–109, 1984.

[97] E. Dobray and P. Freundel. A new power mosfet with a fast-recovery internal inverse diode. In *International Power Conversion Proceedings*, pages 152–161, 1983.

[98] Siemens SIPMOS Power Transistor Data 1996.

[99] David Halliday and Robert Resnick. *Fundamentals of Physics Volume One.* John Wiley and Sons, New York, 1988.

[100] E. U. Condon and Hugh Odishaw. *Handbook of Physics.* McGraw-Hill Book Company, New York, 1967.

[101] C. H. Edwards Jr. and David E. Penney. *Elementary Differential Equations with Boundary Value Problems.* Prentice Hall, New Jersey, 1989.

[102] Clifton G. Fonstad. *Electronic Devices and Circuits.* Massachusetts Institute of Technology course notes, 1991.